UNIVERSIDADE DE LISBOA
FACULDADE DE CIÊNCIAS

Weather extremes in a changing climate: variability, mechanisms and societal impacts

"Documento Definitivo"

Doutoramento em Ciências Geofísica e da Geoinformação
Especialidade de Meteorologia

Riccardo Hénin

Tese orientada por:
Doutora Margarida L.R. Liberato
Doutor Alexandre M. Ramos
Doutora Célia M. Gouveia

Documento especialmente elaborado para a obtenção do grau de doutor

2021

2021

UNIVERSIDADE DE LISBOA

FACULDADE DE CIÊNCIAS

Weather extremes in a changing climate: variability, mechanisms and societal impacts

Doutoramento em Ciências Geofísica e da Geoinformação

Especialidade de Meteorologia

Riccardo Hénin

Tese orientada por:

Doutora Margarida L.R. Liberato

Doutor Alexandre M. Ramos

Doutora Célia M. Gouveia

Júri:

Presidente:

- Doutor João Manuel de Almeida Serra, Professor Catedrático e Presidente do Departamento de Engenharia Geográfica, Geofísica e Energia da Faculdade de Ciências da Universidade de Lisboa

Vogais:

- Doutora María Cruz Gallego Herrezuelo, Catedrática de Universidad, Facultad de Ciencias da Universidad de Extremadura, Espanha;
- Doutora Raquel Olalla Nieto Muñiz, Profesora titular de universidade, Facultad de Ciencias da Universidad de Vigo, Espanha;
- Doutora Margarida da Conceição Rasteiro Magano Lopes Rodrigues Liberato, Professora Auxiliar, Departamento de Engenharias da Universidade de Trás-os-Montes e Alto Douro (orientadora);
- Doutor Emanuel Nemésio de Sousa Dutra, Investigador Doutorado, Instituto Português do Mar e da Atmosfera, na qualidade de individualidade de reconhecida competência na área científica;
- Doutor Ricardo Machado Trigo, Professor Associado, Faculdade de Ciências da Universidade de Lisboa.

Trabalho financiado pela Fundação para a Ciência e a Tecnologia (PD/BD/114479/2016)

Documento especialmente elaborado para a obtenção do grau de doutor

2021

Acknowledgments

More than 5 years passed since my first day in Lisbon and my first day as a researcher. I was given a great opportunity and I want to thank all the people that made this possible.

At first, I say thanks to my supervisors: Prof. Dr. Margarida Liberato, Dr. Alexandre Ramos and Prof. Dr. Celia Gouveia. I feel you gave me all the opportunities a Ph.D. candidate expect. You gave me the motivation and the pressure I needed to pursue my objectives: it was not easy to balance all those inputs but in the end I am proud of what I did, the publications, the experience, and the confidence I gained over the years. I also thank Dr. Joaquim Pinto and Dr. Patrick Ludwig for welcoming me to their research group at KIT. I consider those months an important part of my Ph.D. experience.

Going back to 2016, I would have not even applied for a Ph.D. without the support of Dr. Silvio Davolio, who supervised my Master thesis, guided me in the very first steps after university (and also after the Ph.D.). Sometimes people underestimate the power of the right words told at the right time.

All over these years, a lot of people made my Portuguese experience extraordinary. I want to thank the Earthsystems' friends, the 8.207 crew. I felt part of the Portuguese family from the very beginning. A special thanks to Andreia, my counterpart, always loyal and sincere. They sat in other offices, but they are still part of this: João and Rodrigo, thank you very much for the time we spent together.

A big thanks goes to Alex, Chiara and Francesco: the expat-feeling made us a wonderful group. It was hard to see some of you leaving Lisbon soon but be sure our friendship is not gone, despite the time and the distance that is taking us apart. Thank you very much, Alex, for being my sidekick all this time!

The last year of Ph.D. was marked by the covid pandemics: very hard times I spent with my wonderful Brazilian family from Rua Lopes and with you, Emma and Tommaso. It was so important for me you two were living in Lisbon at that time.

A final mention to my parents, my brother and, for the first time, to the little Gioele. You are an extraordinary example of patience and integrity. Even if I hardly admit it, you continue to be an example. These last times made all these feelings even stronger.

Agradecimentos

Mais de cinco anos já passaram desde o meu primeiro dia em Lisboa, que foi também o meu primeiro dia como investigador. Agora vejo isto como uma grande oportunidade que eu tive e quero agradecer todas as pessoas que contribuíram para este percurso.

Primeiro, quero agradecer os meus orientadores: Prof. Dr. Margarida Liberato, Dr. Alexandre Ramos e Prof. Dr. Célia Gouveia. Sinto que tenho recebido por vossa parte as ferramentas e as oportunidades que um estudante de doutoramento precisa. Vocês deram-me a motivação e a pressão necessária para perseguir os meus objetivos: não foi fácil balancear todos esses inputs, mas enfim posso dizer que sou orgulhoso do que eu fiz, das publicações, da experiência e da confiança que eu ganhei ao longo do tempo. Quero agradecer também o Prof. Dr. Joaquim Pinto e Dr. Patrick Ludwig para o acolhimento que tive no vosso grupo de investigação no KIT. Considero aqueles meses uma parte importante do meu doutoramento.

Regressando ao 2016, tenho que admitir que nem sequer ia candidatar-me para um doutoramento sem o apoio e o suporte do Dr. Silvio Davolio, orientador da minha tese de Mestrado, que me guiou nos primeiros passos depois da Faculdade (e, na realidade, também agora depois do Ph.D.). Às vezes, as pessoas subestimam a importância das palavras certas no tempo certo.

Nestes anos, muitas pessoas contribuíram para que a minha experiência portuguesa fosse extraordinária. Quero agradecer os amigos do Earthsystem, especialmente a malta da sala 8.207: sentiu-me parte da família portuguesa desde o princípio. Um agradecimento especial para a Andreia, uma parelha sempre leal e sincera. Eles estavam sentados noutras salas, mas são parte disto tudo: João e Rodrigo, obrigado por tudo o que fizemos nestes tempos.

Um grande abraço ao Alex, a Chiara e ao Francesco: acho que o expat-feeling nos tornou num grande grupo. Foi realmente muito difícil os-ver deixar Lisboa antecipadamente, mas podem estar certos de que a amizade que me liga a vocês sempre fica aqui, apesar do tempo e da distância. Muito obrigado, Alex, por ter sido o meu parceiro o tempo todo!

O último ano que passei em Lisboa foi marcado para o surto da pandemia do covid-19: foram dias difíceis que eu tive a sorte de partilhar com a minha família brasileira da rua Lopes e com vocês Emma e Tommaso. Foi mesmo muito importante para mim vocês estar em Lisboa naqueles meses.

Enfim, um agradecimento especial aos meus pais, ao meu irmão Stefano, e pela primeira vez, ao pequeno Gioele. Vocês são um extraordinário exemplo de paciência e integridade e continuam a ser uma fonte de inspiração para mim, apesar de eu não conseguir admitir isto tão facilmente. Os últimos tempos tornaram estes sentimentos ainda mais fortes.

Abstract

Extreme weather events and associated impacts have been gaining increasing attention from researchers, stakeholders and the general public. Among extreme weather events, extratropical cyclones (ETCs) do represent one of the major causes of disruption as they are often associated with extreme precipitation and wind. The Iberian Peninsula (IP) is a key area in this regard due to its location, south of the North Atlantic (NA) storm track exit region. This thesis analyses the North-Atlantic cyclones variability, its link to large-scale frontal system variability and to precipitation and wind extremes, in a compound weather extreme perspective.

Several precipitation data sources are assessed over the IP, including the last reanalysis product from ECMWF (ERA5). The methodology is based on grouping precipitation days according to anomalies thresholds, considering both the intensity and the spatial extent. The main result is that ERA5 overperforms the other products, although satellite data have very good performances when the precipitation anomalies are large.

Therefore, ERA5 is used to compute a novel ranking of concurrent precipitation and wind events for the IP. The top100 concurrent events are detailed in terms of the attending cyclones and the spatial pattern of meteorological extremes. Novel subregional characterization of concurrent precipitation and wind events and associated cyclones is produced for the IP, showing that the northwestern domain is the most affected by concurrent events.

Within ETCs, the precipitation and wind spatial patterns, which determine the damage swath, are organized around the cyclone's center and along the fronts. A methodology to objectively associate precipitation to fronts at a sub-daily basis is applied to gridded data sets, including a novel sensitivity test for the optimal size of the allocating area. This new approach enables a comprehensive analysis of the long-term climatology and trend of frontal precipitation on the NA domain.

Key words: Weather extremes, extratropical cyclones; compound events; atmospheric fronts; precipitation and wind extremes.

Resumo

Nas últimas décadas, os eventos meteorológicos e climáticos extremos responsáveis por impactes socioeconómicos sérios têm vindo a receber cada vez mais atenção entre investigadores, *stakeholders* e o público em geral. Existem várias abordagens na literatura científica para identificar e classificar os extremos climáticos. Estes extremos são estritamente dependentes da definição de extremo que é utilizada e, consequentemente, das métricas consideradas. Por outro lado, há um consenso em como as perdas económicas e os impactes sociais associados a eventos climáticos estão a aumentar em todo o mundo: isso fica a dever-se não só ao aumento da severidade dos eventos, mas também ao aumento da exposição e vulnerabilidade social.

Esta tese trata principalmente do primeiro aspeto, contribuindo para um conhecimento mais aprofundado e melhores abordagens de caracterização da variabilidade e dos mecanismos das tempestades do Atlântico Norte, conhecidos como depressões extratropicais. As depressões extratropicais são um elemento chave do estado do tempo e do clima, nas latitudes médias e elevadas, contribuindo fortemente para a variabilidade sinóptica e para a ocorrência de eventos extremos nessas latitudes. A tese foca-se também na ligação entre as depressões extratropicais e a variabilidade do sistema frontal em larga escala, assim como a precipitação e extremos de vento, na perspetiva de eventos extremos compostos, com foco na Península Ibérica. Do conjunto dos eventos climáticos extremos, as depressões extratropicais representam uma das principais causas de perturbação, pois são frequentemente associados a precipitação e ventos extremos. As depressões extratropicais, são ciclones que se formam nas latitudes médias e altas. Estes ciclones geralmente desenvolvem-se em regiões de grande baroclinicidade, i.e., forte gradiente horizontal de temperatura, designadas por zonas frontais, neste caso no Atlântico Norte. A Península Ibérica é uma área chave neste sentido, devido à sua localização especifica no Sul do caminho de passagem destas tempestades.

A presente tese está organizada em três capítulos principais, sendo cada um deles um artigo científico publicado em revista ISI e revisto por pares. Em cada capítulo, é abordado um aspeto diferente da variabilidade e dos impactes das depressões extratropicais que ocorrem no Atlântico Norte. O primeiro ponto abordado relaciona-se com a validação de diferentes bases de dados de precipitação. O objetivo é avaliar quais os dados de precipitação mais adequados para caracterizar extremos de precipitação na Península Ibérica. Para este trabalho, o período

analisado abrange os anos de 2000 a 2008, devido à consistência temporal entre as diferentes bases de dados consideradas. São utilizados dados de satélite e de reanálise, incluindo o último produto de reanálise disponível do ECMWF (ERA5), lançado em 2018, e dois produtos derivados de observações por satélites do *Tropical Rainfall Measuring Mission* (TRMM). O desempenho de cada uma das bases de dados é comparado com a base de dados em malha de precipitação a 0.2º (IBERIA 02, IB02), obtida através de observações de precipitação de estações meteorológicas em Portugal e Espanha e que constituía, até ao momento da publicação do artigo, a melhor base de dados em termos de resolução espacial disponível para a Península Ibérica. Os dias de precipitação são agrupados de acordo com a sua anomalia em relação à média considerando não só a intensidade, mas também a sua extensão espacial. Os resultados mostram que as estimativas de precipitação ERA5 apresentam maior acerto quando comparado com o IBERIA02, quando as várias métricas de comparação são analisadas (correlação, viés e erro médio quadrático). Por outro lado, os dados de precipitação estimados por satélite subestimam drasticamente a precipitação média, embora não tão notoriamente quando são apenas considerados os dias mais extremos de precipitação (com valores de anomalia mais elevados). Em segundo lugar, através da decomposição de viés, as diferentes fontes de erro são também calculadas, evidenciando que a principal contribuição para a tendência da precipitação ERA5 (TRMM) deriva de falsos alarmes (acertos), enquanto as outras fontes de viés foram reduzidas com sucesso em relação à base de dados anterior de reanálise, a ERA-Interim.

No segundo capítulo, são utilizados dados meteorológicos relativos à reanálise do ERA5, desde 1979 até ao presente, para melhorar duas bases de dados de eventos extremos de precipitação e de vento na Península Ibérica. O objetivo final é construir uma nova classificação de eventos extremos compostos de precipitação e de vento. A coocorrência de dois ou mais extremos climáticos é atualmente um tema altamente debatido na comunidade científica. Ou seja, para melhor caracterizar o risco meteorológico geral, é comum assumir uma abordagem composta que considera o papel potencial de múltiplos extremos meteorológicos contribuindo para um impacte isolado ou para impactes compostos. Dentro deste pensamento, os 100 principais eventos diários simultâneos de precipitação e vento na Península Ibérica são identificados e analisados através da sua ocorrência em termos de intensidade e do padrão espacial. Posto isto, a ocorrência de depressões extratropicais associados a Rios Atmosféricos e a possibilidade de os mesmos serem forçadores destes eventos compostos foi também estudada. Esta análise permitiu uma nova caracterização sub-regional da ocorrência simultânea de extremos de precipitação e vento e depressões associados ao domínio em estudo, sendo as principais

conclusões desta análise as seguintes: (1) é mais provável que extremos de vento ocorram independentemente da precipitação, especialmente no quadrante sul da Península Ibérica (PI); (2) pelo menos 80% dos 100 principais eventos extremos ocorridos na Península Ibérica entre 1979 a 2018 estão claramente associados a depressões extratropicais; (3) os Rios Atmosféricos têm maior probabilidade de estarem associados aos eventos mais extremos de precipitação e (4) entre vários subdomínios, o Norte de Portugal é o mais afetado pela ocorrência simultânea de eventos de precipitação e vento extremos.

As regiões mais perto do núcleo dos sistemas de baixas pressões extratropicais estão geralmente associadas a extremos de vento, enquanto a ocorrência de precipitação extrema está associada aos seus sistemas frontais. As frentes atmosféricas refletem a zona de transição entre diferentes massas de ar e podem servir para localizar fluxos de ar. No entanto, é um desafio relacionar objetivamente os extremos meteorológicos com uma característica da atividade ciclónica específica. No terceiro capítulo desta tese, é apresentada uma nova metodologia que permite associar objetivamente a precipitação aos sistemas frontais numa escala sub-diária. O método é baseado na co-localização de precipitação a cada 6 horas entre a reanálise do Era-Interim e dos sistemas frontais calculados a partir de um método objetivo de deteção usando a mesma reanálise. Este método de deteção é baseado em gradientes de temperatura potencial equivalente a 850 hPa Esta metodologia aplica-se a conjuntos de dados em grelha, como os dados de reanálise, e permite a análise da climatologia e da tendência da precipitação frontal para o Atlântico Norte, distinguindo as contribuições das frentes frias e quentes. Neste estudo, é considerado o período 1979-2018, verificando-se que a precipitação frontal é responsável por até 80% da precipitação total na região do *storm track*, com máximos de 50% nas regiões costeiras da Europa Ocidental. Esses valores são mais elevados no inverno e no outono, épocas durante as quais a frequência das depressões extratropicais é mais elevada. Para além disso, existe um aumento (estatisticamente significativo) observado para a precipitação frontal na região Oeste do Atlântico Norte, sugerindo um deslocamento para os polos da precipitação frontal na região da *storm track*, impulsionada principalmente por frentes frias.

Em resumo, esta tese explora a variabilidade e os mecanismos das depressões extratropicais, estando focada nos seus impactes relacionados com precipitação e vento. São propostas novas abordagens para descrever e classificar extremos compostos de precipitação e ventos extremo. Relacionou-se também a variabilidade de precipitação com os sistemas frontais, no que diz respeito à região Euro-Atlântico e ao domínio da Península Ibérica. É importante notar que a

maioria das metodologias apresentadas pode ser facilmente ajustada a outros domínios de interesse e / ou adaptada a outros domínios. A metodologia para associar objectivamente precipitação e frentes atmosféricas pode ser vista como um caso específico do problema mais geral da associação de *weather features*, que hoje em dia é abordado também na perspectiva da Inteligência Artificial. Espera-se que a implementação de tais metodologias em previsões meteorológicas operacionais forneça informações potencialmente novas para a avaliação de riscos e processos de tomada de decisão no que diz respeito aos riscos meteorológicos relacionados com depressões extratropicais.

Palavras-chave: extremos meteorológicos, depressões extratropicais; eventos compostos; frentes atmosféricas; precipitação e ventos extremo.

Table of Contents

List of Figures

List of Tables

List of Acronyms and Abbreviations

ARs	Atmospheric Rivers
CE	Common Era
DWD	Deutscher Wetterdienst
ECMWF	European Centre for Medium-Range Weather Forecasts
EPEs	Extreme Precipitation Events
ERA5	ECMWF Reanalysis 5th Generation
ERA-Interim	ECMWF Re-Analysis Interim Generation
ETCs	Extratropical Cyclones
FB	False Bias
FCT	Fundação para a Ciência e a Tecnologia
GCMs	Global Circulation Models
HB	Hit Bias
IB02	Iberia02
IDL	Instituto Dom Luiz
IP	Iberian Peninsula
ISI	International Scientific Indexing
IPCC	Intergovernmental Panel for Climate Change
IPCC AR6	IPCC Assessment Report 6th
IPCC-SREX	IPCC – Special Report on Managing the Risks of Extreme Events and Disasters to Advance Climate Change Adaptation
IVT	Integrated Vapor Transport
MAE	Mean Absolute Error
MB	Miss Bias
MSLP	Mean Sea Level Pressure
NA	North Atlantic
NAO	North Atlantic Oscillation
NH	Northern Hemisphere
NWP	Numerical Weather Prediction
PV	Potential Vorticity
RMSE	Root Mean Squared Error
SST	Sea Surface Temperature

TMPA	TRMM Multi-Satellite Precipitation Analysis
TRMM	Tropical Rainfall Measuring Mission
TRMM RT	Tropical Rainfall Measuring Mission Real-Time
UTC	Coordinated Universal Time
WMO	World Meteorological Organization

1

Introduction

1.1 Weather extremes in a changing climate

Weather and climate extremes affect the everyday life of billions of people worldwide. These events are sporadic but recurrent and they play a crucial role in determining climate and weather variability (Rummukainen, 2012). The ever-increasing interest in weather extremes worldwide is fostered by the disruptive impacts and damages they are responsible for, in terms of economic, natural and societal losses. Weather extremes comprehend a wide range of events on different spatial and temporal scales (Ren et al., 2018). Spatially, they can persist over large areas, or they can be localized. For example, heat waves and cold spells or prolonged dry and wet conditions are typically described at the synoptic scale. On the contrary, heavy precipitation and strong (gusty) wind affect the regional and sub-regional scale. Sometimes, extremes show more complex patterns as it is for convective cells embedded in cyclonic systems or for the urban heat island exacerbated by a heat wave. The same variety applies to the impacts of extreme events whose temporal and spatial scales span from minutes (wind gust) to months (drought) and spatially from the very local to the continental scale (Bouwer, 2019). This thesis aims at characterizing such variability of extremes, by assuming the study case of extratropical cyclones affecting the midlatitudes, namely the North Atlantic (NA) and European domain, and their related precipitation and wind impacts, in a compound weather perspective.

By definition, extreme events are not expected to occur many times. However, the frequency and the importance of record-shattering extremes is increasing, given that they are an integral part of the climate system and as such, they are being affected by climate change within emission-dependent scenarios (Fischer et al., 2021). In the last decades, several weather extreme events affected the European domain as, for example, the exceptional 2013/2014 winter stormy season in the UK (Kendon and McCarthy, 2015) which turned out as the wettest winter on record for the region since 1910 (Muchan et al., 2015), due to an unprecedented frequency of extratropical cyclones (around one cyclone every 2.5 days – Priestley et al., 2017). In October 2017 the storm Ophelia, the farthest east major hurricane on record in the Atlantic Basin (Moore, 2021), affected Portugal and Ireland and it represented a striking example of the complex interplay among weather drivers and compound impacts: intense winds following the major drought of the last 50 years over Iberia (Garcia-Herrera et al., 2018) triggered the most intense wildfires of the last century in Portugal and caused tens of victims (Augusto et al., 2020). Moreover, extended storms surges and coastal flooding in Ireland were also observed (Guisado-Pintado and Jackson, 2020). Ophelia was only the last one of a series of isolated and

exceptional storms that affected Iberia and Western Europe in the last decade as for Xynthia (Liberato et al., 2013) or Gong (Liberato, 2014) which caused unprecedented natural and economic losses. Prolonged dry spells and heat waves are also becoming more frequent in the context of global warming, as confirmed by the long record of episodes that affected Europe in the last years: the continental-scale heat waves in 2003 which caused more than 70000 additional deaths in Europe (Robine et al., 2008), the Russian drought in 2010 (Cherenkova et al., 2013), the abovementioned Iberian drought in 2016/2017 and, more recently, the 2018 and 2019 consecutive summer droughts in Central Europe (Hari et al., 2020).

According to the Intergovernmental Panel for Climate Change (IPCC) and World Meteorological Organization (WMO) definition (IPCC, 2014), an extreme event is referred to as the occurrence of a value of a weather or climate variable above (or below) a certain threshold near the upper (or lower) ends ('tails') of the range of observed values of the variable. In this sense, the definition accounts for both the intensity (peak-over-threshold) and the rarity (the threshold depends on the distribution of the variable) of the event. Meteorological extremes that typically occur over a longer period as heat waves, cold spells and droughts call for different criteria. For those cases, the computation of specific (climatic) indices, based on a combination of the main weather variables involved, is the most common approach (Sillmann et al., 2017). For the other cases, extremes are based on the exceedance of a relative or absolute threshold (IPCC, 2021), either defined as a percentile, an absolute value or an index that quantifies this exceedance, as for the wind speed loss indices developed in the context of wind impacts and insurance (Pinto et al., 2007; Mornet et al., 2015).

However, for a weather event to be extreme not all the meteorological variables, physical processes or factors involved must be necessarily extreme. It might happen that a combination of them and/or a concurrence in time and space end up being extreme, as for the many examples of recent European extreme events mentioned in the previous paragraph. Within such a wide perspective, more complex events can be identified, and extremes can be attributed. These events are referred to as *compound events*, a rather recent concept that came to the attention of the scientific community and the public because of the increasing complexity of observed extreme events and impacts (Leonard et al., 2014). For example, a coastal flood is not only due to high rain rates over a specific location but rather depends on factors such as rivers run-off, severe wind, storm surges and soil moisture content which combine in a way that leads to flooding (Bevacqua et al., 2017). Another typical example of compounding extremes and impacts is that of a heat wave occurring after or during a drought period, triggering wildfires

(Gouveia et al., 2017, Sutanto et al., 2020) and crop losses (Ribeiro et al., 2020a). The very first definition of compound events was eventually proposed in the IPCC-SREX (2012) and it was further detailed in a series of studies by Zscheischler et al. (2018; 2020a; 2020b) and lastly by Bevacqua et al. (2021), Messori et al. (2021) and in the last IPCC AR6 (IPCC, 2021).

Compound events are now a crucial part of the IPCC risk assessment framework, and they are referred to as "a combination of multiple drivers and/or hazards that contributes to societal or environmental risk and impact". The drivers or hazards may not be (all) extremes themselves but their spatial and/or temporal combination can lead to extreme impacts. Therefore, several cases are accounted within this definition namely (1) cases where multiple drivers lead to an impact or, conversely, a single driver leads to multiple impacts (multivariate), (2) circumstances where extremes are enhanced by underlying pre-existing climate-driven common conditions (preconditioned) and (3-4) cases where two or more extremes occur simultaneously or clustered (temporally and/or spatially compounding). Furthermore, several studies term compound events only when a statistical dependence among drivers is established, based on multivariate probabilistic analysis (e.g., Bevacqua et al., 2017; Manning et al., 2018, Ai et al., 2018; Ribeiro et al., 2020b). Several extreme weather events that occurred in Europe in the recent past have been analyzed by assuming this new perspective such as compounding coastal floods and precipitation events (Santos et al., 2021, Sanuy et al., 2021). On the other hand, reanalysis data enables assessing the long-term variability of compound events and mapping the general dependency among drivers. Again, this is the case of storm surges, in association with river discharge (Bevacqua et al., 2020a), Atmospheric Rivers (ARs) (Ridder et al., 2018) and heavy precipitation (Wu et al., 2018), or the case of extreme precipitation and ARs (Ramos et al., 2018), ARs and cyclogenesis (Eiras-Barca et al., 2018b) and the case of precipitation and wind (Owen et al., 2021; Zscheischler et al., 2021) which is of greatest interest for the current thesis.

Detecting and analyzing weather extremes requires long-term, homogeneous and quality-checked measuring networks. The lack of high-quality data from the past is often a limitation for extreme studies as it intrinsically prevents any assessment of rare events (Easterling et al., 2016). Moreover, very localized extreme events are likely missed by gauge networks (Alexander et al., 2019). The satellite era enables an unprecedented coverage and flux of data which was beneficial for weather extreme studies albeit they cover only a few decades (Benjamin et al., 2018). Still, this posed new challenges about the way to handle dramatic amounts of data: for example, the increased availability of high-quality and high-resolution

real-time data from multi-satellite missions put a strain on data assimilation techniques in forecast applications (Sorooshian et al., 2000). However, the climate and weather research over the last decades have benefited also from a constant increase of computational power, advances in machine learning techniques and novel crowd-engaging initiatives which all together contribute to meet the demand for quick and effective data processing (Abhigna et al., 2018). For example, deep learning techniques for automated identification of features in raw data facilitate quick and effective image processing (Lagerquist et al., 2019). This represents a great potential for detecting meteorological patterns in satellite data or gridded weather fields, as for cyclones (Bonfanti et al., 2018) or fronts (Biard and Kunkel, 2019) and it provides automatic guidance to forecasts and thus to decision making processes (McGovern et al., 2017).

1.2 Temporal and spatial variability of extratropical cyclones

Cyclones are among the weather phenomena that mostly affect the daily weather variability. Therefore, a better understanding of cyclone variations is fundamental for both operational forecasts and climatological studies. Characterizing the intrinsic internal variability of cyclones is essential to define a baseline so that recent changes and future trends can be put into a longer-term perspective. However, this requires very high-resolution climate model output, to enable the identification and tracking of the storms in the past. These kinds of data sets are not trivial, as they often include ensembles of historical simulations (e.g., Pinto and Ludwig, 2020; Raible et al., 2021). For example, Raible et al. (2018) analyzed variations in cyclones statistics (duration, core depth, radius, associated precipitation) from 850 to 2100 CE in the NA Ocean: they found pronounced variations on interannual and decadal timescales, but no external forcing imprint is found before 1850. In the recent past, cyclone characteristics are dominated by decadal variability and connections to modes of variability in both hemispheres. Lastly, the anthropogenic signal is determining a general decrease of the total number of cyclones but also an increase in associated precipitation and cyclones core intensity due to an increase of moisture availability.

Generally speaking, (human-induced) climate change does play a role in modifying local climate and weather variability, both in time and space and therefore also in modifying cyclones and associated meteorological extremes. Transitional climatic zones as the midlatitudes are paramount in this sense: most of the mechanisms that are being affected by climate change at the global scale reflect in the midlatitude variability and extremes as for

Arctic amplification (Francis and Vavrus, 2012), Arctic Sea ice loss (Simmonds and Govekar, 2014), amplified planetary waves (Screen and Simmonds, 2014), $C0_2$ forcing (Grise and Polvani, 2014), changes in circulation modes (Stephenson et al., 2006).

Some of these phenomena are known to have a direct and/or indirect effect on the characteristics of extratropical cyclones (ETCs) and their variability. For example, it was found that a positive (negative) phase of the North Atlantic Oscillation (NAO) corresponds to a stronger (weaker) jet stream, thus to a more (less) intense storms activity. It is also associated with positive (negative) anomalies of precipitation and wind in Central and Northern Europe and to negative (positive) anomalies in Southern Europe and Mediterranean sectors, especially in winter (Hurrel et al., 2003; Trigo, 2008; Woollings et al., 2014). Moreover, there is evidence that the relationship between the NAO and precipitation is strengthening over most of Europe (López-Moreno and Vicente-Serrano, 2008).

The cyclones' variability over time and space is described in terms of frequency, based on the storm track density (Ulbrich et al., 2009; Liberato et al., 2011). The cyclones' intensity variability is less straightforward to assess, mainly because it requires a consensus on the definition of intensity. Usually, the instant of maximum intensity is considered as the one with minimum MSLP at the core of the cyclone (Neu et al., 2013) and thus strong cyclones are those with min (MSLP)<980hPa. However, a more informative variable is the deepening rate of the MSLP, which allows evaluating the maximum pressure drop, used as a criterion to distinguish between explosive (drop ≥ 24hPa/24h relative to 60° of latitude) and non-explosive cyclones (Sanders and Gyakum, 1980).

Despite being different from each other's, cyclones might share certain characteristics, and this is the basis of several classification studies. For example, Karremann et al. (2016) grouped windstorms according to the location of the storm tracks, Reale et al. (2019) provided for separated climatology for explosive and non-explosive cyclones and Eiras-Barca et al. (2018b) distinguished between (explosive) cyclones that are attended by ARs and those who are not. They showed that the western sectors of the ocean, especially in the NA Ocean, are more prone to faster and deeper explosive cyclogenesis, due to stronger SST gradients and air-sea interactions. Ranking studies of extreme events are less frequent than classification studies, they mainly address the impacts and only in a second step ranked events are characterized in terms of synoptic characteristics or temporally/spatially compounding weather phenomena. For example, daily (Ramos et al., 2015) and multi-daily (Ramos et al., 2017) precipitation events rankings are produced for the IP, based on both the local intensity and the spatial extent of the

rainfall and they found that ARs mostly concur to the top-ranked events. The role of moisture advection, through upper air troughs, in enhancing the magnitude of extraordinary rainfall events is established also for the top-ranked daily and sub-daily precipitation events for northwestern Italy (Pinto et al., 2013). Rankings of extreme events at longer timescales are also possible, such as for the dataset of rankings of the most extreme, prolonged, widespread dry and wet periods in the IP for aggregated timescales of 6 to 24 months presented in Liberato et al. (2021), based on drought indices time-series.

The Iberian Peninsula is an interesting domain to explore the effect of such variability on the daily weather as it is a recognized hot spot for climate change and climate extremes at the regional scale (e.g., Giorgi, 2006; Gomez-Navarro et al. 2010; Jerez et al. 2013; Cardoso Pereira, 2020). The location of the IP in a transitional area between the midlatitudes and the subtropics leads to a remarkable diversity of regional climatic conditions, mainly dependent on precipitation variability. The annual variability of rainfall regimes over the IP is heterogeneous: the total annual precipitation ranges from more than 3000mm/year over the mountain chains to the northwest to locally less than 200mm/year to the southeast, one of the lowest values of all Europe (Acero et al., 2018). Most of the inner continental lands receive less than 500mm/year, except for the highest mountain ranges. Extremes also affect southern Iberia where most of the total annual precipitation comes from a few intense stormy events.

Wind regimes are also extremely diverse across the IP. Lorente-Plazas et al. (2015) analyzed the annual cycle of wind speed on the IP showing interesting results in terms of both wind variability and wind extremes. Their results suggest that wind speed regimes and extremes are controlled by extratropical cyclones variability. For example, they showed that northerly wind dominates along the Atlantic coast, whereas westerly and northwesterly wind dominates almost elsewhere. Moreover, they showed that wind speed maxima in the North of Iberia (including North of Portugal) occur in winter when cyclones' frequency is also at its maximum. Conversely, eastern Iberia shows different behavior, as it is mainly characterized by a land-sea pattern driven by sea-breeze regimes and enhanced by coastal mountains. Indeed, the Mediterranean coast clearly shows a bimodal cycle in wind intensity, influenced by both sea-breeze and cut-off lows events. At the IP regional scale, it was shown that the ratio between extreme wind and the mean wind speed is particularly high, mostly in winter, with respect to other European regions (Laurila et al., 2021). Eventually, this indicates the predominant role of extratropical cyclones in shaping wind extremes in the region.

Vicente-Serrano et al. (2017) provided for a comprehensive review of published studies on the last decades' trend of several atmospheric variables on the IP among which is worth mentioning an expected increase in mean temperature (+0.3°/decade), a decrease of annual precipitation (-18.7mm/decade) and a seasonal dependent trend signal for wind, characterized by a decrease (increase) in observed daily peak wind gusts in winter (summer) semester (Azorin-Molina et al., 2014; Laurila et al., 2021). Moreover, several studies pointed towards a lengthening of the dry summer season over the region in the post-1979 period (Peña-Ortiz et al., 2015; Guerriero et al., 2016), which is going to be characterized by longer and more frequent heatwaves (DellaMarta et al., 2007; Pereira et al., 2017). These tendencies eventually concur with an increase in drought and fire risks (Coll et al., 2017; Russo et al., 2017).

However, despite the general decrease of annual precipitation observed and expected for the IP, it is still unclear how this reflects on extreme precipitation events (and associated cyclones). Theoretically, a warmer climate promotes an ever-increasing uneven distribution of precipitation, with less but more intense rainy and stormy days. This happens because of increased moisture availability, increased latent heat release from the sea body and the energy balance constraint (e.g., Trenberth, 2011; Pendergrass and Knutti, 2018; Santos et al., 2019). In practice, results vary widely depending on the data sets, the time period and the methodology considered to quantify extremes in each study. Several authors agree on a generalized increase (decrease) of extreme precipitation events in autumn (spring) (e.g., Espirito-Santo et al., 2014; Serrano-Notivoli et al., 2018; Pereira et al., 2020). Regional differences are also noteworthy: in northwestern Iberia, wintertime extreme precipitation is more likely associated with extratropical cyclones and therefore its variability is influenced by cyclones' climatology and by the larger-scale dynamics such as for the occurrence of ARs (e.g., Santos and Fragoso, 2013; Ramos et al., 2015; Sousa et al., 2016). In this regard, Gallego et al. (2011) found that the contribution of extreme precipitation days to total precipitation increased during the 20th century, although it mainly increased in the first half whereas it decreased later. However, this is explained by the prevalent positive phase of NAO over the last decades which is known to be correlated with less precipitation on the whole European Sector. The role of teleconnection patterns in modulating extreme precipitation events is well documented also for southeastern Iberia. Precipitation extremes in this region are more likely linked either to the frequency of cut-off lows (Nieto-Ferreira, 2021) or to the Mediterranean influence in terms of moisture availability (Halifa-Marin et al., 2021).

1.3 Extratropical cyclones mechanisms and impacts

Most of the variability and uncertainty discussed in the previous section, regarding the IP, ensue from extratropical cyclones (ETCs) and their mechanisms. These cyclones typically originate over the midlatitudes oceans, sometimes in the wake of weakened tropical cyclones. The northern and northwestern sectors of Iberia are typically more exposed to the impacts of these storms, but it is also possible that such storms end up affecting the entire peninsula (Trigo, 2008). When the jet stream is displaced to the south, it favors cyclogenesis to occur right in the middle of the NA Ocean and the storms are dragged towards Europe at unusual low latitudes, for example, as occurred for the Klaus storm in 2009 (Liberato et al., 2011). Such events undergo explosive development and produce extreme impacts once they make landfall. Over the last decade, other well-studied European cyclones besides Klaus were Kyrill (Fink et al., 2009), Xola (Pinto and Belo-Pereira, 2010), Xynthia (Liberato et al., 2013), Gong (Liberato, 2014) and Stephanie (Ferreira et al., 2016) and, more recently, the storm Miguel (Coll-Hidalgo, 2021) as well as entire families of consecutive cyclones (Sefton et al., 2021; Stojanovic et al., 2021). From the climatological point of view, the passage of these systems has been associated with high fractions of total accumulated precipitation over the IP (up to 90 % according to Catto et al., 2012) as well as extreme precipitation (Catto and Pfahl, 2013) and extreme wind (Nissen et al., 2010).

The ETCs variability on the North Atlantic and European Sector is tightly bound to the dynamics of the zonal flow between 50°N and 60° N, represented by the eddy-driven polar jet stream at high altitudes, and reflected in the prevailing westerly wind at the surface. Cyclones form as wavelike disturbances of the polar jet, through which warm air is pushed northward and colder air slips southward, spinning around the low-pressure center. Therefore, a leading warm front and a trailing cold front follow through the cyclone until the occluded phase is reached as the cyclone deepens. A vertical wind shear develops as the cold air mass easily spreads at the surface, forcing the warm sector to lift.

Both upper-level and lower-level forcing have been suggested as potential mechanisms for weak polar jet disturbances (e.g., Uccellini, 1990; Hewson and Neu., 2015; Graf et al., 2017). For example, a local dip of the tropopause, which is associated with a Potential Vorticity (PV) anomaly, modifies the thermal field at the lower levels thereby inducing a cyclonic circulation. The same can happen when a warm air advection at the surface or an enhanced local heat release, as it occurs over the water bodies, produces a local convergence (divergence) of air

flows at lower (higher) levels. Most of the cyclones form and develop due to a combined action of the two mechanisms and a measure of their relative incidence has been suggested (Deveson et al., 2002). Therefore, it is the meandering of the jet stream that determines the sequence of troughs and ridges, the cyclogenesis and the associated storms tracks (Pinto et al., 2009; Athanasiadis et al., 2010; Hanley and Caballero, 2012). A sustained zonally extended jet is also a precondition for successive secondary cyclogenesis, referred to as cyclone clustering, in the exit region of the storm track (Priestley et al., 2020).

Through observations and numerical simulation, several authors (e.g., Uccellini, 1990; Schultz and Zhang, 2007; Davies, 2010) suggest that the essential pre-condition for cyclogenesis is the presence of an upper-level forcing enhanced by baroclinic instability rather than a fracture in a front-like structure. As a matter of fact, cyclones might form without a pre-existing front, as for cyclogenesis on the leeward side of a mountain chain, which is typical of the Mediterranean basin. Therefore, the extent cyclones and fronts attend to each other is still under debate (Schemm et al., 2018). For the Northern Hemisphere (NH), it is found that at the time of maximum intensification the majority of all cyclones do have associated fronts and by the time of cyclosis around half of all cyclones do maintain associated fronts, even those cyclones that only acquired a front at a later stage. It can be assumed that fronts are potential proxies for cyclones' activity (Berry et al., 2011b).

However, both fronts and cyclones are not constituent elements of the atmosphere but rather are transient features. Therefore, any statistics regarding their frequency ultimately depend on the criteria established for their detection. For several decades, manual tracking of fronts and cyclones on synoptic charts was accepted as a standard procedure, although it was affected by a high degree of subjectivity and personal biases. The satellite era and the availability of global reanalysis data sets favor the development of objective and automated routines. Nowadays, there is not yet a consensus on a specific methodology, and several schemes have been tested instead for both cyclones (e.g., Raible et al., 2008; Ulbrich et al., 2009; Neu et al., 2013) and fronts (Thomas and Schultz, 2019 for a comprehensive review).

This variety of approaches reflects the different points of view assumed by each author on what a front is. To remove such a degree of subjectivity, a wealth of recent studies explores the use of machine learning techniques and crowd-trained routines. They are applied to reanalysis data sets as well as to process satellite images, with the common objective to automatically identify, label and track the different phases and local features of cyclones evolution, exactly as a meteorologist would do (Fig.1.1).

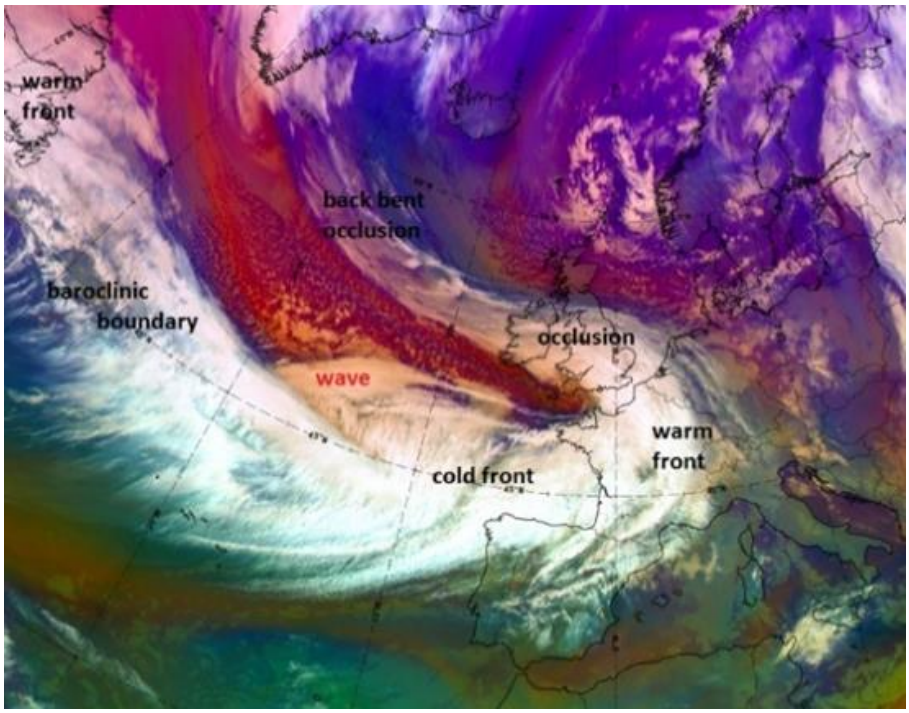

Figure 1.1 Satellite image of Windstorm Ana, 10 Dec 2017 06 UTC. [https://www.eumetsat.int/]

Over the last decades increasing attention was devoted to the mechanisms of moisture transport in the lower atmosphere and the role it plays in enhancing the precipitation embedded in cyclonic systems. For example, a Lagrangian approach applied to air particles in the region of the cyclone showed that the transport of moisture from tropical latitudes was responsible for the heaviest precipitation event of the twentieth century in Lisbon, the 18-19 Nov 1983 event (Liberato et al., 2012). Other studies confirmed that several flooding events in Western Europe are related to such a feature (e.g., Lavers et al., 2011; Trigo et al., 2014; Ferreira et al., 2016), referred to as Atmospheric Rivers (ARs). Climatological and comprehensive studies confirmed that ARs do contribute to extreme precipitation, especially for the most extreme events (e.g., Ramos et al., 2015; Ramos et al., 2016a; Eiras-Barca et al., 2018b). ARs are detected as Integrated Vapor Transport (IVT) departures from climatology over a large band behind the cyclone Moreover, the occurrence of ARs is associated with strong anomalies in the MSLP field at the midlatitudes (Fig. 1.2).

In addition to the synoptic-scale features of the jet stream and ARs, ETCs are typically described through airflow analysis at lower levels (Hewson and Neu, 2015). These features (called jets) represent the mechanisms through which a storm is sustained, and they are associated with well-defined signatures in the weather fields, as for the atmospheric fronts (Hewson and Neu, 2015). Going deeper into this topic is not the main purpose of the thesis.

However, it is important to mention that airflows are linked to specific clouds, precipitation and wind patterns and they are key aspects to describe the dynamic of the storm. As an example, warm airflows are responsible for the moderate-to-heavy stratiform precipitation band along the cold front, whereas it is in the cold airflow that most of the strongest showers occur, including embedded convection cells (Houze, 2004).

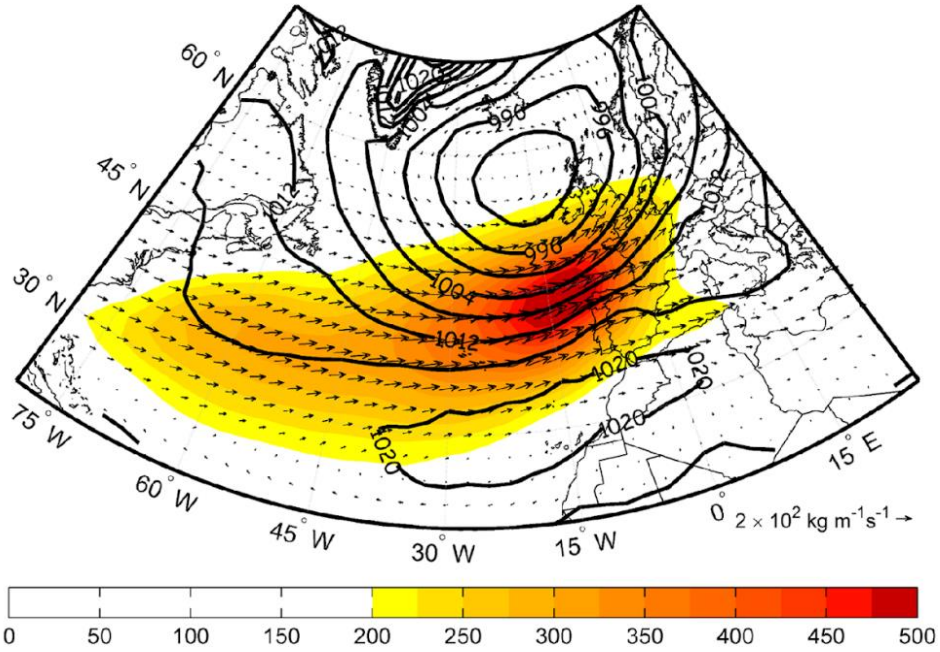

Figure 1.2. (Mean composites of IVT direction (vectors) and intensity (kg m^{-1} s^{-1}; color shading) and SLP (hPa; contours) fields during the occurrence of the persistent ARs that affect the IP (679 persistent cases corresponding to 3837 timesteps). [Ramos et al., 2015]

In the Numerical Weather Prediction (NWP) models, the spatio-temporal structure of clouds and precipitation within ETCs has been the core topic of several studies (e.g., Field and Wood, 2007; Catto et al., 2010; Govekar et al., 2014). Not only cloud and precipitation but roughly all the mechanisms described in the previous paragraphs have been studied and characterized directly on real case studies simulations.

Extreme weather impacts are often addressed independently of each other, and they are linked to a specific economic sector loss. For example, hail events have been linked to economic losses in agriculture (Changnon et al., 2009; Punge and Kuntz, 2016) as well as to buildings (Hirsch et al., 2013) and, more generally, to the insurance sector (Brown et al., 2015; Púčik et al., 2019). Similarly, droughts events have been also studied in terms of induced crop losses (Musolino et al., 2018; Ribeiro et al., 2019) but also by quantifying their effects on the water supply chain (Rossi and Cancelliere, 2013) and livestock (Salmoral et al., 2020). The

energy sector is highly affected by extreme weather: for example, hailstorms damage photovoltaic plants (Muehleisen et al., 2018) but also the effects of wind (precipitation) extremes on the wind (hydro)-power generation is widely studied (e.g., Andrade et al., 2011; Santos et al., 2015; Gonçalves et al., 2020).

The meteorological impacts of ETCs are mainly due to precipitation and wind extremes. Localized extreme precipitation rain rates typically lead to local flooding whose effects might be enhanced by urbanization. This is the case of urban flash floods, which are frequent in the Mediterranean basin (Gaume et al., 2016; Faccini et al., 2018) and in Iberia as for the Lisbon metropolitan area case study (Leal et al., 2018; Trigo et al., 2016). On the other hand, sparse prolonged moderate to high rain rates over longer time periods (days to weeks) more likely produce extended river flooding and landslides over larger areas (e.g., Vicente-Serrano et al., 2011; Rebelo et al., 2018; Pereira et al., 2018). As already mentioned, the continuous moisture supply through ARs does play a role in the maintenance of rainy and stormy conditions and for this very reason, ARs start to be considered as proxies for such events (Ramos et al., 2020). Extreme precipitation develops in convective environments, along with lightning, hailstorms and strong gusty winds that provoke falling trees and power outages (e.g., Gardiner et al., 2010; Dowdy and Catto, 2017; Tervo et al., 2021). Damaging winds within cyclones are often related to an abrupt descent of upper-level airflow (downbursts). Enhanced downbursts develop within squall lines, and they provoke a clear damage swath, as it occurred during the Vaia storm that affected northeastern Italy in October 2018 with unprecedented severity, leading to the disruption of millennial forests on the flanks of several Alpine valleys (Vaglio Laurin et al., 2021). The event has been widely studied also because of the potential role played by an AR, exceptionally located in the Mediterranean basin (Davolio et al., 2020). Downbursts are recognizable as arc-shaped signals in radar reflectivity maps (bow-echo: Wakimoto et al., 2006; Mathias et al., 2017). Typically, the most affected infrastructure by wind is the electric power supply network as it might take days to restore its functionality (e.g., storm Xola - Pinto and Belo-Pereira, 2020; storm Tilo - Kettle, 2019). However, not only gusty wind but also persistent intense wind is associated with disruptive impacts. Over longer timescales, intense winds might affect the landscape and the ecosystems through coastal erosion and modification, land degradation and vegetation stress (Otero et al., 2013: Borrelli et al., 2014). Wind extremes are typically used as a proxy in storm loss models used by insurance companies (e.g., Klawa and Ulbrich, 2003; Pinto et al., 2009; Donat et al., 2011). Donat et al, (2011) performed multi-model simulations with global and regional climate models to assess and project wind loss

potential in Europe. They found that the mean loss ratio will increase in the Western and Central European regions whereas a slight decrease is expected for Iberia, consistently with extratropical cyclones' track changes.

Besides direct impacts, the concurrent effect of several meteorological extremes can lead to indirect impacts or to cascading/concurrent impacts. In recent years, the compound weather extremes perspective also embraced the extreme impacts analysis. That is, more and more studies cover wide ranges of interconnected impacts rather than a single impact: for example, this holds for droughts, heat waves and fires and their combined effects on vegetation stress and food security as for the Russian 2010 episode (Hunt et al., 2021). Situations of greater interest for this work are those of compounding precipitation and wind occurring within cyclones, and leading to storm surges, coastal flooding, landslides and compromised infrastructures, among the others (e.g., Zscheischler et al., 2018; Bevaqua et al., 2019; Khanam et al., 2021). Still, ETCs are the primary cause of most of the economic and societal weather impacts in the IP. In this regard, the DISASTER database provides the most complete data collection on flood and landslides events that occurred in Portugal since 1865 (Zêzere et al., 2014; Pereira et al., 2018). It was observed that more than 2/3 of the events in Central and Northern Portugal are associated with a cyclonic activity over Portugal or under the influence of the frontal system activity. The authors also searched for the frequency of ARs on the disaster days (45%) and the role of precipitation as a triggering factor for the disaster, finding that almost all the events are associated with extreme accumulated rainfall percentiles. The results of this study confirm that the impacts of cyclones might affect a wide area, wider than the punctual storm track. In a warmer climate, the swath damage of both extreme precipitation and extreme wind associated with extratropical cyclones is expected to widen because of the increasing intensity of the storms and this poses new challenges for impact studies (Phibbs and Toumi 2016; Sinclair et al., 2020). There is a lot of uncertainty in future extratropical cyclones trend except for two aspects: (1) there is medium confidence that serial clustering of storms will increase in most of Europe, in the wake of the poleward shift of storm tracks and (2) a slight increase in amplitude and frequency of storms is expected for Northern and Central Europe (IPCC, 2021).

The impact-centric perspective is gaining more and more attention over the years for both extreme precipitation and wind (e.g., Leal et al., 2019; Koks and Haer, 2020), especially in the context of compound events (Zscheischler et al., 2018). This is happening because of (1) increasing awareness of the interdependence and compounding effects of meteorological

extremes and impacts, (2) increasing adverse impacts affecting the life and goods of people and (3) because similar approaches are welcomed by stakeholders. The degree of a meteorological impact varies depending upon many factors, depending in the first place on the severity of the events itself, the timing and location. However, the meteorological hazard is only one of the players when referring to impacts and risks. According to the conceptual framework developed by the IPCC for risk assessment, the risk associated with a climate or weather extreme is defined as a measure of the probability of the occurrence of a hazard and its consequences (impacts), where the consequences come from the interplay of natural, societal and economic exposure and vulnerability, as depicted in Fig. 1.3 (IPCC, 2012). Fighting against disaster risks includes acting on both sides, that is mitigating climate changes to reduce the hazard and promoting adaptation and resilience measures.

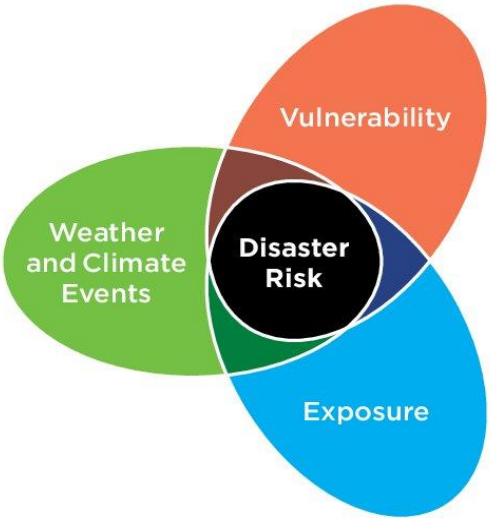

Figure 1.3 Schematic overview of the components included in risk analysis (hazard, exposure and vulnerability). [IPCC, 2012]

As a matter of fact, human-induced climate change has already affected the frequency and intensity of extreme events (e.g., the last annual report from the Bulletin of the American Meteorological Society - Herring et al., 2021). Heavy precipitation events increased systematically over most of the land regions worldwide whereas changes in winds extremes are strongly tied to the future changes of storms, including tropical and extratropical cyclones (Fischer and Knutti, 2016; Outten and Sobolowski, 2021). As global warming continues, we will likely experience unprecedented extreme events, in terms of frequency, magnitude, timing and location. Moreover, the combined occurrence of multiple unprecedented extremes may result in large and unprecedented extreme impacts in the future, inducing major socio-economic losses. Such increasing knowledge on climate change risks and weather hazard

changes enables institutions and stakeholders acting towards more resilient systems, to mitigate the adverse impacts of extremes on lives, goods and nature (IPCC, 2021; Bouwer, 2019).

Within this thesis, the hazard component of the scheme presented in Fig. 1.3 is addressed. However, differently from the traditional approaches which mainly consider each hazard independently from the others, several features of extratropical cyclones and their related impacts are combined together, to disentangle their intrinsic mutual relationships, also through the identification of the individual processes involved. Therefore, the work focused on precipitation and wind extremes first, and traces back to the drivers and to the potential compounded occurrence of these drivers. Still, precipitation and wind extremes are directly relatable to impacts. As mentioned at the beginning of this Introduction, this approach implies that objective criteria to identify the individual extremes are set (as in Chapter 2 for precipitation and Chapter 3 for wind speed). Then, also the compounded occurrence of extremes needs to be defined, in time and space (as for concurrent precipitation and wind, Chapter 3). Finally, extremes are put into a relationship with the underlying weather features (Chapter 3 and Chapter 4).

1.4 Objective and structure of the thesis

The ever-increasing concern about weather-driven natural hazards is the leading motivation for this research. In broad terms, the characterization of high-impact weather events such as extratropical cyclones (ETCs) and related precipitation and wind extremes affecting the IP is the main objective. More in detail, this thesis aims at describing and providing new insights on the relationship between North Atlantic storms, precipitation and wind extremes, including the potential co-occurrence of different weather features, both at local and at the large-scale, which produce multiple hazards.

The current thesis is presented in the form of a paper-based manuscript that is, each of the main chapters consists of a research paper published (chapters 2 to 4). Therefore, all chapters are intended to be independent, and they follow the typical structure of a research paper, from Introduction to Conclusion through Data, Methods, Results and Discussion. For the sake of clarity, the first page of each chapter includes some highlights. In this regard, the author acknowledges potential repetitions, mainly affecting background information and data sources which, to a certain extent, are shared among the research topics considered.

More into detail, this manuscript is organized as follows:

- Chapter 1 presented the state-of-the-art of research themes that have been tackled during the Ph.D. After a wide introduction of the most common approaches to the study of extreme weather events (Section 1.1), more insights are provided on precipitation, wind and cyclones variability, focusing on Iberia (Section 1.2). In Section 1.3 the main mechanisms related to cyclones activity over the North Atlantic and European Sector are discussed. This includes a short description of the potential research and methodological approaches for their characterization. Local-scale impacts associated with ETCs are commented in Section 1.3.

- Chapter 2 includes research on the performances of different types of daily precipitation estimates (namely, reanalysis and satellite-based) toward a benchmark ground-based gridded data set for IP (IB02). This work yields a better knowledge of the most common data sources available for investigating precipitation extremes and related impacts and thus it represents a reference for any future study focusing on the IP (Hénin et al., 2018a).

  The main research questions addressed here are:

  - Are the most widely used precipitation data sets adequate to represent extreme precipitation events on the IP?
  - Does ERA5 bring added value in reproducing extreme precipitation on the IP, especially if compared with the previous ERA-Interim release?
  - Which are the main error sources that affect precipitation data sets on the IP?

- Chapter 3 aims to produce a unified ranking for precipitation and wind extreme events over the IP along with an analysis of the corresponding cyclones' properties. As for the previous chapter, this research will serve as a reference for future research on the IP (Hénin et al., 2021). The main research questions addressed here are:

  - How often do concurrent extreme precipitation and wind events affect the IP?
  - Which are the cyclones' properties associated with such events?
  - Is there any regional variability or trend?

- In Chapter 4 a systematic analysis of the co-occurrence of precipitation and atmospheric fronts is pursued, for the Euro-Atlantic and European domain (Hénin et al., 2018b). This chapter broadens the view to the synoptic scale and provides for a methodology, based on a search box approach, to objectively evaluate the fraction of precipitation that can be ascribed to the presence of atmospheric fronts. The algorithm is applied to the North Atlantic domain both systematically and to a case study and it is, to a certain extent, tunable so that it can be adapted to other geographical domains, as well as it can serve as a base for other similar studies. The main research questions addressed here are:
    - Is there a method to assess the amount of precipitation relatable to atmospheric fronts systematically and objectively?
    - Which fraction of total precipitation is associated with fronts? Are there seasonal differences and/or trends?

- Finally, Chapter 5 provides for a comprehensive review of the conclusions presented in each paper, providing consistent and robust answers to the research questions raised in the introduction and further callings for potential new research goals and future perspectives.

It is worth mentioning that the research presented in this thesis is relevant in the context of two research projects, both with international partnerships, funded by the Portuguese Foundation for Science and Technology (FCT) during years 2017 to date, namely:

- Expert Crowdsourcing for Semantic Annotation of Atmospheric Phenomena (eCSAAP) headed by the Institute for Systems and Computer Engineering, Technology and Science (INESC TEC - Porto, Portugal) in collaboration with Instituto Dom Luiz (IDL – Lisbon, Portugal) and the Carnegie Mellon University (CMU – Pennsylvania, USA). The project aimed at exploring the potential of crowdsourcing for atmospheric and climate research tasks such as identifying and tracking extratropical cyclones. The core idea is that human-based semantic annotation of weather features can be integrated with automatic methods in a future hybrid approach. A key component of this process is the development of algorithms for objective detection and association of weather features in gridded data sets, as is shown for precipitation and atmospheric fronts in Chapter 4.

- Weather extremes in the Euro-Atlantic region: assessment and impacts (Wex-Atlantic). The project addresses hydrometeorological and wind extremes in the North Atlantic and European Sectors, related to the occurrence of extratropical cyclones. The projects aimed at characterizing weather extremes, the underlying physical mechanisms such as moisture transport and frontal systems, their variability and expected changes under global warming, as well as their impacts. Further research tasks relate to the capability of current GCMs to reproduce such extreme events and to the major changes to be expected in climate-change scenarios. This thesis mainly addressed the first aspects. Chapter 2 shares fundamental information in this sense, about which data set to use to characterize precipitation extremes. The ranking developed in Chapter 3 provides novel information on the variability of hydrometeorological extremes on the IP. Chapter 4 includes novel and updated information on the seasonal climatology and historical trend of frontal precipitation on the Euro-Atlantic and European sectors.

2

Precipitation data sets and extreme events on the IP

This chapter is based on a manuscript that is an original contribution of this thesis published in Water, in 2018, under the title *"Assessing the Use of Satellite-Based Estimates and High-Resolution Precipitation Datasets for the Study of Extreme Precipitation Events over the Iberian Peninsula"*, with the DOI: 10.3390/w10111688.

The research included in this chapter was supported by the project eCSAAP (CMU/CS/0012/2017) and by Instituto Dom Luiz (IDL, UID/GEO/50019/2013), funded by Fundação para a Ciência e a Tecnologia, Portugal (FCT) and Portugal Horizon2020. Riccardo Hénin was supported by an FCT doctoral grant (PD/BD/114479/2016) and Alexandre M. Ramos was supported by an FCT postdoctoral grant (FCT/DFRH/SFRH/BPD/84328/2012).

Graphical Abstract

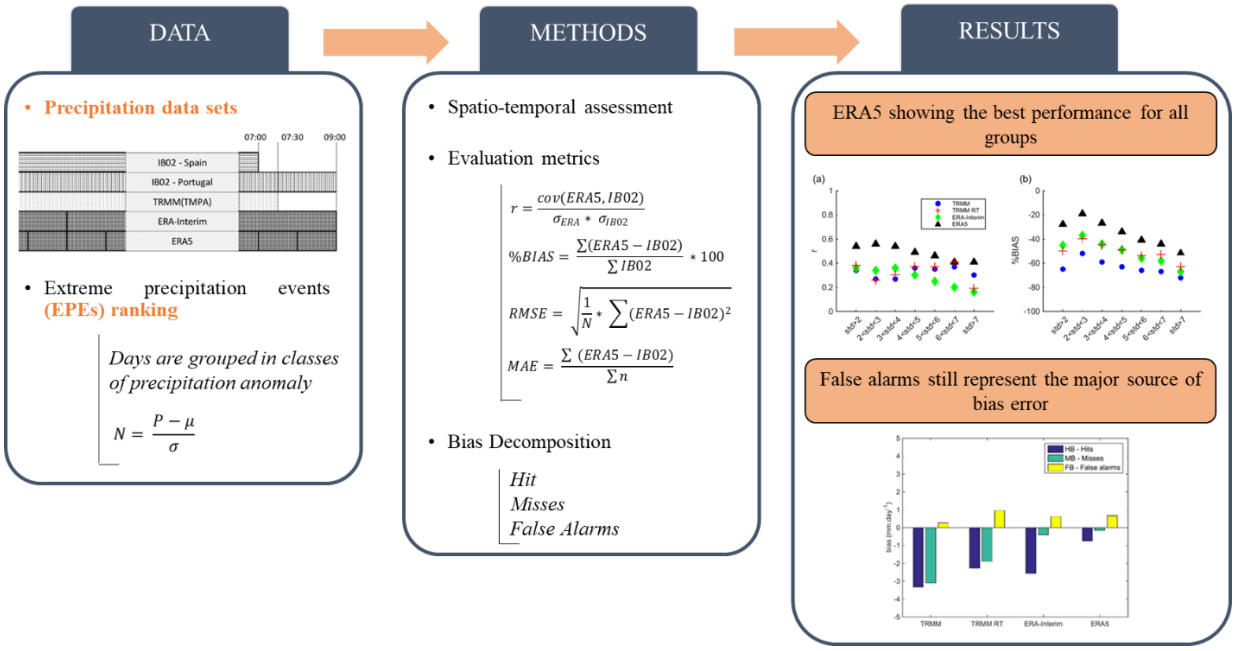

Highlights

- Context and motivation

Extreme precipitation is hard to measure because of its uneven nature. Precipitation estimates from reanalysis products and satellite missions are widely used in weather and climate studies nowadays, besides a wealth of well-known shortcomings. An assessment of daily precipitation sums from different sources is presented for the Iberian Peninsula (IP) on annual and seasonal scales, eventually focusing on a subset of extreme precipitation events (EPEs).

- Data (common period considered: 2000-2008)

- IB02 (Belo-Pereira et al., 2011; Herrera et al., 2012)
- ECMWF reanalysis (both ERA-Interim and ERA5)
- TRMM TMPA 3B42 near-real-time and post-real-time releases
- Ranking of Extreme Precipitation Events (EPEs) for the IP (Ramos et al., 2014a)

- Methods

A set of accuracy metrics, namely the Pearson linear correlation coefficient (*r*), the percentage bias (%BIAS), the Root Mean Square Error (RMSE), and the Mean Absolute Error, (MAE) are analyzed for different quartiles of daily precipitation amounts. Additional insights are provided for the top-ranked EPEs on the IP. Bias decomposition into Hit Bias (HB), Missed Bias (MB) and False Bias (FB) is also explored.

- Results

Results show that both reanalysis and multi-satellite data sets overestimate (underestimate) daily precipitation sums for the least (most) extreme events over the IP. Contrary to some literature, it is shown that the TRMM (TMPA) precipitation estimates from the near-real-time product can be considered for EPEs assessment over these latitudes. Finally, it is found that the more recent ERA5 reanalysis accounts for large improvements over ERA-Interim and it outperforms also the satellite-based data sets. HB is the prevailing component of the total bias.

Keywords: TRMM (TMPA) dataset; real-time satellite retrievals; extreme precipitation; extreme precipitation events (EPEs); Iberian Peninsula; ERA5.

2.1 Introduction

Extreme precipitation events (EPEs) are responsible for a relevant number of natural disasters worldwide, including landslides, flash-floods, and material destruction. The socio-economic impacts associated with EPEs, namely human casualties and rebuilding costs, have become of great interest for both decision-makers and insurance companies (Swiss Re, 2008; Pitt, 2008). As a matter of fact, precipitation extremes affect the water cycle as a whole, with several implications also for hydrology and water reservoir management (Jiang et al., 2017).

Over the Iberian Peninsula (IP) an objective ranking of EPEs has been provided at daily (Ramos et al., 2014a) and multi-day scales (Ramos et al., 2017) for the extended wintertime season (October to March), based on the high-resolution (0.2° × 0.2°) ground-based precipitation dataset IB02 (further details are provided in Section 2.2). Some significant EPEs which occurred in the past have been examined both in terms of mechanisms and related impacts (Liberato 2013; Trigo et al., 2016; Trigo et al., 2014; Rebelo et al., 2018; Nieto et al., 2007). Given the high temporal and spatial variability of the IP climatology (Ramos et al., 2014b; Lionello, 2012), some studies also focus on sub-regions of the IP that are affected by specific weather regimes (Nieto Ferreira, 2017; Hidalgo-Muñoz et al., 2011; Liberato and Trigo, 2014). The precipitation enhancement over the IP includes different mechanisms, mostly convection to the south (Serrano et al., 1999; Paredes et al., 2006), synoptic forcing and water vapor transport to the west and to the north (Ramos et al., 2015; Lavers and Villarini, 2015; Hénin et al., 2018a), and orographic effects (Khodayar et al., 2018). Depending on the season, different precipitation regimes have been observed over the IP: for some regions, most of the annual precipitation is observed during the winter months, whereas summer can be totally dry (Martín-Vide and Gomez, 1999; de Luis et al., 2010). The annual cycle of precipitation captured by the IB02 and other global precipitation data sets (including ERA-Interim) is described in Belo-Pereira et al. (2011).

The spatial and temporal variability of accumulated extreme precipitation typically shows local maxima that can be detected only using high-resolution gridded products or data from traditional weather stations. A ground-based network is able to map the precipitation pattern only at a coarse scale, especially over complex topography and over the oceans, where the coverage provided by rain-gauges and weather buoys is inhomogeneous. However, accurate estimates of rainfall are essential for the risk assessment of any water-related natural hazards. In this sense, reanalysis data sets and satellite-based measurements are highly beneficial as they

fill the observational gaps and they guarantee continuous spatial and temporal data coverage, even if the extreme precipitation days are not modeled very accurately (Rhodes et al., 2015). Since the early modern satellite era, several missions have been operating, but intrinsic limitations of the specific onboard sensor technology as well as propagation and atmospheric attenuation effects still limit the quality of the data (Levizzani et al., 2007; DeMoss et al., 2007). Increasing the spatial resolution of a single sensor always implies higher uncertainties for the final product but thanks to new algorithms that combine data from different sources, high resolution and high-quality products are being made available (e.g., Huffman and Bolvin, 2015; Adler et al., 2003; Behrangi et al., 2009; Joyce et al., 2004). The latest advances of the most recent multi-satellite missions include coincident measurements from both active and passive onboard sensors with cross-calibration techniques and additional post-processing routines. The Tropical Rainfall Measuring Mission (TRMM) (Huffman et al., 2009), headed by the National Aeronautics and Space Administration (NASA) and the Japanese Aerospace Exploration Agency (JAXA), provides data from November 1997 and releases different precipitation products (both in near-real-time and post-real-time) widely used for monitoring, modeling, and research, also beyond the tropics. The TRMM has been recently incorporated into the wider Global Precipitation Measurement Mission (GPM) and its products serve as a reference for the new generation of GPM precipitation retrievals (Skofronick-Jackson, 2017; Huffman, 2018). The main goal is to promote advances in the quality of satellite estimates beyond tropical latitudes, for them to be beneficial for the study of extratropical cyclones and related precipitation.

Although EPEs are quite common over the IP, it is not ascertained yet which product, either reanalysis or satellite estimates, is the most appropriate for studying extreme precipitation days. An inter-comparison of different reanalysis data sets to ground truth is pursued in Belo-Pereira et al. (2011), showing that there is a seasonal cycle of the ERA-Interim performance over the IP, with the best scores attained in winter. On the contrary, satellite products such as the ones provided by the TRMM have been barely studied at the extratropical latitudes, and their potentiality has not yet been fully assessed over the IP. In a study by Liu and Zipser (2014) the need for such an analysis, to be conducted for in-depth case studies and under different precipitation regimes is stressed. The present work is intended as a follow-up to Liberato et al. (2017) where a preliminary assessment of four EPEs that occurred over IP has been carried out using both ERA-Interim and TRMM data. It aims at assessing which high-resolution precipitation data sets provides for the most reliable estimates during heavy rain

episodes over the IP, thus being beneficial for any future investigation of EPEs over the region. Additional data sources with respect to Liberato et al. (2017) are considered, namely ERA5 and the near-real-time product of TRMM mission. Given the increasing interest in multi-satellite products, this analysis will also serve as an extensive test for TRMM precipitation estimates over the midlatitudes, which are beyond the optimal operational band of the onboard instruments used for retrieval. Finally, new insights are provided through the intra-products comparison, at the regional scale, between the near-real-time and the post-real-time TRMM products during EPEs over the IP.

The paper is organized into four sections. After the introduction, the different data sets used are described in Section 2.2, namely the reanalysis and satellite data for precipitation (Section 2.2.1 to 2.2.3) and the dataset for extreme precipitation events over the IP (Section 2.2.4). Section 2.2.5 explains how data from different sources are manipulated to be effectively combined in time and space and how the assessment is conducted. Results are presented and discussed in Section 2.3, firstly focusing on the assessment of precipitation all over the common period (Sections 2.3.1 and 2.3.2), and secondly focusing only on a specific subset of EPEs which occurred during the extended wintertime season (Section 2.3.3). Finally, conclusions are drawn in Section 2.4.

2.2 Data and Methods

2.2.1 Ground-based precipitation dataset IB02

In the present study, different data sources are considered for precipitation estimates. At first, the most comprehensive gridded, high-resolution (0.2° × 0.2°) available database of daily precipitation for the IP is used as ground truth (IB02 hereafter). It is produced by joining two individual national data sets from Portugal (PT02) and Spain (SP02), respectively (Belo-Pereira et al., 2011, Herrera et al., 2012). Both data sets refer to the same 0.2° × 0.2° latitude/longitude grid, obtained by interpolation of rain gauge data through an ordinary kriging method and an additional inverse distance weighting method (IDW) for the Portuguese dataset only. Albeit with some inevitable temporal variations in the rain gauges density, both the Spanish and Portuguese networks cover the period from 1950 to 2008. Totally, more than 2400 weather stations provided data for IB02. Several quality control procedures have been applied to the data, such as a plausible value check, internal consistency checks, and a standard normal

homogeneity check (the authors refer to Belo-Pereira et al. (2011) for more details and references on these procedures as well as for network coverage).

In IB02 precipitation records are summed to provide for daily values, but the accumulation period is slightly different for Spain and Portugal. Given a day n, daily precipitation over Portugal is accumulated between 09:00 UTC of day n − 1 and 09:00 UTC of day n. On the contrary, daily precipitation over Spain ranges from 07:00 UTC of day n to 07:00 UTC of day n + 1. For consistency, the Portuguese dataset is shifted one day forward in IB02. It is believed that, unless an event strictly peaks during the time lag, the defined accumulation period is robust and no artificial features are found at the border between the two countries. Other studies made use of precipitation data from IB02 for real case study analysis (e.g., Rebelo et al., 2018; Liberato et al., 2017) and for more extensive assessments (e.g., Sousa et al., 2016; Durán and Barstad 2018; Guerreiro et al., 2016).

2.2.2 Reanalysis dataset

Precipitation estimates from the widely used ERA-Interim reanalysis product of the European Centre for Medium-Range Weather Forecast (ECMWF) are considered for comparison with the ground-based IB02 dataset. ERA-Interim global reanalysis (Dee et al., 2011a) is available from 1979 onwards, but only the period 2000–2008, the common period of the satellite-based dataset and the EPEs ranking, is considered in this study. The ERA-Interim 6-hourly values of accumulated precipitation are extracted and aggregated into daily sums. Precipitation data originally come at 0.75° of horizontal resolution and they are projected through bilinear interpolation onto the same 0.2° × 0.2° grid of IB02 (see Section 2.2.5 for further details). Recently, a new generation of reanalysis product—ERA5—has been released, with hourly data from 2000 to within three months of real-time (but expected to be extended back in time until 1950). ERA5 will eventually replace the ERA-Interim (Hersbach and Dee, 2016). Hence, it is beneficial at this stage to assess both products over the IP. Both the horizontal (from 0.75° to 0.25°) and the vertical (from 60 to 137 levels) resolutions are improved in ERA5. In the following analysis, the same interpolation method as for ERA-Interim is used to match with the IB02 grid.

2.2.3 TRMM TMPA Data sets

In addition, two precipitation products from the Tropical Rainfall Measurement Mission (TRMM) are used (Huffman et al., 2009). The main purpose of the mission is to provide a new understanding of the distribution and variability of precipitation and energy exchanges in the tropical and subtropical regions of the world, especially during storms (Huffman et al., 2007). On-board instruments (Kummerow et al., 1998; Liu et al., 2012) include a visible and infrared scanner (VIRS), a microwave imager (TMI), a precipitation radar (PR), and a lightning imaging sensor (LIS). The TRMM Multi-satellite Precipitation Analysis (TMPA) products are the most popular in the TRMM mission: they account for precipitation retrievals algorithms that incorporate multiple-sensor and multi-satellite data in addition to in-situ observations, yielding to an unprecedented accuracy of precipitation estimates (Huffman et al., 2009). The products belong to Version 7 of the 3B42 algorithm, both in the near-real-time (6–9 h after present time) and post-real-time releases (Huffman et al., 2003). The latest improvements of Version 7 mainly come from additional satellites and a uniform ground-based adjustment (Bolvin and Huffman, 2015; Liu, 2015a). The near-Real-Time product (for simplicity hereafter referred to as TRMM RT) only depends on microwave and infra-red data, and it is computed a few hours after real-time; the research-grade product (hereafter referred to as TRMM) is differently calibrated and is adjusted to monthly values (Huffman et al., 2003). According to Liu (2015b), the former provides quick and less accurate estimates on a global scale, suitable for monitoring activities, whereas the latter is designed to provide estimates more appropriate for research purposes. Data are made available from 1997 and 2000, respectively. For both TRMM and TRMM RT (together referred to as TRMM TMPA products), data are provided onto a 0.25° × 0.25° grid and they cover the latitudinal band 50° N to 50° S even though many efforts are being made, in the framework of the GPM mission, which is going to include the TRMM mission, to further extend the coverage beyond the extra-tropics.

Some studies already focused on areas beyond the inclined latitude band of the TRMM satellites (Yong et al., 2010; Cai et al., 2015) and explore the differences between the two products (Jiang et al., 2017; Chen et al., 2013). The research-grade product is more widely used for regional studies worldwide as in America (Habib et al., 2009; Scheel et al., 2011), in the Mediterranean domain (Lo Conti et al., 2014; Villarini, 2010), and over Iberia (Nieto Ferreira, 2017; Liberato et al., 2017; El Kenawy et al., 2015). In Villarini (2010) and Yong et al. (2014) high (light) precipitation events tend to be under (over) estimated. Cai et al. (2015) and Yong et al. (2014) addressed the suitability of both TRMM TMPA products over river basins in China

for predicting river streamflow and water resources in the context of hydrological extremes. Besides the good results obtained in Chen et al. (2013) for a TMPA-driven hydrological model for river streamflow, large differences were found over latitude by Ebert et al. (2007) with over (under) estimation of precipitation affecting high (low) latitudes. The accuracy of the TRMM TMPA estimates was also shown to vary among seasons: Chen et al. (2013) found the worst performances over three different regions in northern China during winter, also because of the ice and snow cover affecting the retrieval algorithms. On the contrary, winter (and summer) accounted for the best results over Iberia in El Kenawy et al. (2015). However, the accuracy of a single product can change from one region to another (Ebert et al., 2007), mainly because of different rainfall regimes (the more convective the precipitation, the more accurate satellite estimates are), because of the surface conditions and also because of the reliability of the ground-based dataset used for validation. Given this variety of results, further investigations are surely needed.

2.2.4 Extreme Precipitation Events (EPEs) Dataset for IP

In this work, the ranking of high-resolution winter daily precipitation extreme events developed by Ramos et al. (2014a) is used. It is the most comprehensive database available for EPEs over the IP. It accounts for daily accumulated precipitation, from 1950 to 2008, for the extended wintertime (October to March), as summer precipitation is not significant over most of the IP domain (Martín-Vide and Gomez, 1999; de Luis et al., 2010). Given the high spatial variability of precipitation regimes over IP, the events are ranked according to an index that takes into account both the anomaly of precipitation and the extension of the area affected by the anomaly. In more detail, the normalized precipitation departure from seasonal climatology is evaluated for each grid point and for all days and it reads:

$$N = \frac{P - \mu}{\sigma} \tag{2.1}$$

where P is the daily precipitation sum, μ is the 7-day running mean for that day, and σ is the standard deviation from that mean. Then, the area affected is defined by the number of grid points that have precipitation anomalies exceeding two standard deviations (2σ). A mean value for this anomaly is defined over the selected area and the ranking index is defined by multiplying the two quantities. It is worth saying that the 2σ threshold does not substantially differ from the 95th percentile of the daily precipitation distribution, which is typically considered as a reference for attributing extremes. For further details, the authors suggest directly referring to Ramos et al. (2014a).

2.2.5 Temporal-Spatial and Intensity Assessment

The four precipitation data sets described in Section 2.2.1 are matched in time and space for direct comparison and EPEs assessment. That is, precipitation values from ERA-Interim (6 h) and ERA5 (1 h) reanalysis as well as from TRMM TMPA products (3 h) are aggregated into daily (24 h) sums over the common period 2000–2008 and the same 0.2° × 0.2° latitude/longitude grid of the IB02, through bilinear interpolation. However, the accumulated periods do not exactly overlap, because of the different timing each product is made available (Figure 2.1). The IB02 accounts for daily values from 07:00 (09:00) UTC of day n to 07:00 (09:00) UTC of day n + 1 for Spain (Portugal) respectively. ERA-Interim is then accumulated by summing four timesteps (12:00 UTC and 18:00 UTC of day n, 00:00 UTC and 06:00 UTC of day n + 1) so that daily values cover the interval from 09:00 UTC (day n) to 09:00 UTC (day n + 1). The accumulation period for ERA5 is one hour before each timestep. Therefore, ERA5 daily precipitation is computed by summing 24 hourly timesteps (10:00 UTC of day n to 10:00 UTC of day n + 1) so that daily values cover the same interval as for ERA-Interim. On the contrary, TRMM TMPA products are available at 3-h timesteps, making it possible to define a backward (from 07:30 UTC of day n to 07:30 UTC of day n + 1) and a forward (from 10:30 UTC of day n to 10:30 UTC of day n + 1) accumulation period with respect to the reanalysis accumulation period. In order to achieve the best possible match among the four data sets considered, the backward period is used. A mask is applied to all the data sets so that only grid points of continental Iberia with daily precipitation exceeding 2 mm·day−1 are considered for this analysis.

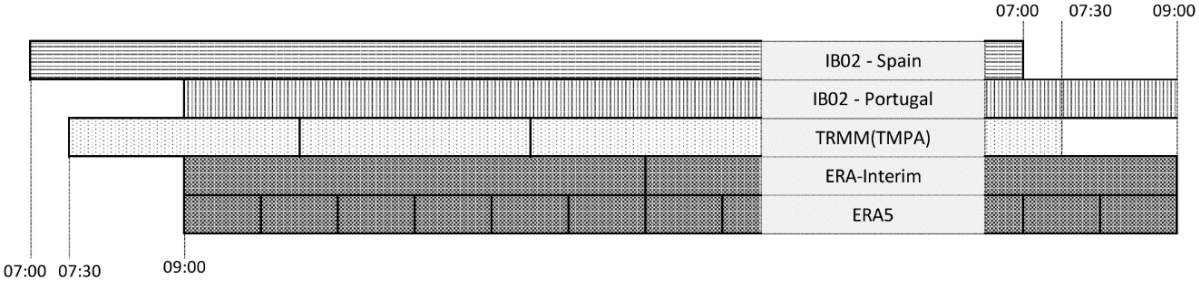

Figure 2.1. Scheme of the daily accumulation period considered for the different data sets used in this study. The left side refers to the beginning of the accumulation period (day n), the right side refers to the end of the accumulation period (day n+1).

For the assessment of precipitation among data pairs a set of four accuracy metrics is considered (Wilks, 2006) namely the Pearson linear correlation coefficient (r, Equation (2.2)), the percentage bias (%BIAS, Equation (2.3)), the root mean square error (RMSE, Equation (2.4)) and the mean absolute error, (MAE, Equation (2.5)). The corresponding formulae read (taking ERA5 as an example):

$$r = \frac{cov(ERA5, IB02)}{\sigma_{ERA} * \sigma_{IB02}} \tag{2.2}$$

$$\%BIAS = \frac{\sum(ERA5 - IB02)}{\sum IB02} * 100 \tag{2.3}$$

$$RMSE = \sqrt{\frac{1}{N} * \sum (ERA5 - IB02)^2} \tag{2.4}$$

$$MAE = \frac{\sum (ERA5 - IB02)}{\sum n} \tag{2.5}$$

where *n* is the number of data pairs considered, *cov* is the covariance and σ is the standard deviation. The equations hold similarly for ERA-Interim, TRMM and TRMM RT.

Each index is evaluated through a grid-to-grid procedure based on the 0.2° × 0.2° IB02 grid. With such an approach, it is worth noting that both the intrinsic interpolation scheme of IB02 and the interpolation required for the other data sets to match with IB02 constitute a source of uncertainty. In those cases, precipitation extremes may be misrepresented, especially over regions of complex topography (Daly et al., 2017). However, the IB02 already accounts for several quality control procedures and internal consistency checks and its robustness has been already assessed (Belo-Pereira et al., 2011). On the other hand, an area average approach would clearly smooth any local extremes (El Kenawy et al., 2015) and it would not be suited for the current analysis.

Finally, in order to have insights on the weaknesses and strengths of each of the data sets considered, the total bias is split into three components (Habib et al., 2009). This procedure allows distinguishing three different bias sources with respect to IB02, namely the bias due to successful detection (hit bias, HB), the bias due to misses (missed rain bias, MB) and the bias due to false alarms (false rain bias, FB). They are defined as follows (taking ERA5 as an example):

$$HB = \sum P_{ERA5}\,(P_{ERA5} > 2\ \&\ P_{IB02} > 2) - P_{IB02}(P_{ERA5} > 2\ \&\ P_{IB02} > 2) \tag{2.6}$$

$$MB = \sum P_{IB02}\ \ (P_{ERA5} < 2\ \&\ P_{IB02} > 2) \tag{2.7}$$

$$FB = \sum P_{datN}\ \ (P_{ERA5} > 2\ \&\ P_{IB02} < 2) \tag{2.8}$$

where P_{ERA5} is the precipitation at the specific grid point from ERA5 (but it holds similarly for the other data sets) and P_{IB02} is the precipitation at the corresponding grid point from IB02. The sums run all over the grid points of continental IP and the sum of the three components gives

the total bias. Given the values described in Eq. 2.6 to 2.8, it is possible either to obtain the fraction of total bias explained by each bias source or the average of each bias source per grid point.

2.3 Results

2.3.1 IB02 Precipitation Dataset

IB02 dataset covers the period from 1950 to 2008, although the spatial coverage of the station network may vary through, as described in Belo-Pereira et al. (2011). However, reanalysis data and satellite retrievals from the TRMM mission are made available only later, since 1979 and 2000, respectively. Thus, a preliminary control on how the common 2000-2008 period is representative of the entire dataset is necessary. The mean daily precipitation is evaluated, for all year and for the wintertime period, from 3 different time windows, namely the entire 59-years IB02 dataset, the standard 30-years climatological mean and the 9-years common period used in this study. As shown by the results summarized in Table 1, no relevant changes occur in the climatology between the 3 considered periods. The mean of daily precipitation, averaged over the whole IP, remained substantially similar between the 50-years and 30-years periods (10.28 $mm.day^{-1}$ and 10.24 $mm.day^{-1}$, respectively). Over the last decade available, the daily mean slightly decreases below the 10$mm.day^{-1}$ threshold. Considering only the extended winter months (October to March), the values of mean daily precipitation are slightly larger than for all-year (Table 1), but they show the same behavior over time on IP. The two standard percentiles thresholds for extremes are also considered. In this case, the mean precipitation daily values over IP are slightly lower during 1979-2008 (29.03 $mm.day^{-1}$ and 48.37 $mm.day^{-1}$ for 95th and 99th percentile, respectively) than during 1950-2008 (29.12 $mm.day^{-1}$ and 48.77 $mm.day^{-1}$) and they decrease again during the last 9 years (28.42 $mm.day^{-1}$ and 47.47 $mm.day^{-1}$). However, all these values are in agreement (28-29 $mm.day^{-1}$ and 47-48 $mm.day^{-1}$, for 95th and 99th percentiles respectively) and thus it may be considered that the 3 periods are comparable. Still, the difference between extended winter and all-year percentiles values serves as proof of the seasonal variability of precipitation over IP.

It should be noted that this control over different time periods is not aiming at dragging conclusions over the climatology of Iberia. The purpose indeed is to show that the last 9 years available are quite well representative of the entire IB02 dataset and this justifies the use of the common period 2000-2008, even though not particularly long, throughout this analysis.

Table 2.1. Main statistics for different temporal subranges of the IB02 dataset.

Time range	Mean (std) [mm.day^{-1}]		95th perc [mm.day^{-1}]		99th perc [mm.day^{-1}]	
	All year	Extended winter	All year	Extended winter	All year	Extended winter
59 yrs (1950-2008)	10.28 (9.98)	10.92 (10.65)	29.12	31.12	48.77	51.75
30 yrs (1979-2008)	10.24 (10.09)	10.95 (10.82)	29.03	30.79	48.37	51.55
9 yrs (2000-2008)	9.90 (9.87)	10.46 (10.41)	28.42	30.23	47.47	50.82

2.3.2 Accuracy metrics for quartiles of precipitation for all year on the period 2000-2008

At first, the accumulated daily precipitation at each grid point during the 2000-2008 common period is classified in quartiles, according to the 25th/50th/75th percentiles for the daily precipitation, evaluated separately for each grid point and for each day of the year. The percentiles are given by the 7-years running mean all over the IB02 dataset (1950 to 2008). Throughout this section, the analysis is conducted for all days of the common period 2000-2008 and for the 4 quartiles separately, Q1 being the weakest one and Q4 the most extreme one.

Fig. 2.2 includes the scatterplots of measured daily precipitation (mm.day^{-1}) from IB02 versus the estimates from TRMM, TRMM RT, ERA-Interim and ERA5, respectively. For TRMM(TMPA) products, Q1 to Q3 data pairs are clustered closer to the satellite estimates. On the contrary, the points belonging to Q4 spread closer to the identity line. ERA-Interim and ERA5 show the same pattern as described for the satellite products, the only difference being a higher correspondence between estimates and ground-based values also for Q3. As it is defined, Q4 includes the data pairs where IB02 daily precipitation exceeds the 75th percentile that is, also the grid points with actual extreme precipitation. The fact that in the related scatterplots, a lot of points still spread close to the zero (of both x and y axes) is to be expected. The first case relates to the underestimation of precipitation by the specific dataset considered, which is larger for extreme events (as shown later). The second case comes from the IP grid points whose 75th percentiles for daily precipitation are very low, as it may occur over some inland and southern areas and during the drier months of the year.

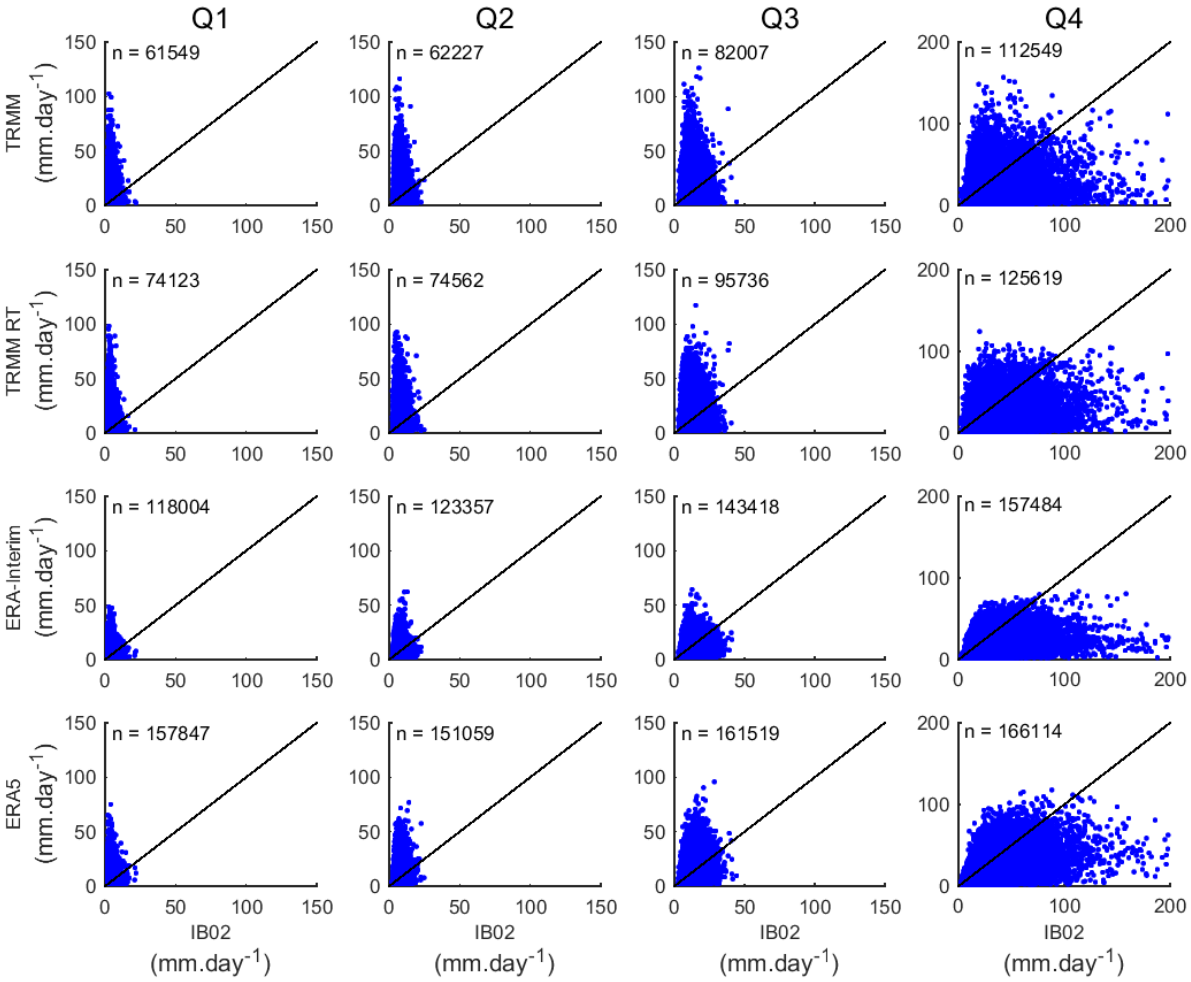

Figure 2.2. Scatterplots of accumulated daily precipitation (mm.day^{-1}) for each dataset vs IB02 (over raws TRMM, TRMM RT, ERA-Interim and ERA5, respectively) and for each quartile (over columns). Data pairs refer to all year for the common period 2000-2008. Only values over 2 mm.day^{-1} are considered. The number of data pairs (*n*) is displayed. Please note that the x-axis limit is different for Q4 (200mm.day^{-1}); however, a certain number of data pairs (11 for TRMM, 10 for TRMM RT, 12 for ERA-Interim and ERA5) is still not displayed in Q4 panels.

The correlations coefficients (Fig. 2.3a) indicate a very low correlation for Q1 (all data sets below 0.2). They indicate low correlation also for Q2 and Q3 and a still poor but higher correlation for Q4 (0.26, 0.34, 0.43 and 0.54 for TRMM, TRMM RT, ERA-Interim and ERA5, respectively). Both the reanalysis products perform better than TRMM(TMPA) products for all the quartiles and the main difference is observed for the intermediate quartiles Q2 and Q3, as suggested by the scatterplots. It is observed that the more the quartile includes higher precipitation data pairs, the more TRMM RT outperforms TRMM.

All the annual data sets considered show a positive (negative) %BIAS for Q1 and Q2 (Q3 and Q4) with respect to IB02 (Fig. 2.3b). That is low(high) daily precipitation events over IP are overestimated (underestimated) by global data sets. The reanalysis products show the best adjustment to IB02 for Q1 and Q2 with ERA-Interim outperforming ERA5. On the contrary,

ERA5 improves ERA-Interim for Q3 and Q4 and it turns out to be the best of all data sets for the most extreme quartile (-30% BIAS). In terms of %BIAS, TRMM RT product equals TRMM except for Q1 where, however, both the TRMM(TMPA) products have poor performance (+144% and +133% BIAS respectively). Both the error metrics, namely RMSE (Fig. 2.3c) and MAE (Fig. 2.3d), increase with the increasing extremeness of the precipitation. Values of RMSE jump from Q3 to Q4 from less than 10 mm.day^{-1} to almost 20 mm.day^{-1}, as clearly visible by the large degree of dispersion around the fitted line in the scatterplots (Fig. 2.2). MAE also increases the most from Q3 to Q4 (4-6 mm.day^{-1} to 9-15 mm.day^{-1}). This behavior is somehow expected as the spatio-temporal pattern of precipitation is more complex for heavy and extreme events because of localized peaks of rainfall and local effects of enhancement. Consistently with the other annual metrics, reanalysis data sets perform better than TRMM(TMPA) products (ERA5 performs best for Q4) and TRMM RT outperforms TRMM as far as the quartiles include more extreme values.

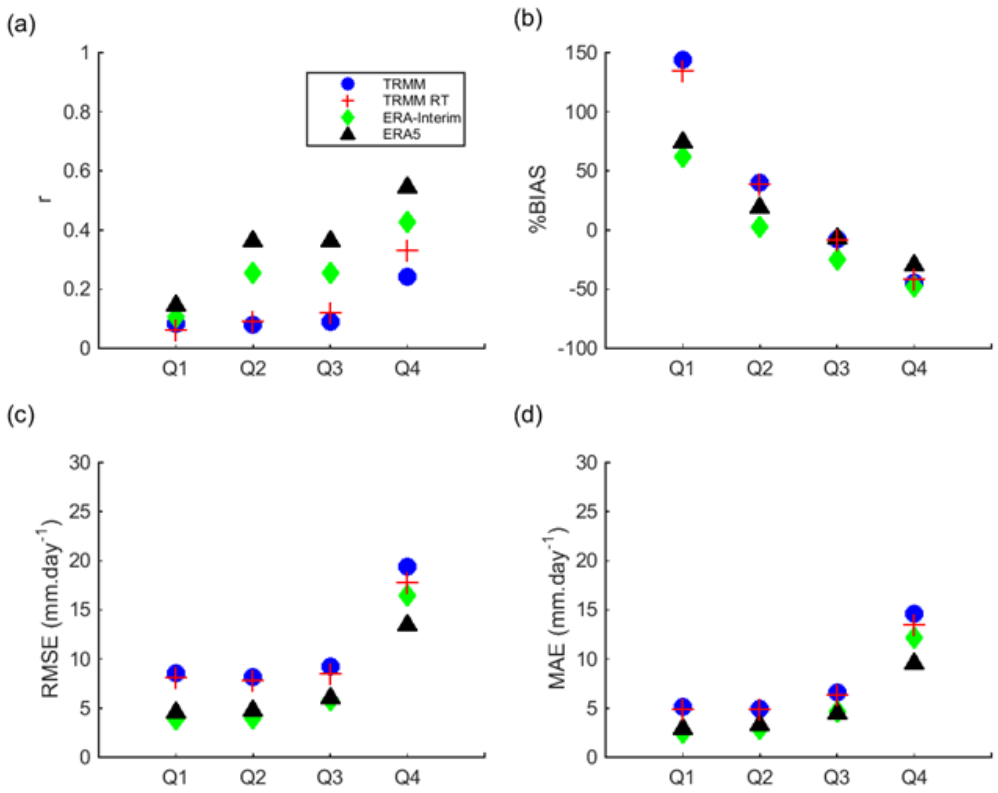

Figure 2.3. (a) Correlation coefficient, (b) percentage bias (%BIAS), (c) Root Mean Square Error (RMSE) and (d) Mean Absolute Error (MAE) for accumulated daily precipitation (mm.day^{-1}) of TRMM (blue circle), TRMM RT (red cross), ERA-Interim (green diamond) and ERA5 (black triangle) versus IB02. Metrics are plotted for different quartiles of daily precipitation for all year and for the common period 2000-2008.

2.3.3 Insights on the last decile of EPEs for extended winter on the period 2000-2008

As pointed out by the assessment presented in Sec. 3.2, the accuracy metrics for Q4 often show a different pattern with respect to the other quartiles, with larger errors but a better adjustment in terms of correlation to the IB02 ground-truth. At the same time, the related scatterplots show that Q4 still includes a significant number of grid points from IB02 whose precipitation cannot be considered as extreme. As a follow-up to the previous analysis, a set of objectively identified extreme events has been chosen and studied separately. The events are selected from the EPEs ranking dataset in Ramos et al. (2014a) and described in Sec. 2.2, limited to the 2000-2008 common period. Then, only daily precipitation values falling into the last decile (90th) are considered, which gives a total number of 84 events (the full list can be consulted in the Supplementary Material).

As before, it is first assessed whether the subset of events obtained from the full ranking over the common years can be considered representative of the longer dataset. As the ranking of EPEs only includes the extended wintertime months, the analysis from now onwards will account only for events that occurred between October to March. In addition, summertime is known to account for different precipitation regimes over IP (de Luis et al., 2010; Belo-Pereira et al., 2011) with relevant regional patterns (Nieto Ferreira, 2017; Martín-Vide and Gomez, 1999). Therefore, it would require a different methodology to produce a valuable ranking. The main statistics are shown in Table 2: as previously found, mean daily precipitation has only a very slight decrease when the time window is shortened to the common period. Still, it cannot be said to what extent this small change is due to a decrease in total precipitation or to actual changes in the mechanisms enhancing the extremeness of the events – which is out of the scope of this study.

Table 2.2. Main statistics for different temporal subranges of IB02 (extended wintertime extreme days).

Time range	Mean (std) [mm.day^{-1}]	95th percentile [mm.day^{-1}]	99th percentile [mm.day^{-1}]
59 yrs (1950-2008)	11.46 (10.94)	32.38	53.16
30 yrs (1979-2008)	11.53 (11.22)	32.99	54.25
9 yrs (2000-2008)	11.07(10.88)	31.75	53.0

Daily precipitation from IB02 is plotted against the estimates from TRMM, TRMM RT, ERA-Interim and ERA5 (Fig. 2.4) for all the data pairs of the 84 EPEs previously identified. Only grid points whose precipitation anomalies exceed 2σ are considered, as prescribed in Ramos *et al.* (2014a). The analysis is repeated for anomalies exceeding 3σ to 7σ and the number of grid points considered for each class is shown in each panel of Fig. 2.4. For all the four data

sets, but it is more evident for TRMM (Fig. 2.4 – first row), data pairs show the tendency to be clustered towards IB02. This tendency gets clearer as far as only grid points beyond a certain threshold of standard deviation anomalies are considered. Therefore, also for the last decile of extreme events, it holds that the more the precipitation is extreme, the more the reanalysis and TRMM(TMPA) data sets underestimate IB02 ground truth.

By analyzing the accuracy metrics for all grid points with precipitation anomalies over 2σ (Fig. 2.5), it becomes evident that TRMM RT has slightly higher correlation values than TRMM (r = 0.37 compared to r = 0.32) and lower %BIAS (-45.35% compared to -58.48%), RMSE (25.75 $mm.day^{-1}$ compared to 29.85 $mm.day^{-1}$) and MAE (20.21 $mm.day^{-1}$ compared to 24.28 $mm.day^{-1}$). These results suggest that TRMM RT is more adequate for winter EPEs than TRMM. All the error metrics are lower for the reanalysis products with respect to TRMM (TMPA) products with ERA5 that clearly improves ERA-Interim (-0.28% compared to -0.44% for %BIAS, 19.20 $mm.day^{-1}$ compared to 24.34 $mm.day^{-1}$ for RMSE, and 13.55 $mm.day^{-1}$ compared to 18.26 $mm.day^{-1}$ for MAE).

For subsets of grid points grouped according to the number of standard deviations they depart from the mean, TRMM RT still outperforms TRMM with the only exception of the correlation for $\sigma>7$ (r = 0.30 compared to r = 0.19 for TRMM RT and TRMM, respectively) whose number of grid points is very little in comparison to the other classes. It is observed that while the performance of the reanalysis products decreases for the most extreme classes, TRMM (TMPA) estimates become more reliable. For ERA-Interim, this behavior is quite clear: for IB02 grid points with precipitation anomalies up to 4σ, ERA-Interim and TRMM (TMPA) products still compete in terms of correlation (Fig. 2.5a) but ERA-Interim suddenly drops beyond that threshold, to r ~ 0.2 for $\sigma>6$, whereas TRMM (TMPA) products still approach r ~ 0.4. ERA5 overcame this issue as its correlation never drops below r = 0.4, thus being again the most performing dataset. In terms of percentage of BIAS (Fig. 2.5b), TRMM RT outperforms ERA-Interim only for grid points beyond the 5σ threshold but still, the ERA5 reanalysis is always preferable. TRMM dataset always underestimates by more than 50%. In terms of RMSE and MAE, TRMM RT behaves similarly to ERA-Interim, both outperforming TRMM but still accounting for larger errors than the new ERA5 reanalysis.

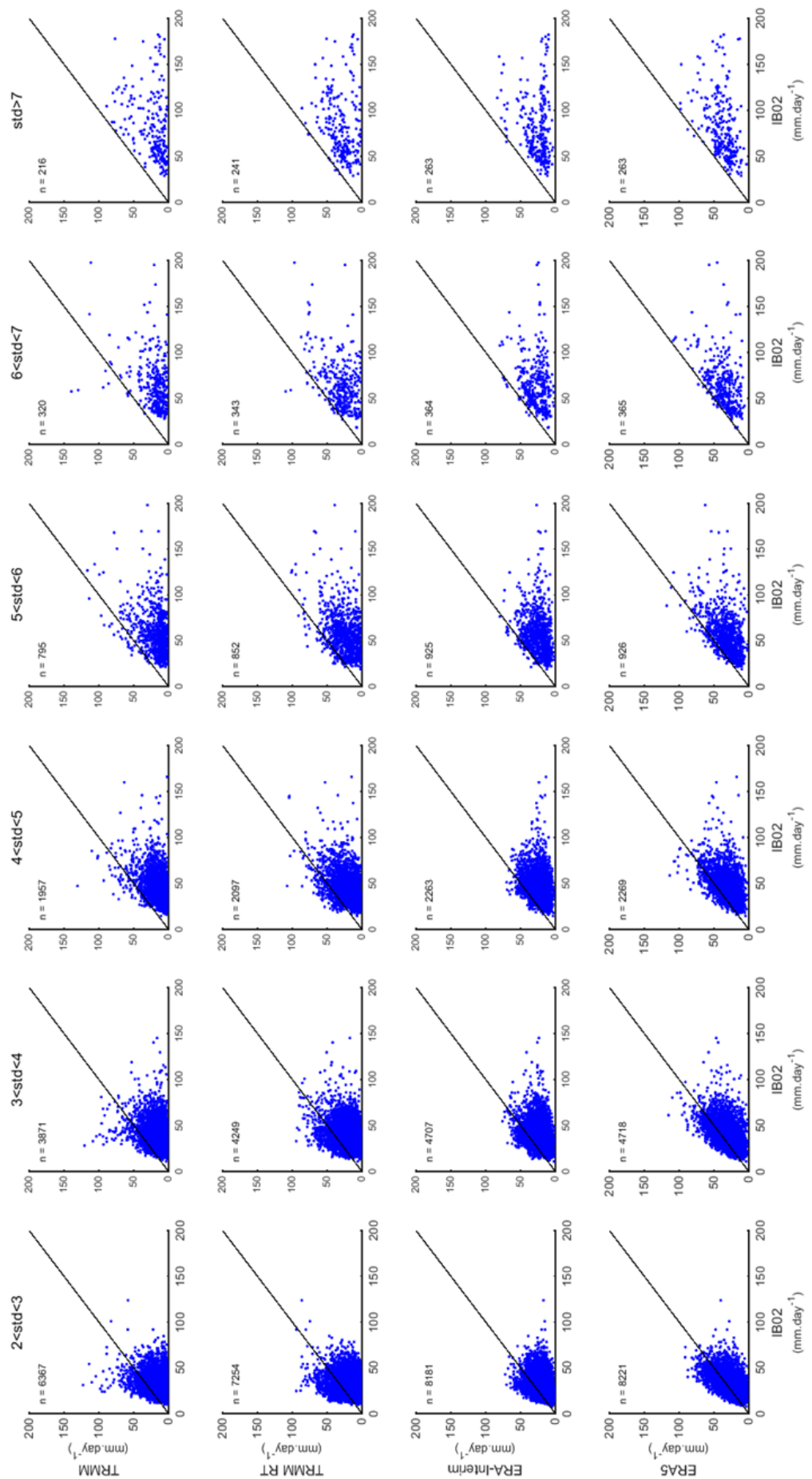

Figure 2.4. Scatterplot of accumulated daily precipitation (mm.day^{-1}) for each dataset vs IB02 (over rows: TRMM, TRMM RT, ERA-Interim and ERA5 respectively) and for different ranges of precipitation anomaly (in σ units) at the grid points. Only days for extended winter and for the common period 2000-2008 beyond the 90th percentile of the ranking developed by Ramos et al. (2014a) are considered. Only values over 2 mm.day^{-1} are considered A certain number of data pairs (7 for each of the data sets considered) is not displayed due to x-axis limits.

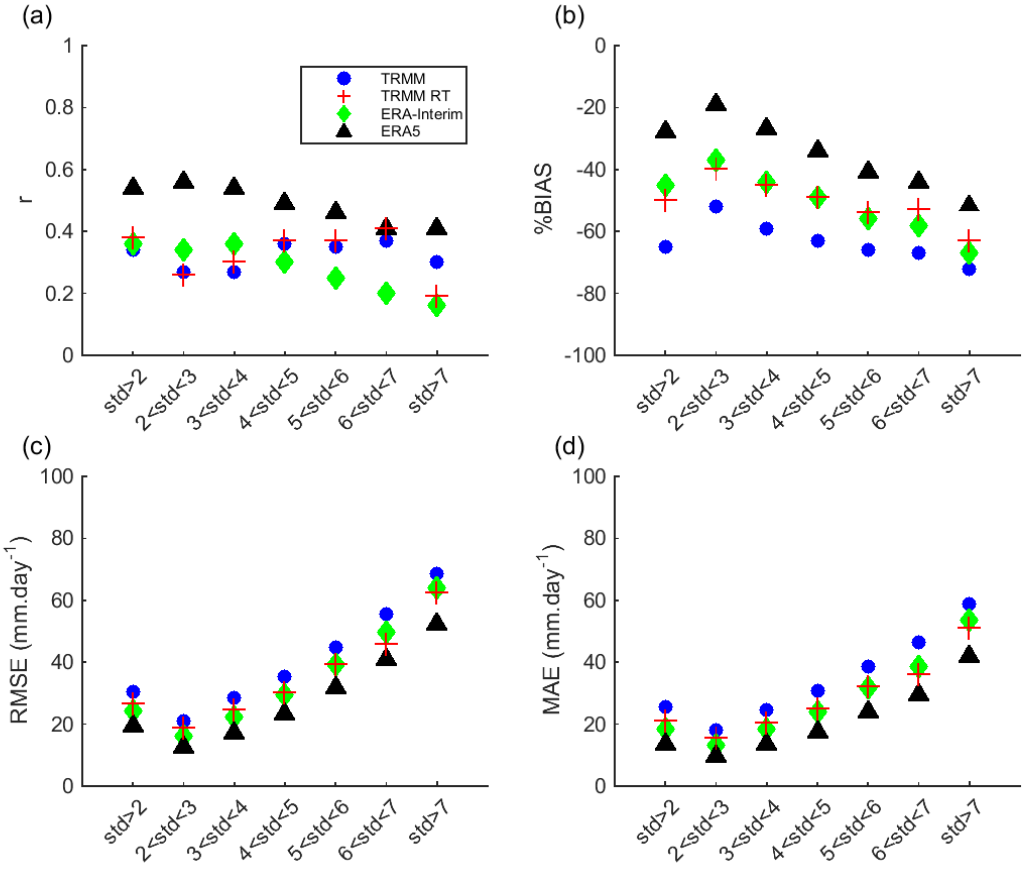

Figure 2.5. (a) Correlation coefficient (r), (b) percentage bias (%BIAS), (c) Root Mean Square Error (RMSE) and (d) Mean Absolute Error (MAE) for accumulated daily precipitation (mm.day^{-1}) of TRMM (blue circle), TRMM RT (red cross), ERA-Interim (green diamond) and ERA5 (black triangle) vs IB02. Only daily precipitation for wintertime and for the common period 2000-2008 that falls beyond the 90th percentile of the ranking developed in Ramos et al. (2014a) is considered. Metrics are plotted for precipitation anomalies over 2σ and for different ranges of precipitation anomalies (in σ units) at the grid points.

According to what has been observed in the scatterplots of Fig. 2.2 and Fig. 2.4, the analysis of the total bias is not always exhaustive. By splitting the total bias into its different components, that is Hit Bias (HB), Missed Bias (MB) and False Bias (FB) as described in Sec. 2.3, new insights are made clearer on each dataset performance. In Fig. 2.6 each bias source is divided by the total number of grid points where bias is observed for the specific dataset so that the average values per grid point are plotted. HB is shown to be the main source of uncertainty for all the data sets. The second source of bias is MB for TRMM(TMPA) products and FB for ECMWF reanalysis. With respect to ERA-Interim, both the hits bias (HB) and missed rain bias (MB) are successfully cleared in ERA5. Regarding TRMM(TMPA) products, it is shown that even though the research-grade release reduced false alarms (from 0.96 mm.day^{-1} to 0.27 mm.day^{-1}), still the underestimation and the missing values are higher than in the real-time version (on average -3.33 mm.day^{-1} compared to –2.27 mm.day^{-1} for HB and -3.09 mm.day^{-1} compared to –1.89 mm.day^{-1} for MB for TRMM and TRMM RT, respectively).

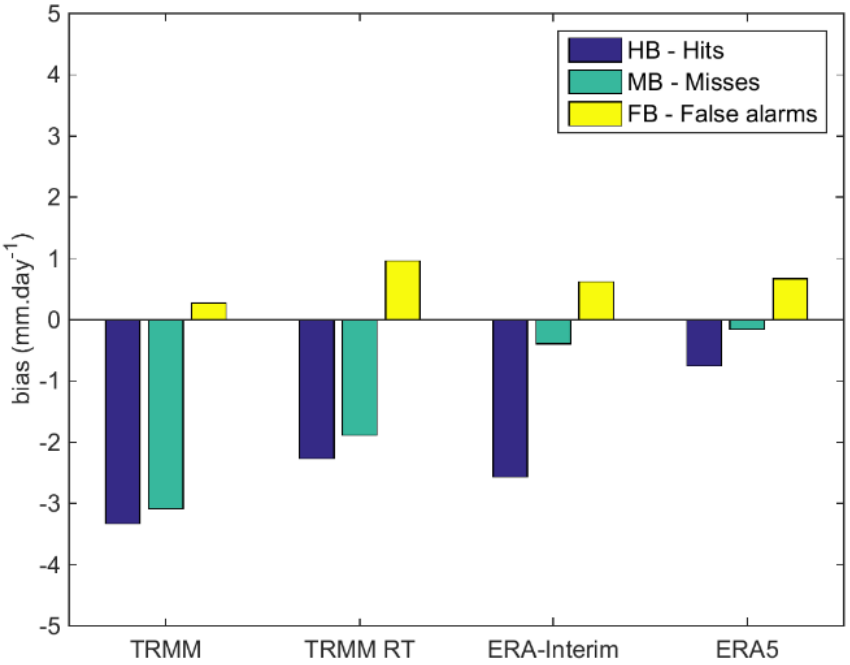

Figure 2.6. Decomposition of total bias for each dataset versus IB02. The total bias is split into contributions from hits (HB - blue), misses (MB - green) and false alarms (FB - yellow) and the values are averaged over the total number of grid points. Only daily precipitation for extended winter and for the common period 2000-2008 that falls beyond the 90th percentile of the ranking developed in Ramos et al. (2014a) is considered.

As an example, the case study of 6/12/2000, the #4 in the ranking for IP of Ramos *et al.* (2014a) and the #1 if considering only Portugal is analyzed, also through the related precipitation maps (Fig. 2.7). In this case, the TRMM RT estimates, perform better than the associated TRMM product when precipitation is extreme, despite the latter being more widely used for research purposes. In this event, two main precipitation spots can be recognized: the first one across the northern border between Portugal and Spain; the second one extending from SW to NE over central Portugal (Fig. 2.7a). Only the first spot is reproduced by ERA-Interim (Fig. 2.7d) and TRMM (Fig. 2.7b), even though it results wrongly displaced to the North. The analysis of this case shows also that ERA5 improved over the previous ERA-Interim dataset and outperforms the other data sets considered. On the contrary, both TRMM RT (Fig. 2.7c) and ERA5 (Fig 2.7e) are able to represent the precipitation over the southern sector. However, in TRMM RT the band is oriented from NW to SE that is almost symmetric with respect to IB02 (Fig 2.7d) whereas in ERA5 it is correctly displaced, although the precipitation amount is underestimated with respect to IB02. For ERA-Interim, the spatial and temporal pattern of precipitation is partially inconsistent with what is shown in (Skofronick-Jackson et al., 2017) where the same case is analyzed. In that case, the precipitation maximum aforementioned is located more to the west. This difference is ascribable to the different resolution of the grid (1° x 1° in Liberato et al. (2017) and 0.2° x 0.2° in the present study) which may lead to

displacements in the plotted field. In the case of TRMM RT, significant amounts of daily rainfall are detected all over eastern and southern IP even though no precipitation occurred according to IB02. This inaccuracy can be only partly explained by the 1h30 time lag between TRMM (TMPA) products and IB02 accumulation period (some of the precipitation over southern Portugal and Andalusia actually falls in the morning of December 7th). Therefore, this is an example of how relevant the contribution of false alarms to the total bias can be for TRMM RT.

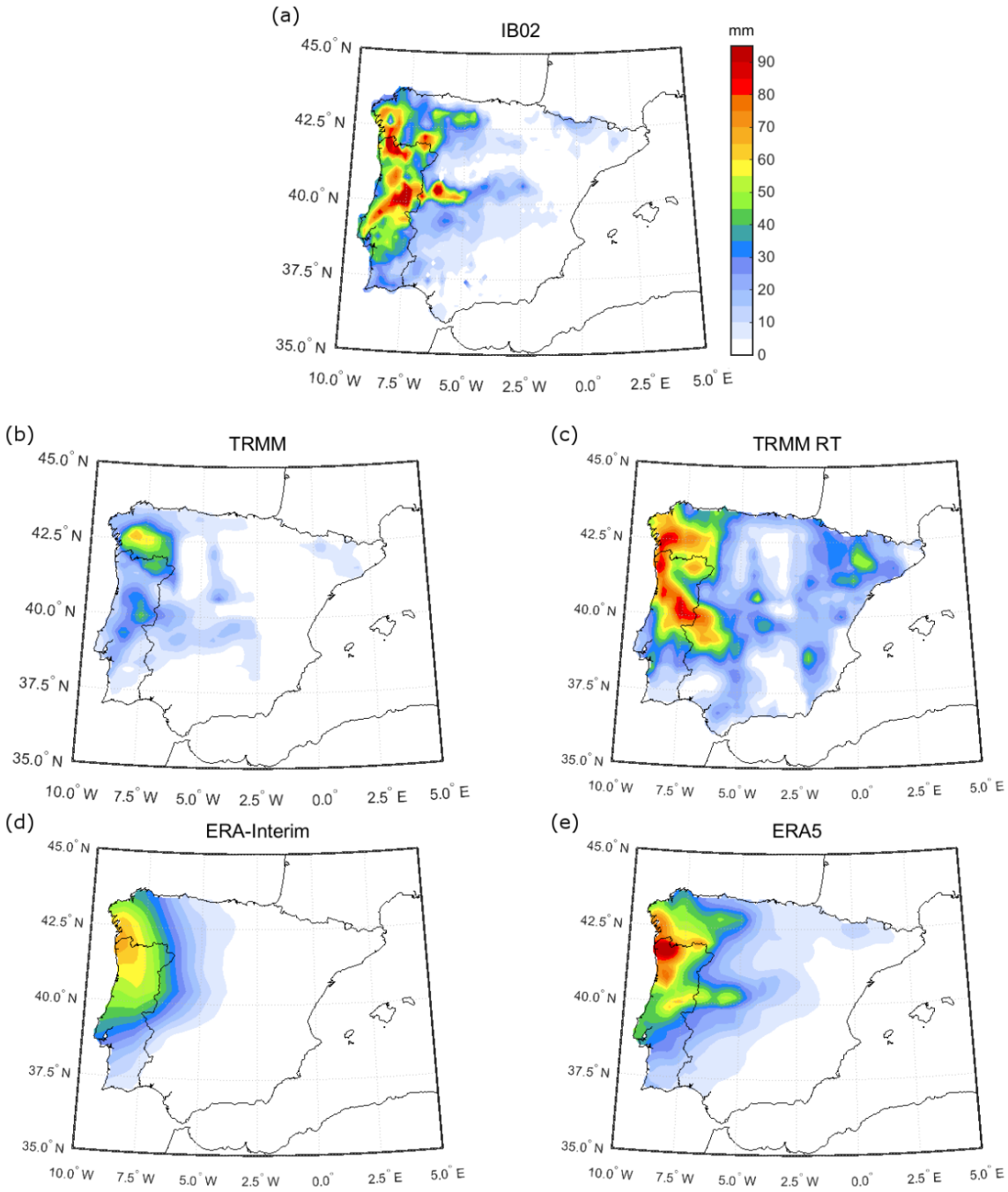

Figure 2.7. Extreme precipitation event on 6 December 2000. Daily precipitation from (a) IB02, (b) TRMM (TMPA) research-grade product, (c) TRMM (TMPA) RT product, (d) ERA-Interim and (e) ERA5.

As for the analysis of the maps, also the main accuracy metrics suggest that TRMM RT is more accurate than TRMM and that ERA5 is the dataset that best performs in reproducing extreme precipitation for this case study (Fig. 2.8). By considering only data pairs whose precipitation anomaly exceeds 2σ, the correlation coefficients differ among the four data sets: ERA5 has the largest correlation (r = 0.63), then ERA-Interim and TRMM RT almost equals each other (r = 0.53 and r = 0.52 respectively) and TRMM has the lowest (r = 0.44). TRMM and ERA-Interim data sets significantly underestimate precipitation (-57.25% and -25.73% of BIAS respectively) whereas, also because of the large occurrences of false alarms, TRMM RT shows a very low negative bias (-8.36%), even lower than ERA5 (-11.17%). The lowest values of both RMSE and MAE come from ERA5, the largest from TRMM.

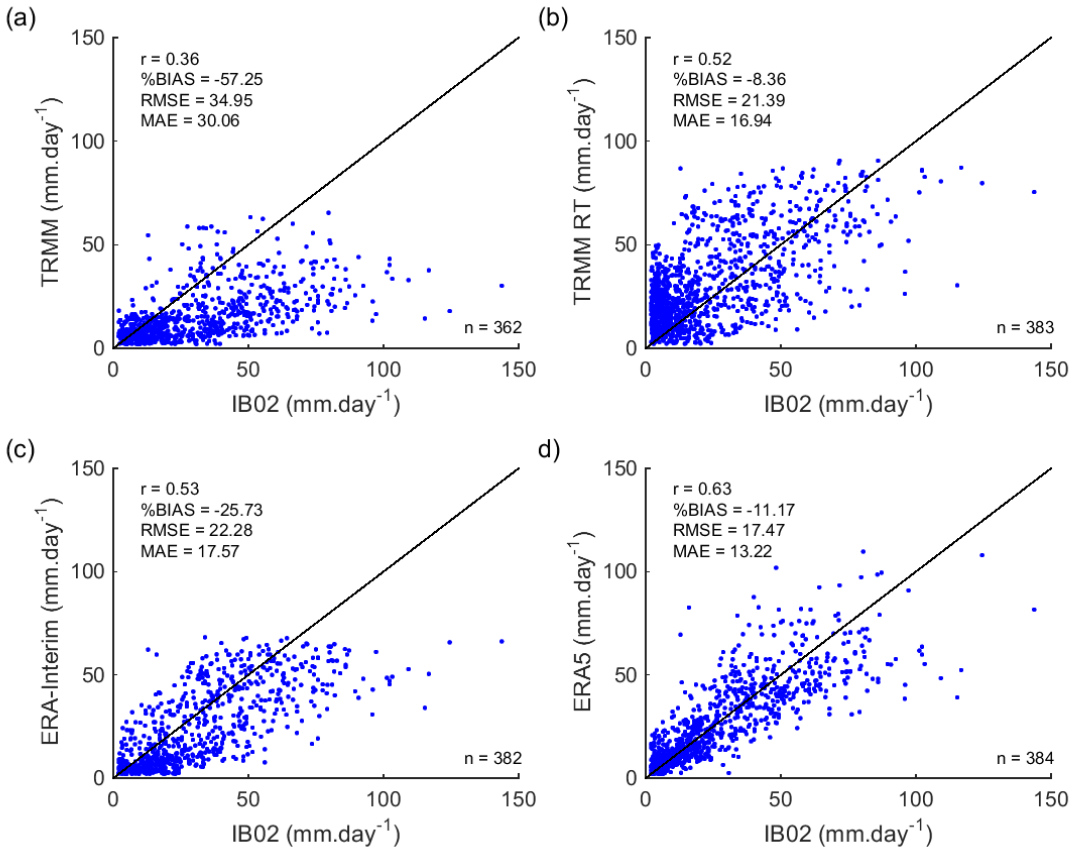

Figure 2.8. Scatterplot of accumulated daily precipitation for the extreme event on 6 December 2000 for (a) TRMM(TMPA) research-grade product vs IB02, (b) TRMM(TMPA) RT product vs IB02, (c) ERA-Interim vs IB02 and (d) ERA5 vs IB02. Only grid points whose precipitation anomaly exceeds 2σ are considered. Number of data pairs *(n)*, correlation coefficient (r), percentage bias (%BIAS), root-mean-square error (RMSE) and mean absolute error (MAE) are displayed.

2.4 Discussion and conclusions

An evaluation of the accuracy of several precipitation data sets in reproducing the spatial and temporal characteristics of extreme precipitation events (EPEs) over the continental Iberian Peninsula (IP) is undertaken. For this assessment, daily accumulated precipitation from a high-resolution (0.2° × 0.2°) ground-based gridded dataset (IB02), from ERA-Interim and ERA5, a new fifth-generation European reanalysis by ECMWF, and from two TRMM (TMPA) multi-satellite products are considered for the common period 2000–2008. Statistical analysis is performed through a set of standard accuracy metrics, including the Pearson linear correlation coefficient (r), the percentage bias (%BIAS), the root mean square error (RMSE), and the mean absolute error (MAE). Different contributions to the total precipitation bias are also analyzed. At first, the study considers all days of the common period, grouping the data pairs into quartiles according to the percentiles of mean daily precipitation computed for each grid point and for each day of the year separately. Then, only the most extreme decile of wintertime EPEs, as ranked in Ramos et al. (2014a), are considered.

Results show that reanalysis products account for the best scores in terms of accuracy metrics for all the quartiles. However, reanalysis products also show different behavior depending on the intensity of the precipitation events: light (heavy) precipitation is overestimated (underestimated). This tendency is even clearer for the multi-satellite TRMM TMPA products. Results from Liberato et al. (2017) already showed that for four of the most extreme precipitation events over the IP (Ramos et al., 2014a), the accumulated daily precipitation is underestimated with respect to IB02 by up to 80%. In El Kenawy et al. (2015), TRMM is assessed at regional scale over the IP for different thresholds of daily precipitation, and it is shown that it has a reasonable skill for moderate daily precipitation amounts (up to 25 mm·day−1) but a low skill for extremely light and strong events. Yong et al. (2014) showed that over two river basins in China, both TRMM TMPA products dramatically underestimate heavy precipitation. To the author's knowledge, there are only a few studies directly comparing the accuracy of TRMM to TRMM RT (e.g., Liu, 2015b; Habib, 2009; Yong et al., 2014). According to Liu (2015b), the variation of individual differences between the two products is small (heavy) over regions of heavy (light) rain. Yong et al. (2014) concluded that the month-to-month gauge adjustment applied in post-real time resulted in improved data accuracy of the related retrievals. On the contrary, clear improvements of TRMM RT over TRMM have been found in the present analysis and it is shown that the difference between TRMM RT and TRMM does not change for quartiles Q1 to Q3, but it does for Q4. These differences with

earlier studies likely depend on the different regions considered but also on how the classes of precipitation are defined: in Liu (2015b) and Yong et al. (2014) the classification of the events relies on fixed thresholds of daily precipitation, whereas in this study extreme days are objectively defined according to percentiles. Therefore, a group typically accounts for different daily precipitation amounts at the individual grid points, depending on the local climatology. On the other hand, the current results conform to those in Habib et al. (2009), which studied six tropical-related heavy rainfall events over Louisiana (USA) and found a larger agreement for TRMM RT with respect to TRMM when considering the upper tail of the distribution of rain rate.

As a first assessment of ERA5 over the IP, this study concludes that the new reanalysis product has considerably novel skills in estimating extreme precipitation with respect to previous releases and also to TRMM TMPA products. Indeed, improvements compared to ERA-Interim have been found regarding correlation (values for r increasing of ~0.1 for quartiles Q2, Q3 and Q4,) whereas for the other metrics, ERA5 clearly outperforms ERA-Interim for the most extreme quartile Q4.

However, when considering only the most extreme wintertime events and only those grid points with the most extreme precipitation values, the multi-satellite products considered become more competitive in this study. ERA5 still performs best, but the correlation coefficient is better for TRMM and TRMM RT for anomalies greater than 4σ and 5σ, respectively, as compared to ERA-Interim. Beyond 5σ, TRMM RT outperforms ERA-Interim also in terms of %BIAS, thus showing a better performance than the corresponding research-grade version. All metrics actually show that TRMM RT has a fairer agreement with extreme daily precipitation events than TRMM, including lower errors and higher correlation. The fact that the real-time product better identifies the spatial and temporal characteristics and intensity of extreme precipitation events gives a new perspective about the significance of this product for the midlatitudes regions. Indeed, most earlier studies rely on the solely research-grade product (e.g., Cai et al., 2015; Scheel et al., 2011; Lo Conti et al., 2014; Villarini, 2010), which is believed to be more accurate because of the added value given by the post-processing and by the different calibration period. Similarly, most of the studies that made a direct comparison of TRMM RT to its counterpart TRMM found better agreement in terms of reproducing daily precipitation for the latter (e.g., Chen et al., 2013; Liu, 2015b; Jiang et al., 2017).

This analysis also suggests that the main accuracy metrics were not able to characterize extensively all the weaknesses and strengths of the data sets considered. Through total bias

decomposition, the different contributions to the total error are identified and the bias due to successful detection was identified as the dominant component. Results also show that the research-grade of TRMM TMPA products successfully removes false alarms with respect to TRMM RT. On the other side, it accounts for larger missed bias and for an overall larger total bias. Habib et al. (2009) also found similar inconsistencies between the two TRMM TMPA versions for a small set of tropical-related case studies. The current analysis extends those findings to the midlatitudes and consolidates them through a more extensive set of events. Finally, it is shown that most of the error sources are successfully removed in ERA5 as compared to ERA-Interim. Nevertheless, it should be noted that this work is the first assessment of ERA5 for precipitation estimates over the IP, and thus requires additional investigations.

2.5 Supplementary material

Table 2.1S: List of the 90th percentile of (84) extreme daily precipitation events extracted from the ranking described in Ramos et al. (2014a) over IP all over the common period 2000-2008.

#event	Year	Month	Day
1	2001	2	6
2	2006	10	22
3	2001	3	1
4	2000	12	6
5	2001	3	2
6	2003	10	30
7	2006	11	24
8	2007	11	19
9	2004	3	29
10	2001	3	3
11	2003	2	25
12	2005	10	27
13	2007	11	20
14	2001	1	26
15	2005	12	1
16	2000	11	30
17	2004	3	28
18	2006	10	24
19	2000	11	22
20	2001	10	19
21	2001	1	5
22	2000	12	21
23	2000	10	23
24	2004	10	19
25	2004	10	27
26	2007	2	8
27	2001	3	20
28	2003	11	15
29	2004	2	24
30	2006	1	27
31	2000	11	5
32	2006	11	23
33	2003	3	27
34	2002	12	26
35	2001	12	23
36	2007	3	7
37	2006	3	23
38	2003	2	26
39	2000	12	23
40	2005	10	13
41	2006	11	15
42	2004	2	20
43	2002	3	3
44	2003	1	18
45	2003	10	25
46	2005	10	30
47	2004	10	26
48	2006	2	26
49	2004	3	11
50	2001	3	21
51	2000	12	5
52	2002	10	9
53	2001	3	4
54	2007	3	27
55	2003	12	9
56	2002	1	22
57	2001	1	28
58	2003	2	24
59	2006	3	17
60	2007	2	17
61	2002	3	13
62	2003	1	2
63	2004	12	1
64	2007	10	1
65	2006	10	17
66	2005	10	28
67	2006	2	25
68	2000	1	14
69	2003	11	22
70	2001	1	10
71	2003	10	1
72	2006	10	19
73	2006	3	4
74	2003	10	31
75	2004	2	23
76	2000	10	20
77	2000	10	22
78	2000	11	1
79	2008	2	18
80	2006	10	23
81	2000	12	7
82	2000	10	21
83	2003	1	20
84	2003	1	30

3

A ranking of concurrent precipitation and wind extreme events for the IP

This chapter is based on a manuscript that is an original contribution of this thesis published in the International Journal of Climatology, in 2021, under the title *"A ranking of concurrent precipitation and wind events for the Iberian Peninsula"*, with the DOI: 10.1002/joc.6829.

The research included in this chapter was supported by the Portuguese Science and Technology Foundation (Fundação para a Ciência e a Tecnologia - FCT) through the projects UID/GEO/50019/2019, PTDC/CTA-MET/29233/2017 (WEx-Atlantic) and CMU/CS/0012/2017 (eCSAAP). Riccardo Hénin was supported by an FCT doctoral grant (PD/BD/114479/2016) and Alexandre M. Ramos was supported by the Scientific Employment Stimulus 2017 from FCT (CEECIND/00027/2017). J. G. Pinto thanks AXA Research Fund for support.

Graphical Abstract

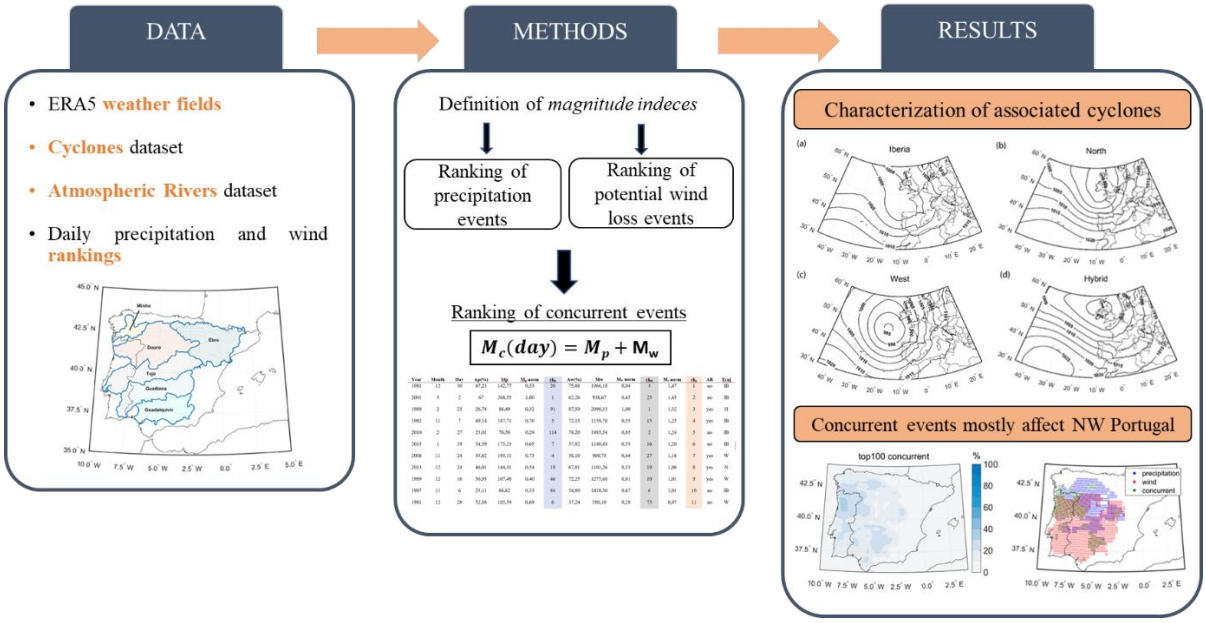

Highlights

- Context and motivation

Extreme precipitation and severe winds are responsible for notable economical and societal losses in the Iberian Peninsula (IP). Very often such extreme weather phenomena develop within cyclonic systems and their related mechanisms as for the horizontal water vapor transport through Atmospheric Rivers (ARs). The concurrence of precipitation and wind extremes has been investigated for some well-known recent storms whereas very few studies aim for a more comprehensive (regional) analysis.

- Data (period considered: wintertime 1979-2018)

- Weather fields from ECMWF ERA5 reanalysis;
- Cyclones database (Trigo, 2006);
- Atmospheric Rivers (ARs) database (Ramos et al., 2016a).

- Methods

Concurrent extreme precipitation and wind events on the IP and its main river basins are ranked according to a magnitude index that is obtained by combining two existing indices for precipitation and wind, respectively. Composite and manual analysis of the underlying synoptic conditions is pursued over the top100 most extreme concurrent events including (1) cyclones' trajectories, (2) the presence of an Atmospheric River (AR), (3) recurrent patterns in the locations affected by precipitation and wind extremes, (4) possible long-term trends.

- Results

It is more (less) likely for wind (precipitation) extremes to occur independently from precipitation (wind) extremes. Afterward, it is found that 85% of the top100 concurrent precipitation and wind extreme events are relatable to cyclonic features, which in most of the cases either cross the IP or pass to the northwest. Indeed, concurrent events are more frequent in the western sectors of the IP and during wintertime whereas, in recent decades, a decreasing trend is observed in autumn. ARs are more likely associated with the top-ranked events, especially those affecting the northwestern sector of the IP (Douro and Minho river basins).

Keywords: frontal climatology, frontal precipitation, fronts, midlatitudes, North Atlantic storm track.

3.1 Introduction

The concept of compound weather and climate events has been gaining more attention in recent years since the IPCC introduced this new paradigm for studying extremes and adapting to weather-related risks (Seneviratne et al., 2012), and stressed the need for new approaches that assume the impacts' perspective. Some authors have further discussed on the concept of compound events, completing the framework proposed by the IPCC with statistical insights (Leonard et al., 2014; Zscheischler and Seneviratne, 2017; Hao et al., 2018). The societal, natural and economic impacts of extreme compound events typically show complex causal chains, described by the joint probability of several inputs (Sadegh et al., 2018). For example, evaluating coastal flood risk based exclusively on sea-level rise scenarios or storm surges has the caveat that it does not consider the role of precipitation and its control on river discharge and soil moisture content, which might locally enhance the size of the coastal flood (e.g., Moftakhari et al., 2017; van den Hurk et al., 2015; Kew et al., 2013).

On the other hand, a certain wind regime might combine with long-term drought and with a local heatwave, triggering wildfires (Ruffault et al., 2017). Therefore, one of the most acknowledged definitions of compound weather event refers to it as a combination of drivers and/or hazards that contribute to societal or environmental risks (Zscheischler et al., 2018). The drivers might not be extremes themselves, but they can be responsible for an extreme impact when acting simultaneously. In the framework of compound events, several other combinations of concurrent drivers have been explored: concurrent cyclones, fronts, and thunderstorms (Dowdy and Catto, 2017), concurrent Atmospheric Rivers (ARs) and precipitation (Ramos et al., 2015; Lavers and Villarini 2013), concurrent ARs and cyclogenesis (Ferreira et al., 2016; Eiras-Barca et al., 2018b).

In the midlatitudes, it is common to experience concurrent precipitation and wind events: they are typically associated with the same mesoscale and/or synoptic features like extratropical cyclones (e.g., Reale and Lionello, 2013; Pfahl, 2014; Raveh-Rubin and Wernli, 2015), which are enhanced by local features such as the orography or the presence of water bodies (Veals et al., 2015; Martius et al., 2016). Within extratropical cyclones, concurrent wind and precipitation are likely to occur along with frontal structures (Catto and Pfhal, 2013; Schemm et al., 2016) and their intensity scales with the frontal strength (Schemm et al., 2017; Raveh-Rubin and Catto, 2019). For the Iberian Peninsula (IP) extreme windstorms and extreme precipitation are among the costliest natural hazards (Lorente et al., 2008; Pereira et al., 2018;

Liberato and Trigo, 2014). This topic has become of great interest to the general public, stakeholders, and reinsurance companies, which deal with increasing rebuilding costs and due compensations, in the framework of increasing risk under climate change (Munich Re, 2018; Aon-Benfield 2018). As a matter of fact, precipitation and wind extremes have been mostly approached individually in the literature, as if they were unrelated to each other.

Pinto et al. (2012) provided evidence that the projected increase of windstorm-related losses for the XXI century in Europe can be largely attributed to changes in the meteorological severity of the events. Other studies suggest that even if the total number of extratropical cyclones remains stable, the number of extreme cyclones affecting Western Europe in the future may slightly increase in association with an intensified polar jet extended towards Europe (e.g., Pinto et al., 2009, Ulbrich et al., 2009; Raible et al., 2018; Catto et al., 2019). For these reasons, shorter return periods for extreme windstorms and associated losses are estimated for most of Europe (e.g., Della-Marta and Pinto, 2009; Donat et al., 2011; Karremann et al., 2014). Factors such as changes in the damage swath of a cyclone (Hewson and Neu, 2015) relative to highly populated areas are also important to explain the trend for estimated losses.

Extreme precipitation over Western Europe has been explored through case studies analysis (e.g., Fragoso et al., 2010; Vicente-Serrano et al., 2011; Trigo et al., 2014; Liberato, 2014; Trigo et al., 2016) and more systematic approaches such as for cyclone clustering (Pinto et al., 2014; Priestley et al., 2017) and daily precipitation ranking (Ramos et al., 2014a; Ramos et al., 2017). In Ramos et al. (2014a) extreme precipitation days have been ranked over the entire IP and several sub-domains, considering both the intensity of the precipitation and its spatial extent. Indeed, it is known that the precipitation regimes of the IP exhibit marked spatial and temporal variability (Trigo, 2008; Gallego et al., 2011): convection mainly affects southern Iberia and the Mediterranean coast (e.g., Paredes et al., 2006; Nieto et al., 2007; Hidalgo-Muñoz et al., 2011) whereas larger-scale features such as water vapor transport are responsible for precipitation enhancement in the northwestern sectors (e.g., Ramos et al., 2015; Lavers and Villarini, 2013; Ferreira et al., 2016). Eventually, mountainous areas experience a topographic enhancement of precipitation on the windward side and wind enhancement and drier conditions leeward (Martius et al., 2016; Khodayar et al., 2018).

Concurrent precipitation and wind events have been only recently explored at a global scale (Martius et al., 2016; Dowdy and Catto, 2017) whereas regional comprehensive analyses,

such as for the Iberian Peninsula are still missing. This study aims to quantitatively assess the intensity and the frequency of precipitation and wind concurrent events on the IP during the last decades, looking for similarities and differences with solely extreme precipitation and extreme wind episodes. This is achieved by exploring a ranking of concurrent precipitation and wind extreme events, obtained through an update of two available daily rankings, one for potential wind loss events (Karremann et al., 2016) and one for extreme precipitation days (Ramos et al., 2014a). In light of the abovementioned discussion, the top100 concurrent events are characterized in terms of synoptic underlying conditions and the concurrence of ARs is searched.

All data sources and methodologies used to detect and rank weather features and hazards are described in Section 3.2. The results are presented in Section 3.3. Conclusions and Discussion complete the paper (Section 3.4). In the Supporting Information, the full list of the top100 concurrent events is shown.

3.2 Data and Methods

3.2.1 Weather fields

MSLP, precipitation and wind fields are obtained from the last release of the European Centre for Medium-Range Weather Forecast (ECMWF) reanalysis ERA5 (Hersbach et al., 2020), on an hourly basis, with a horizontal spatial resolution of 0.25° (31km) on a latitude/longitude grid. The dataset covers the period 1979-2018 and only extended winter months (October to March) are considered in this study. Daily precipitation sums correspond to the precipitation accumulated between 00 UTC (timestep 01 UTC of day n) and 00 UTC on the next day (timestep 01 UTC of day n+1). Hourly instantaneous 10m-wind components are provided in ERA5 for wind speed values computation.

3.2.2 Cyclones detection and tracking

Cyclones' centers are located and tracked over the Euro-Atlantic European sector according to the methodology proposed in Trigo (2006), based on ERA-Interim data. Potential storms are searched as minima in the geopotential height field at 1000 hPa, after applying a set of tunable thresholds for the geopotential gradient (see Trigo, 2006 for details). The cyclones tracking is based on the nearest neighbor approach in the previous field, given a maximum

speed for the center of the storm of 300km/6h in the westward direction and of 660km/6h in any other direction. Finally, this dataset only accounts for cyclones with a minimum lifetime of 24h. This detection and tracking methodology was shown to be appropriate for applications in the extra-tropics, both in terms of systematical and climatological analysis and individual case studies (Neu et al., 2013).

The extratropical cyclones are then classified according to their trajectories following Karremann et al. (2016) methodology which includes four categories: cyclone tracks that cross over Iberia (Iberia), cyclone tracks that cross north of Iberia steering to Central Europe (North), cyclone tracks that cross west of Iberia steering to the British Isles (West) and a fourth category (Hybrid) that includes situations in which the cyclone itself is not determinant for the weather extremes, as it might happen when strong and persistent pressure gradients extend on the IP. This classification was devised to characterize extreme windstorms and related potential wind-loss events but, as discussed in the Introduction, the authors believe this scheme can be applied consistently also to concurrent wind and precipitation events.

3.2.3 Atmospheric Rivers (ARs)

The dataset of occurrences of persistent ARs for the IP is obtained through the methodology described in Ramos et al. (2016a) which relies on an Integrated Vapor Transport (IVT)-based detection scheme successfully employed in previous studies (Lavers et al., 2012; Lavers and Villarini, 2013; Ramos et al., 2015). The detection scheme is applied in this work to 6-hourly IVT fields from ERA5 reanalysis by ECMWF, covering the extended winter months for the 1979-2018 period.

ARs affecting the IP are searched at each grid point and at each time step between 35°N and 45° N along a reference meridian located at 9.75° W and they are defined as local exceedance of the 85th percentiles of the maximum IVT values. For a grid point whose IVT exceeds the local threshold to be labeled as part of an actual AR, a minimum length criterion is applied to the neighborhood grid points, filtering ARs shorter than 1500km. Finally, the persistency of ARs is also requested, through a minimum duration threshold of 18h (that is, the AR is detected for three continuous timesteps and within 4.5° from the first IVT maximum considered). It was shown that this methodology only retains the most extreme ARs and therefore their frequencies are not that high as compared with other studies (Shields et al., 2018). The entire procedure and detection scheme are presented in detail in Ramos et al. (2016a).

3.2.4 Precipitation and wind ranking

The precipitation ranking technique is derived from Ramos et al. (2014a). The ranking covers the period up to 2008 as it is based on IB02, the most comprehensive ground-based daily precipitation dataset available for the IP (Belo-Pereira et al., 2011; Herrera et al., 2012), whose records are not available for recent years. In this study, ERA5 reanalysis data are used instead, given the outcomes of Hénin et al. (2018b) where different precipitation data sources were compared to IB02 on the IP and ERA5 accounted for the best accuracy metrics. Eventually, the ranking produced here covers the period 1979-2018 and daily accumulated precipitation is obtained as the sum of hourly values, as described in Section 3.2.1.

The precipitation anomaly is defined as the normalized daily precipitation departure from seasonal climatology, which is evaluated at all grid points, as in the following:

$$N_{ij} = \frac{(P_{ij} - \mu_{ij})}{\sigma_{ij}} \tag{3.1}$$

where P is the daily precipitation sum, μ is the 7-day running mean for that day and σ is the standard deviation from that mean. Any departure greater than 2σ is considered as a precipitation anomaly. Given the high spatial variability of precipitation regimes over Iberia, a magnitude index is computed for each day considering both the extension of the area affected by the precipitation anomaly (A, as a fraction of all the IP grid points) and the mean of the anomaly over the area (M). The magnitude index is thus given by the product of the two quantities:

$$M_p(day) = A \times \mathrm{M} \tag{3.2}$$

As indicated in Ramos et al. (2014a), the 2σ threshold does not substantially differ from the 95th percentile of the daily precipitation extremes, which is more commonly used as a reference for attributing extremes.

The wind ranking is derived from Karremann et al. (2016). The methodology ultimately relies on the work of Klawa and Ulbrich (2003) and following updates (Pinto et al., 2007; Pinto et al., 2012). It is based on a potential wind-loss model where extreme wind days are ranked according to a magnitude index that grows as the cube of maximum wind speed (assuming a cubic relationship between wind speed and kinetic energy flux) as follows:

$$M_w(day) = \sum_{i=1}^{N} \sum_{j=1}^{M} \left(\frac{v_{ij}}{v_{ij}^{98}}\right)^3 \times I\left(v_{ij}, v_{ij}^{98}\right) \tag{3.3}$$

$$I\left(v_{ij}, v_{ij}^{98}\right) = \begin{cases} 0 & v_{ij} < v_{ij}^{98} \\ 1 & v_{ij} > v_{ij}^{98} \end{cases} \quad (3.4)$$

where v_{ij} is the largest of 24 hourly 10m wind speed values for the specific grid point and v_{ij}^{98} is the 98th percentile for the grid point based on climatology. M and N indicate the total number of grid points in the zonal and meridional directions (continental IP). The use of ERA5 allows for a more accurate search for maximum daily wind speed with respect to Karremann et al. (2016), where 6-hourly data from ERA-Interim were used. As for precipitation, the new wind ranking produced in this study is updated to 2018.

3.2.5 Ranking of concurrent precipitation and wind events

A unified ranking of concurrent wind and precipitation days is obtained by combining the two individual rankings previously described, with equal weight. The magnitude indices for both precipitation and wind (namely Mp and Mw) are first scaled into the range [0, 1] and summed to produce a unique normalized magnitude index for each day. Then, only the days whose both magnitude indices are greater than 0 (which means that at least one grid point recorded extreme precipitation and extreme wind, respectively) are retained.

However, in this study, only a shortlist of the most extreme events is considered for in-depth analysis. At first, the top100 extreme days from the ranking of concurrent precipitation and wind are considered. Each of the selected days is then characterized in terms of large-scale atmospheric conditions, namely by identifying the low-pressure system that is compatible with the local precipitation and wind extremes footprints. Cyclones from the database of Trigo (2006) are searched over a domain that covers the Eastern Atlantic Ocean, the IP and the English Channel. The cyclone tracks are compared to the ERA5 fields (MSLP, wind and precipitation) to verify consistency. Based on this analysis, the tracks are assigned to the four classes and to the spatial pattern of wind and precipitation anomalies. This warrants a consistent and robust classification, although ultimately subjective.

Afterward, whenever it is noted that two consecutive days that appear in the top100 of the concurrent ranking are related to the same cyclone, those particular days are considered as belonging to the same event. This might happen in three situations: (1) when the cyclone is slowly moving and extremes are recorded over several days, (2) when the most intense part of an event occurs close to midnight and (3) when the dynamics of the event is characterized by strong pre-frontal precipitation bands, followed by extreme wind that is recorded on the next day.

Given this new "event" perspective, every time two (or more) days within the top100 shortlist are referred to as a unique event, other days are included in the shortlist, scrolling down the original daily ranking of concurrent precipitation and wind, until a total number of 100 events (daily or multi-daily) is reached again. Eventually, 12 two-day events are found for Iberia. For those occurrences, only the day that ranked higher is included in the top100 concurrent list of precipitation and wind events (the full list is provided in Tab. 3.1.S in Supporting Information). The entire procedure to obtain top100 precipitation and wind concurrent extreme events described in the previous paragraph is repeated for Portugal and Spain separately (Fig. 1a), for the six main river basins of the IP, namely Minho, Douro, Tejo, Guadalquivir, Guadiana and Ebro (Fig. 3.1b) and for 4 geographical quadrants used to regionalize the IP (Fig. 3.1a). These kinds of regionalization are inspired by previous studies that focused on precipitation and wind extremes (e.g., Nieto et al., 2007; Lorente-Plazas et al., 2015; Ramos et al., 2014a).

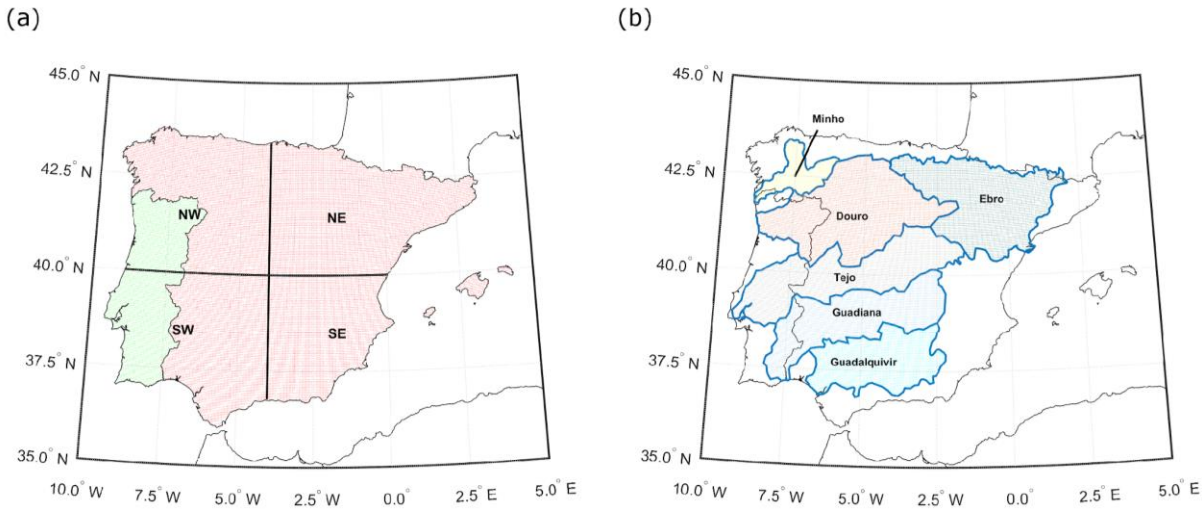

Figure 3.1. Main domains considered in this study: (a) Spain, Portugal and the 4-quadrants regionalization and (b) the 6 main river basins, namely Minho, Douro, Tejo, Guadiana, Guadalquivir and Ebro.

3.3 Results

3.3.1 Revision of existing rankings

The individual rankings for precipitation and wind extremes obtained in this paper for the period 1979-2018 can be considered as consistent updates of the two mentioned available rankings, by Ramos et al. (2014a) and Karremann et al. (2016), respectively. Correlation analysis for the magnitude (and thus, the position in the ranking) of extreme days for the respective common periods is pursued. For 1979-2008 daily precipitation extremes, the IB02-based ranking from Ramos et al. (2014a) and the ERA5-based ranking presented in this study have a correlation coefficient of 0.92 (Kendall's Tau rank correlation test). On the other hand, the correlation coefficient between the ERA-Interim-based ranking of potential wind-loss days from Karremann et al. (2016) and the corresponding one produced for this study is 0.79 (Kendall's Tau correlation test), for the common period 1979-2015. This suggests that the use of hourly ERA5 data had a greater effect on the wind magnitude index than on the precipitation index although the correlation of the new rankings with the corresponding former versions is strong. Therefore, the revision presented in this paper is robust and allows for any further extension of the rankings and related analysis to the present time. Afterward, rank correlation is searched between the new precipitation and wind rankings for the top20, top50 and top100 most extreme concurrent events. The non-parametric Wilcoxon rank-sum test, applied to the distributions of the scores, shows that there is no statistical evidence for differences between the rankings ($z=-1.284$ and $p=.199$, $z=-0.299$ and $p=.764$, $z=0.419$ and $p=.675$ for top100, top50 and top20 respectively) with a confidence level $\alpha=0.05$.

3.3.2 Decadal and seasonal variability

In the first part of this study, the ranking of concurrent precipitation and wind extreme events for the IP is compared with the two new individual rankings of extreme precipitation and extreme wind, by considering the respective top100 records (Tab. 3.1). For the IP, 69% (54%) of the days of the top100 precipitation (wind) rankings are also included in the top100 concurrent precipitation and wind event ranking. That is, wind extremes are more likely to occur independently of precipitation extremes. This is valid also for Spain and the SW sector while the opposite behavior is observed in the NW sector that is, extreme precipitation events are less frequently associated with wind. In Portugal and the northernmost river basins, the fraction of days that appear in both the individual and the concurrent ranking is substantially

equal for precipitation and wind. Less than 50% of the top100 extreme wind days are associated with extreme precipitation in the SE sector as well as in Tejo, Guadiana and Guadalquivir river basins. The Ebro river basin shows a completely different pattern with only 38% of the top100 extreme precipitation days associated with extreme wind.

Table 3.1. Fraction of days that appear in both the concurrent precipitation and wind rankings and the respective individual rankings (%).

month	IP	SP	PT	Minho	Douro	Tejo	Guad	Guadalq	Ebro	NW	NE	SW	SE
prec	69	64	63	55	58	57	61	53	38	59	50	70	47
wind	54	52	66	58	59	49	47	47	52	71	51	50	40

The 10-year running mean (the choice is arbitrary but in agreement with previous similar studies) for the number and intensity of extreme precipitation days, extreme wind days and concurrent extreme precipitation and wind events is explored on the IP for different intensities (top20, top50 and top100 - Fig. 3.2). No clear changes are observed over the last decades in terms of the intensity of the events (Fig. 3.2b). However, a certain variability affects the yearly frequency of the extremes and this holds for precipitation, wind and concurrent precipitation and wind events (Fig. 3.2a). Until 1996, the frequency of the extremes is steady, with very few occurrences of top20 extreme precipitation days. Then, for a decade, the yearly number of extreme events (precipitation, wind and concurrent precipitation and wind) increases for top50 and top100. Over the same period, top20 concurrent and wind events remain stable whereas top20 precipitation events peaks in 2000-2001. The following decade is characterized by a slight drop from 2005 to 2010, followed by another increase until the present time, which is more robust for the top100 and top50 sets of events, and less pronounced for the top20. Over this last period (2005-present), the average number of wind extremes events is steadily larger than extreme precipitation events, especially for the top20. The frequency of top100 concurrent extreme events (but this holds also for precipitation and wind separately) increased over time but no remarkable changes affected top20 and top50: the number of events that ranked in the top100 passed from around two to almost three over the last decades. However, this is likely driven by two remarkable stormy winter seasons: 2013-2014 (as documented in Matthews et al., 2014; Muchan et al., 2015; Priestley et al., 2017) and 2017-2018 (Leitão et al., 2018). Indeed, the very last winter season accounts for 7 over 100 events in the Iberia ranking and 6 of these 7 events come from March 2018, when Portugal experienced a record-brake number of storms.

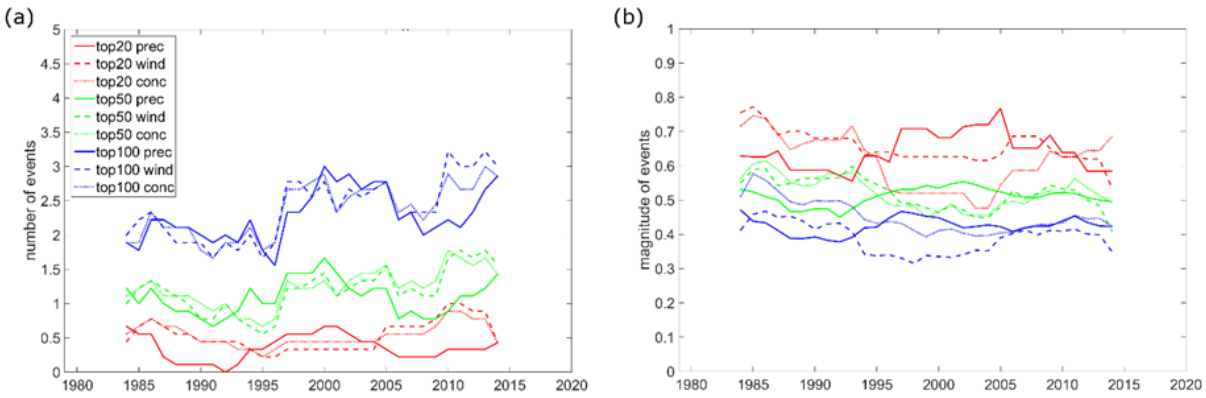

Figure 3.2. (a) 10-year running mean for the number of events per extended winter and (b) 10-year running mean for the normalized magnitude of the events. In both panels, red, green and blue lines refer to top20, top50 and top100 extreme concurrent events, respectively. Solid, dashed and dotted lines refer to precipitation, wind and concurrent precipitation and wind extremes, respectively.

The temporal variability of the top100 concurrent extremes on the IP is analyzed also at the seasonal scale. As the period considered covers 4 decades, any attribution of trend should be done with caution. For concurrent precipitation and wind events (Fig. 3.3a), no clear signal is found of a relationship between the intensity of the events (given by their position in the ranking) and the seasonality, nor clear changes of seasonality over time. Considering wind and precipitation extreme events separately (Fig. 3.3b and 3.3c, respectively), still no clear trend is found for the intensity of the events whereas there is a certain variability of seasonality: it is observed that from 1979 to 2018, the number of extreme wind(precipitation) events occurred in March is 18 (21) of which only 3 (4) occurred in the first half of the time period (1979-1999). This increase in the number of late-winter occurrences maintains even if the exceptional March 2018 is neglected. On the other side, there is a weak signal of a recent decrease in the number of occurrences in autumn: the fraction of top100 precipitation (wind) events that occurred in the first half of the extended winter season (OND) diminished from 57% (62%) during the period 1979-1999 to 37% (33%) during 2000-2018. Early autumn is particularly affected: since 2010, no top100 extreme precipitation events are recorded in October and no top100 extreme wind events are recorded in both October and November.

Relative frequencies of precipitation and wind concurrent extreme days during the extended winter season are compared among the different domains (Tab. 3.2). For the whole IP and Spain, extreme concurrent days most likely occur in the second half of extended winter (58% vs 42%), mainly because November and especially October do not provide for several occurrences (15% and 6% respectively). However, October accounts for slightly more records than March in Portugal (17% vs 15%) and therefore, on average, extreme concurrent days are

more equally spread over time. A similar pattern is observed for Minho, Douro and Tejo river basins whereas Guadiana, Guadalquivir and Ebro slightly differ for having fewer occurrences in early autumn. This pattern reflects in the 4-quadrant regionalization: NW and SW sectors behave quite identically, with higher frequencies in December and January, followed by February, whereas for the NE and especially the SE sectors the season of concurrent precipitation and wind events is shifted ahead. Therefore, the months with the largest relative frequencies are either December or January for all the domains but Ebro and the SE sector, whose peak (23%) occurs in February and March, respectively.

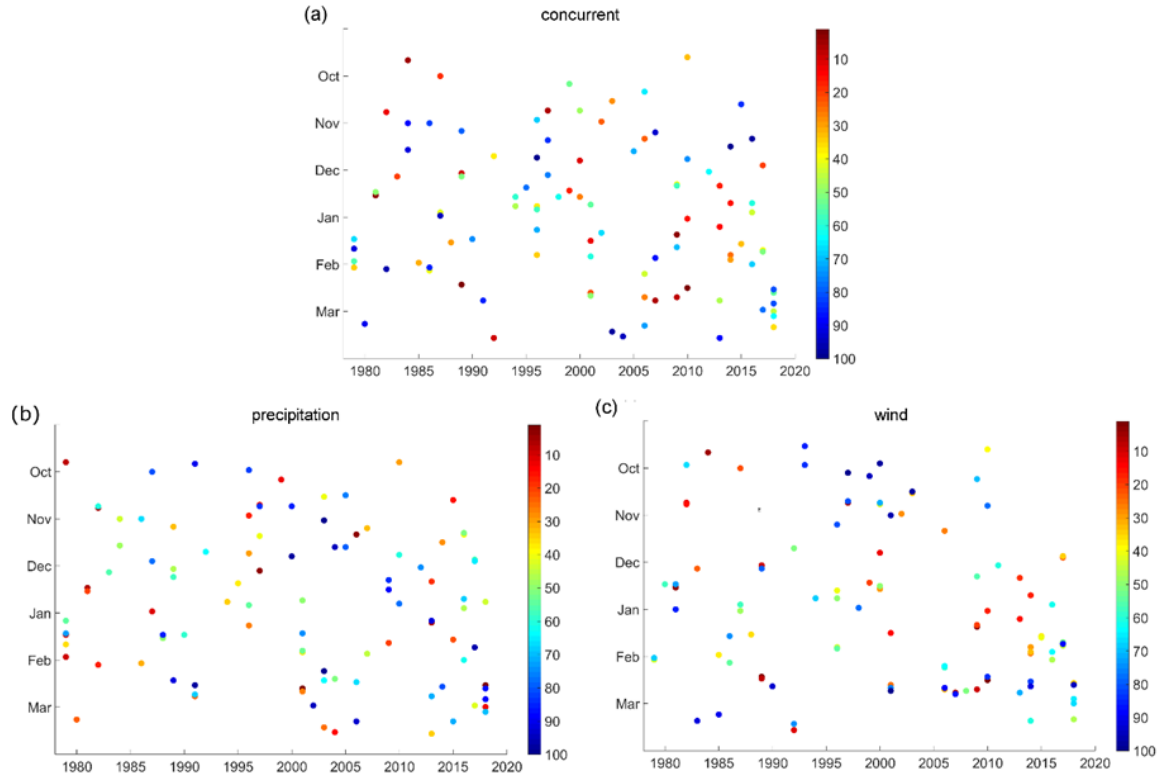

Figure 3.3. (a) Time distribution of top100 concurrent extreme events for extended winters 1979-2018 on the IP. Colors represent the rank of the event. Same for precipitation extremes (b) and wind extremes (c).

Table 3.2. Frequencies (%) of extreme concurrent days.

month	IP	SP	PT	Minho	Douro	Tejo	Guad	Guadalq	Ebro	NW	NE	SW	SE
Oct	6	6	17	15	19	15	10	12	10	13	12	12	7
Nov	15	15	9	10	12	11	12	16	10	12	10	12	12
Dec	21	20	22	22	15	20	23	21	19	23	21	23	20
Jan	19	20	19	25	22	22	22	18	19	21	19	22	21
Feb	20	20	18	15	14	17	20	18	23	14	21	16	17
Mar	19	19	15	13	18	15	13	15	19	17	17	15	23

3.3.3 Associated Atmospheric Rivers and cyclones

The concurrency of extreme precipitation and wind events with potential drivers such as ARs pouring on the IP and extratropical cyclones is explored. ARs are detected according to the spatio-temporal criteria described in Section 3.2.4 and both persistent and non-persistent ARs are considered (Tab. 3.3).

Table 3.3. Frequencies (%) of persistent (non-persistent) Atmospheric Rivers for different subsets of the most extreme concurrent events list.

	IP	SP	PT	Minho	Douro	Tejo	Guad	Guadalq	Ebro	NW	NE	SW	SE
top100	17(26)	17(27)	16(29)	22(35)	20(31)	15(28)	12(20)	12(19)	8(18)	22(34)	11(19)	12(22)	10(12)
top50	22(36)	20(30)	24(40)	28(40)	32(42)	20(28)	18(24)	10(20)	4(14)	28(44)	14(24)	18(26)	14(18)
top20	35(50)	35(45)	40(50)	40(55)	40(55)	25(35)	15(25)	15(20)	5(10)	45(60)	15(25)	20(25)	20(30)

In the IP, and in Spain and Portugal separately, fewer than 20 of the top100 precipitation and wind concurrent events, do show an associated persistent AR (detected for at least 3 consecutive time steps, that is, 18h). ARs play a major role in the northernmost river basins, namely Minho and Douro, where they are detected in 22% and 20% of the top100 cases, respectively. Consequently, in the NW sector, a similar value is observed. The ARs frequency for the southern and eastern river basins, and so it holds for the NE, SE and SW sectors, decreases to 12% for Guadiana and Guadalquivir and to 8% for Ebro. The Tejo river basin represents a transition zone, with 15% of the top100 events attended by an AR. All these frequencies increase by around ten percentage points if also non-persistent ARs are considered (that is, an AR detected for at least one-time step - values in brackets in Tab. 3.3) except for the SE sector. The frequencies also increase with the increasing intensity of the events. For the IP and Spain, 35% of the respective top20 do have an associated persistent AR. Portugal and the northernmost river basins top 40%, whereas for the other river basins no relationship is observed between ARs and the intensity of the events. If also non-persistent ARs are included in the statistics, up to 55% of the top20 concurrent events are associated with an AR in Minho and Douro river basins, and up to 50% in Portugal and the whole IP. The frequencies increase to 25%, 20% and 10% for Guadiana, Guadalquivir and Ebro river basins, respectively. The Tejo river basin behaves more similarly to the northernmost basins even though the frequency of ARs is generally lower. With the 4-quadrant regionalization, the NW sector stands out as the most relatable to ARs. Frequencies of ARs are higher than all the other sectors, and they top 45% (60%) out of the top20 events for persistent and non-persistent ARs, respectively. The

frequency of ARs in the other sectors never exceeds 30% and is less sensitive to the extremeness of the events as well as to the persistency of the ARs.

Eventually, the top100 concurrent precipitation and wind extreme events are characterized through the underlying synoptic pattern which is, in most of cases, driven by a clear cyclonic structure. Bearing in mind the classification scheme suggested by Karremann et al. (2016), this holds for the Iberia (IB), North (N) and West (W) categories whereas the Hybrid category includes all the other situations where the cyclone appears far away from the IP but still, its influence extends over the IP domain. Therefore, the synoptic patterns associated with the top100 concurrent precipitation and wind events are classified: the relative frequencies for each category are shown in Tab. 3.4 whereas the MLSP composites are shown in Fig. 3.4.

Table 3.4. Frequencies (%) of cyclones trajectories for top100 and top20 (in brackets) concurrent events.

traj	IP	SP	PT	Minho	Douro	Tejo	Guad	Guadalq	Ebro	NW	NE	SW	SE
IB	43 (45)	46 (50)	40 (45)	22 (35)	31 (45)	50 (55)	45 (45)	52 (65)	33 (40)	28(30)	37(60)	48(65)	43(40)
N	18 (5)	17 (15)	17 (15)	35 (35)	23 (25)	15 (5)	14 (10)	14 (15)	12 (12)	30(25)	14(5)	14(10)	14(25)
W	25 (35)	21 (30)	36 (30)	31 (15)	30 (30)	33 (35)	25 (35)	25 (20)	7 (5)	31(30)	9(10)	34(25)	9(5)
H	14 (15)	16 (5)	7 (10)	12 (15)	16 (0)	13 (5)	11 (10)	9 (0)	47 (40)	11(15)	40(25)	4(0)	34(30)

Within the top100 most extreme events, the cyclones that directly cross the IP are dominant (>40%) in both Spain and Portugal (and thus the entire IP and its four quadrants). Cyclones belonging to the N class are also equally frequent in the three main domains (17%/18%). The categories W and H are differently represented instead: while the former is more common in Portugal than in Spain (36% vs 21%), the latter is more common in Spain (16% vs 7%).

Regarding the six river basins, it is shown that the IB category is the most frequent also for Douro, Tejo, Guadiana and Guadalquivir. For Tejo and Guadalquivir around half of the events are associated with an IB cyclone. In the Minho river basin, most of the concurrent extreme events are related to the N category (35%), followed by W (31%) and IB comes only in third position (22%). In fact, in the Douro river basin IB and W are almost equal (31% and 30% respectively). In terms of frequency, the W category proceeds N in the majority of the river basins except, as highlighted before, Minho and also Ebro where, however, both W and N have low occurrences (19% in total). Indeed, the frequency pattern for the Ebro river basins is rather polarized between H and IB (47% and 33%). The above-described pattern gets sharper when considering only the 20 most extreme concurrent events (values in brackets in Tab. 3.4). Of notice are the following features: (1) IB becomes the most frequent category also for Douro

and Minho (for the latter IB equals N); (2) the H category is under-represented in all the domains with respect to the top100.

Regarding the four-quadrants regionalization, the IB category is predominant in the southern sectors whereas in the NE it is second to H, and in the NW sector no preferential trajectory is observed, given that IB, W and N are equally frequent, and they explain one-third of the events each. In the eastern sectors, the H configurations are well represented because of the signal due to the cut-off lows which have been included in this category and represent an important climatological feature for these regions (Nieto et al., 2007). Conversely, cyclones whose trajectory is N or W rarely yield to extremes far east in the peninsula (together they represent less than 25% of the occurrences in the top100 events for the NE and SE sectors).

Even though the cyclones' trajectories have been classified into four groups the accurate screening that has been pursued all over the 100 concurrent precipitation and wind events that occurred in each of the domains considered, revealed a certain internal variability within some of the categories. For clarity, this further classification is not included in Tab. 3.4 of the manuscript, but further details on possible sub-categories are provided in Tab. 3.2.S and following paragraphs in Supporting Information.

Besides the classification of the cyclones associated with the top100 concurrent precipitation and wind events, any recurrent pattern on the IP regions that are affected by extremes is searched. The main purpose is to identify any possible hotspot for precipitation, wind and concurrent precipitation and wind extremes (Fig. 3.5) and secondly to associate them with each of the four classes considered for cyclones' trajectories (Figs. 3.6 to 3.8). Therefore, the analysis is based on the relative frequency of weather extremes at each grid point where extreme precipitation is defined as a departure from seasonal climatology greater than 2σ (Eq. 3.1) and extreme wind is based on the exceedance of the local 98th percentile (Eq.3.3).

Within the top100 concurrent events, the areas that are most frequently affected by wind extremes extend further south than for precipitation (Fig. 3.5b vs Fig. 3.5a), exceedances of the local 98^{th} percentile of wind speed are mainly observed (70%) in the SW sector of the IP, corresponding to the administrative regions of Alentejo (Portugal), Extremadura and Andalusia (Spain). Around 50 out of the top100 concurrent events do show precipitation extremes in the North of Portugal and in Central/Northwestern Spain, an area that almost exactly corresponds with the Douro river basin. Finally, concurrent precipitation and wind extremes are mainly observed in the north of Portugal and widespread in Southwestern Spain (Fig. 3.5c).

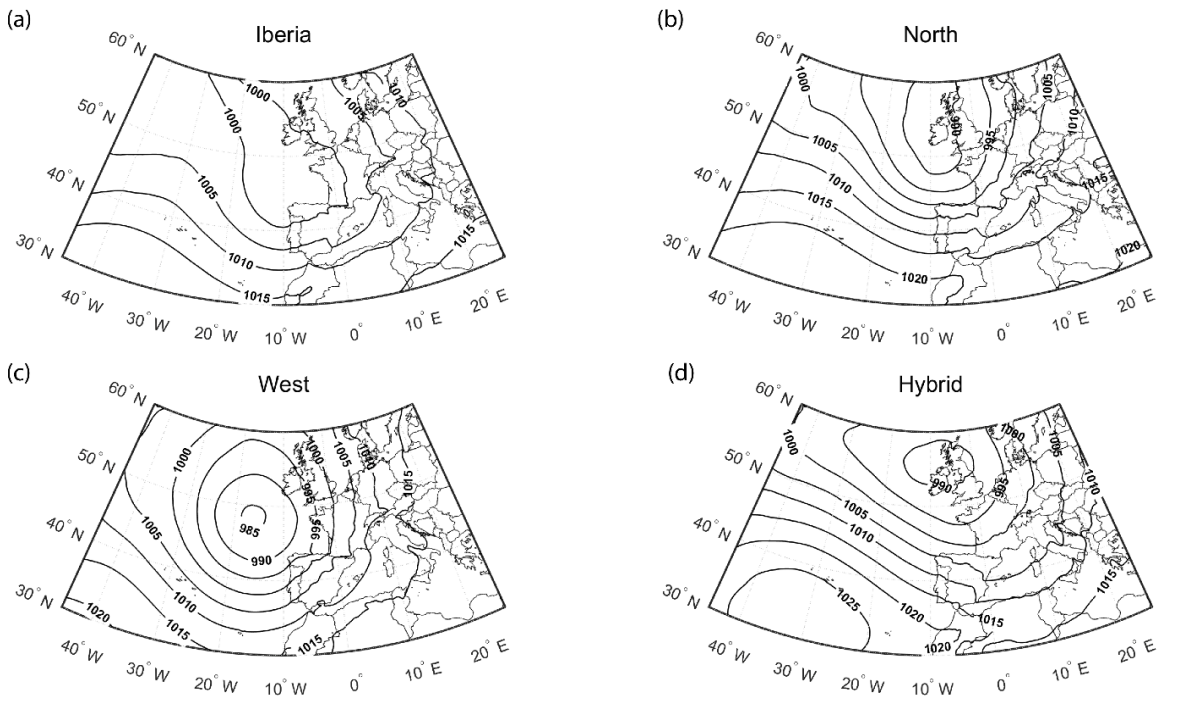

Figure 3.4. MSLP composites for the four categories of cyclones' trajectories: (a) Iberia – 43 events, (b) North – 18 events, (c) West – 25 events, (H) Hybrid – 14 events. Composites are obtained by averaging all the four MSLP fields (00, 06, 12 18 UTC) from each event day.

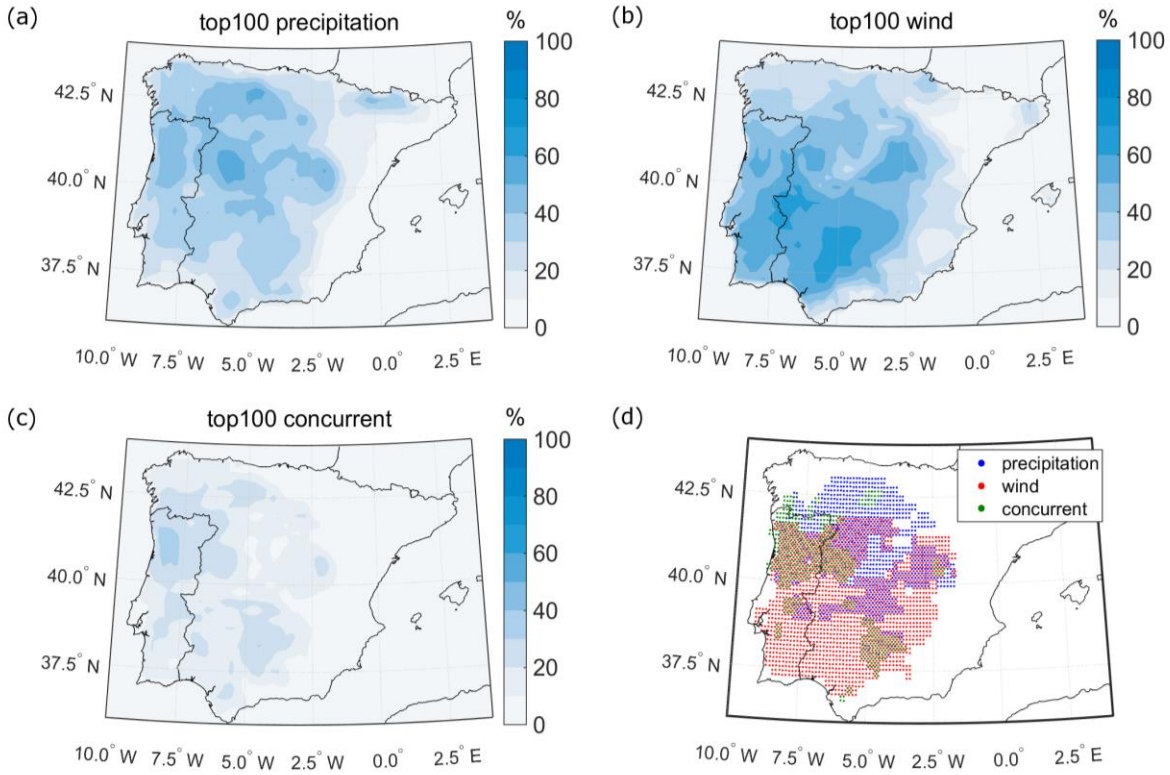

Figure 3.5. Areas affected by precipitation extremes (a), wind extremes (b) and concurrent precipitation and wind extremes (c). Color shading represents the frequency of extreme precipitation, with respect to the top100 concurrent precipitation and wind events. In panel (d) the information of the other panels is summarized. The shaded areas correspond to a normalized frequency >0.7 for each kind of extreme.

The events whose cyclones belong to the IB and W groups do show some similarities in the areas recurrently affected by extreme precipitation (Fig. 3.6a and 3.6c, respectively). These regions are mainly located in the western part of the IP with the IB events affecting slightly more continental sectors than W (maximum frequency observed: 65% and 80% for IB and W, respectively). More than 50% of the events belonging to N (Fig. 3.6b) occur all over an area that includes the Minho and Douro river basins whereas precipitation extremes associated with H events (Fig. 3.6d) insist over Northern Iberia (main peaks over the mountains) and northwestern Portugal. All the categories have secondary peaks of frequency over the Pyrenees.

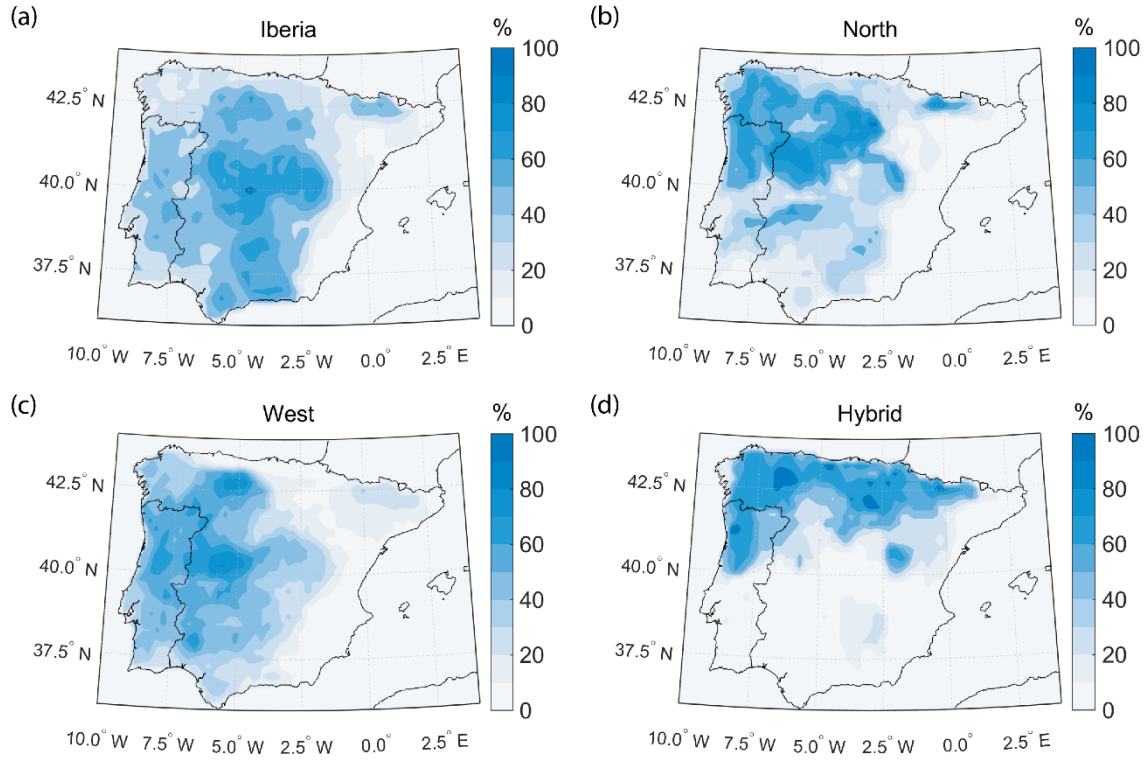

Figure 3.6. Areas affected by extreme precipitation (daily precipitation anomaly exceeding 2σ) in the IP for each of the four categories of cyclones' trajectories considered: (a) Iberia—43 events, (b) north—18 events, (c) west—25 events, (H) hybrid—14 events. Color shading represents the frequency of extreme precipitation, with respect to the total number of concurrent precipitation and wind events of each category.

The spatial pattern for recurrent wind extremes is sharper for the IB and W categories (Fig. 3.7a and 3.7c) compared to precipitation, whereas extremes are more spread all over the IP for N and H categories. The southwestern sector of the IP registered extreme wind for up to 75% of the events belonging to the IB and W classes. For events belonging to the N group (Fig. 3.7b), frequencies up to 70% are observed quite sparsely in the inner sectors of the IP whereas almost no events affected the Mediterranean, the Ebro valley and the northern Iberian coasts. H events (Fig. 3.7d) have a quite similar pattern to N, except for larger frequencies observed in the southern Mediterranean sectors. Therefore, the areas that most often experience concurrent precipitation and wind extremes are mainly located on central and western Iberia

for the IB categories (Fig. 3.8a - only spread spots), on western Iberia for W (Fig. 3.8c - peaks over Portugal and southwestern Spain), on northwestern Iberia for N and H (Fig. 3.8b and 3.8d, respectively), although the latter shows lower and more sparse peaks than N.

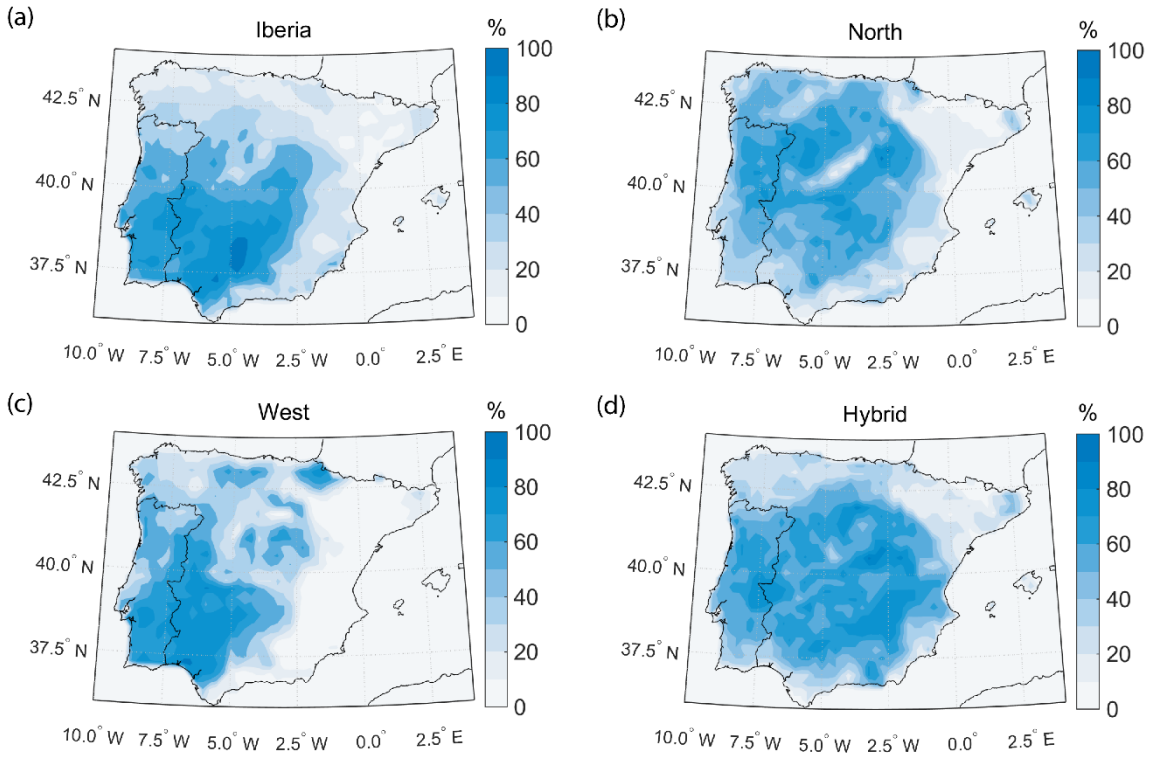

Figure 3.7. Same as Fig. 3.6 but for wind extremes (maximum daily wind speed exceeding 98th percentile).

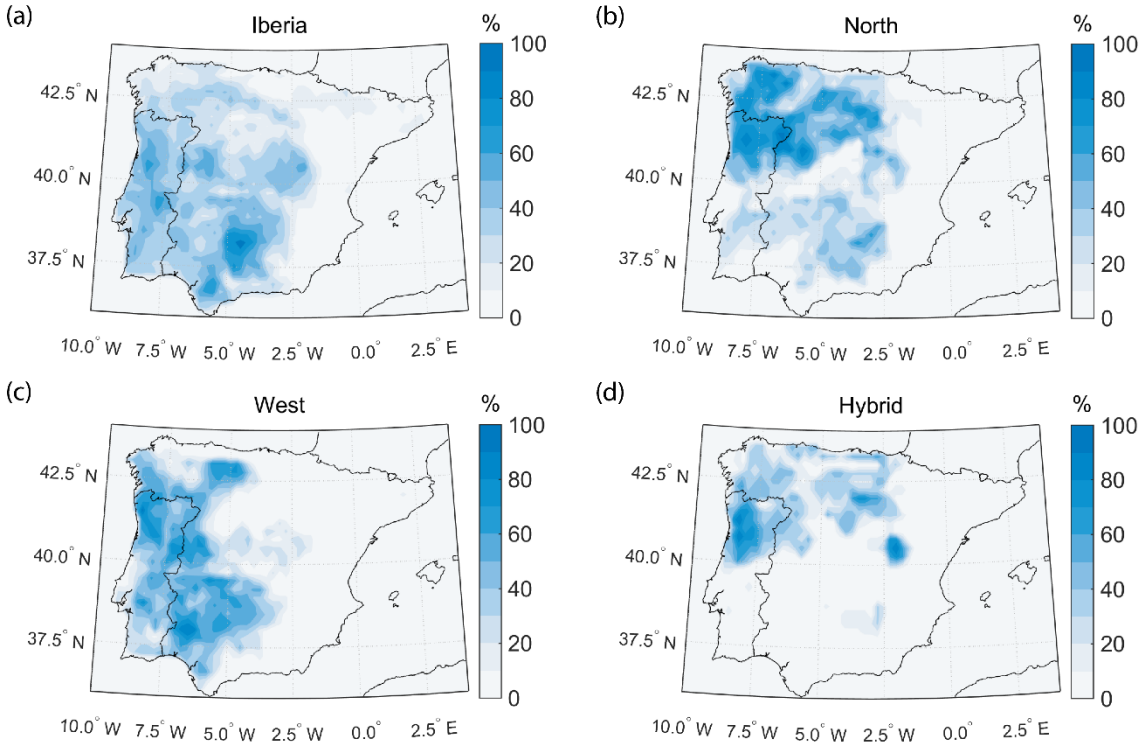

Figure 3.8. Same as Fig. 3.6 but for concurrent precipitation and wind extreme events.

3.4. Discussion and conclusions

Extreme weather events associated with both extreme precipitation and wind are analyzed on the IP domain and the main Iberian river basins. The objective is to provide for a consistent ranking of these events at the local scale, given that Western Europe and Iberia have been indicated as key areas for studying concurrent events. Two available rankings for precipitation and wind extremes, by Ramos et al. (2014a) and Karremann et al. (2016) respectively, are revised and updated based on ERA5 hourly data. A common ranking is produced and characterized in detail: concurrent precipitation and wind events are linked to both the occurrence of ARs and the characteristics of the parent cyclones.

The main results are summarized and discussed as follows:

1) In this study, 85% of concurrent precipitation and wind extreme events are clearly associated with a cyclonic feature. This value is 70% in Karremann et al. (2016), where only wind extremes were considered (and the Hybrid category was included, to describe those situations without a clear cyclone's imprinting). Most of the assigned cyclones belong to the IB category but for the Minho and Douro river basins N and W, respectively, are dominant. Indeed, considering the NW sector of the IP, there is no preferential trajectory for cyclones that produce concurrent precipitation and wind events and the occurrences spread equally among the three categories. The Hybrid category turns out to be prevailing in the eastern sectors and thus only for the Ebro river basin.

2) For each of the four categories of cyclones' trajectory, the locations with the largest frequency of concurrent wind and precipitation extremes are highlighted. Up to 60% of concurrent events belonging to IB and W categories affect specific areas of western Iberia and southwestern Spain. On the contrary, N and H patterns affect recurrently northern Portugal and northwestern Spain.

3) Concurrent precipitation and wind events in the IP and its subdomains prevail in winter, between December and January. Over the last decades, an increase in the frequency of late winter events, together with a decrease of autumn occurrences is observed for precipitation extremes and wind extremes. This is a consequence of (1) strong and prolonged droughts that extend to autumn-time (Coll et al., 2017; Parente et al., 2019) and (2) intense episodes of cyclones clustering on the edge of the extratropical storm track region as occurred in 2013/2014 (Matthews et al., 2014; Muchan et al., 2015; Priestley et al., 2017) and 2017/2018 (Leitão et

al., 2018). However, due to strong long-term variability, no clear trend is appreciable for concurrent precipitation and wind events.

4) The frequency of extreme precipitation, wind and concurrent precipitation and wind events has increased over the last decades (from 2 to almost 3 events per season), but the trend is primarily related to the weaker events of the top100. For wind extremes, this result is slightly different from Karremann et al. (2016), especially for the top100 set of events, where no trend was observed. This difference may be related to the different dataset and temporal resolution used to define the wind extremes. As hourly data from ERA5 are used here, the detection of extremes is expected to be more accurate.

5) Persistent ARs are concurrent to precipitation and wind extremes, especially for the most intense events. In the NW sector of the IP, in Portugal, and Minho and Douro river basins, at least 40% (50%) of the top20 concurrent events are attended by persistent (non-persistent) ARs. This relationship is weaker for the southern IP river basins and almost negligible for Ebro. In Ramos et al. (2015) the contribution of ARs towards extreme precipitation in the IP was also larger for the top-ranked extreme days and the different behavior of the northernmost and the southernmost (including Ebro) river basins was observed too. However, the frequencies of concurrent persistent ARs are sensibly smaller in this study (35% vs 75% on the whole IP). This suggests a stronger relationship of ARs with solely precipitation extremes, as expected considering the role played by moisture inflow in enhancing precipitation. In addition, given the higher threshold for IVT used in this study (following Ramos et al., 2016a), the detection rate of ARs is expected to be smaller compared to Ramos et al. (2015).

6) Portugal, and especially the Minho and Douro river basins (that is, the NW sector of the IP) are the regions that are most likely affected by concurrent precipitation and wind events. Here, the best match among the individual precipitation and wind rankings and the concurrent precipitation and wind ranking is observed: more than 60% of the top100 extreme precipitation (wind) days are also associated with extreme wind (precipitation). Martius et al. (2016), found frequencies between 40% and 50% in Iberia, with higher peaks right on the western coast of the Peninsula. These are the regions most exposed to extratropical cyclones, together with Galicia (Eiras-Barca et al., 2018a), where the winter climatology is mostly driven by the North Atlantic flux and moisture transport. Indeed, the NW sector of the IP is the subdomain with the larger correspondence among rankings. For the other subdomains, it is generally more likely for wind extremes to occur independently of precipitation.

7) The NE (including the Ebro river basin) and the NE sectors of the IB generally show different scores from the rest of Iberia, suggesting that their weather-extremes climatology is driven by different mechanisms. Similar signals, in terms of a weak relationship between meteorological extremes and ARs or extratropical cyclones, were found also in Ramos et al. (2015) and Merino et al. (2016), respectively. Therefore, concurrent precipitation and wind events are not that relevant in these regions, at least within the type of phenomena and the framework proposed here. Most of the extreme precipitation days of the Ebro river basin (62%) occur without a concurrent wind extreme and it is shown that they are mainly related to Mediterranean cut-off lows that are not included in the cyclones' trajectory scheme (but they are accounted as Hmed sub-category, see Tab. 3.2.S in Supporting Information). On the other hand, wind extremes are often related to Hybrid weather patterns where cyclones, and related precipitation, do not play a crucial role.

The ranking of concurrent extreme precipitation and wind events provides a good basis for further systematic analysis of concurrent events on the IP and an updated repository for selecting individual case studies. The trend analysis for the occurrences of these events was limited to the period with available high-resolution reanalysis data sets but it can be extended when ERA5 is released back to 1950. Climate change studies the relevance of concurrent extreme precipitation and wind events may increase in the future: moisture transport in the Northeastern Atlantic is expected to rise dramatically in future scenarios (Ramos et al., 2016b; Sousa et al., 2020) together with an increase in the intensity of fronts and related cyclones affecting Western Europe (Schemm et al., 2017; Catto et al., 2019). As we demonstrated, ARs attend around half of the top20 extreme concurrent events in the IP and extratropical cyclones play a crucial role for at least 85% of these occurrences.

3.5. Supplementary Material

Table 3.1.S. List of top100 precipitation and wind concurrent extreme events. *A(%)* indicates the fraction of the IP domains affected by extremes, *M* indicates the magnitude index, *M norm* indicates the normalized magnitude index, *rk* indicates the position in the respective rankings; *p*, *w* and *c* subscripts refer to precipitation, wind and concurrent precipitation and wind, respectively. AR indicate if a persistent AR was detected and Traj refers to the cyclone trajectory scheme as in Karremann et al. (2016).

Year	Month	Day	Ap(%)	Mp	M_p norm	rk_p	Aw(%)	Mw	M_w norm	rk_w	M_c norm	rk_c	AR	Traj
1981	12	30	47,23	142,77	0,53	20	75,88	1966,18	0,94	3	1,47	1	no	IB
2001	3	2	67	268,55	1,00	1	62,26	938,67	0,45	25	1,45	2	no	IB
1989	2	25	26,74	86,49	0,32	91	87,59	2090,33	1,00	1	1,32	3	yes	H
1982	11	7	49,14	187,71	0,70	5	72,15	1159,70	0,55	15	1,25	4	yes	IB
2010	2	27	23,01	76,58	0,29	114	78,20	1985,54	0,95	2	1,24	5	no	IB
2013	1	19	54,59	175,23	0,65	7	57,82	1140,88	0,55	16	1,20	6	no	IB
2006	11	24	35,62	195,11	0,73	4	56,10	909,75	0,44	27	1,16	7	yes	W
2013	12	24	46,01	144,31	0,54	19	67,81	1101,26	0,53	19	1,06	8	yes	N
1989	12	16	36,93	107,48	0,40	46	72,25	1275,68	0,61	10	1,01	9	yes	W
1997	11	6	23,11	88,82	0,33	84	54,89	1410,30	0,67	6	1,01	10	no	IB
1981	12	28	52,88	185,59	0,69	6	37,24	580,10	0,28	73	0,97	11	no	W
1997	12	17	61,65	226,52	0,84	3	17,05	207,11	0,10	256	0,94	12	no	W
2018	2	28	64,48	228,47	0,85	2	15,14	184,95	0,09	292	0,94	13	no	W
1984	10	4	13,82	39,78	0,15	321	87,59	1596,62	0,76	5	0,91	15	no	IB
2000	12	7	26,44	83,47	0,31	97	68,11	1244,14	0,60	12	0,91	16	yes	W
2015	1	30	35,52	141,6	0,53	22	53,99	786,16	0,38	38	0,90	17	no	H
2018	3	14	49,45	156,52	0,58	12	43,49	618,01	0,30	66	0,88	18	no	W
2009	1	24	0,2	0,45	0,00	2275	85,17	1790,27	0,86	4	0,86	19	yes	IB
1992	3	30	23,41	60,93	0,23	163	69,83	1268,32	0,61	11	0,83	20	no	H
1979	2	10	52,07	166,01	0,62	9	31,69	448,17	0,21	104	0,83	21	no	IB
1983	12	18	33,5	99	0,37	56	66,30	954,38	0,46	23	0,83	22	no	N
1999	10	20	50,05	155,07	0,58	13	35,42	502,80	0,24	94	0,82	24	no	IB
2007	3	7	14,93	43,54	0,16	289	79,92	1364,53	0,65	7	0,81	25	no	N
2017	12	11	34,91	95,95	0,36	65	58,83	952,66	0,46	24	0,81	26	yes	N
2003	10	31	41,57	111,32	0,41	41	53,88	825,05	0,39	32	0,81	27	no	IB
1987	10	15	19,07	89,65	0,33	81	50,35	992,53	0,47	22	0,81	28	yes	W
1988	1	29	31,58	105,37	0,39	49	53,48	799,32	0,38	36	0,77	29	no	H
2001	3	4	44,7	132,25	0,49	26	42,48	569,69	0,27	76	0,76	30	no	IB
1979	1	27	46,82	162,17	0,60	10	23,71	282,96	0,14	188	0,74	32	no	IB
1994	1	6	41,98	120,07	0,45	35	42,38	607,13	0,29	69	0,74	33	no	N
2009	3	5	10,39	32,22	0,12	424	80,83	1280,32	0,61	9	0,73	34	no	H
2010	1	14	15,34	50,37	0,19	234	74,87	1131,39	0,54	17	0,73	35	no	IB
2016	1	10	27,25	106,94	0,40	47	50,55	653,49	0,31	62	0,71	36	no	H
1992	12	4	30,47	96,7	0,36	64	51,56	716,06	0,34	51	0,70	37	no	N

2001	1	28	10,39	32,65	0,12	416	70,74	1177,23	0,56	14	0,68	38	no	IB
1996	11	11	43,29	149,2	0,56	17	19,88	250,64	0,12	210	0,68	39	no	W
2009	12	23	34,11	89,2	0,33	83	39,86	698,47	0,33	56	0,67	41	yes	IB
2014	2	9	24,02	68,26	0,25	141	46,22	825,03	0,39	33	0,65	43	no	IB
2010	10	3	21,59	74,08	0,28	120	54,69	776,75	0,37	39	0,65	44	no	IB
2009	2	1	38,24	142,55	0,53	21	17,86	237,85	0,11	222	0,64	45	no	IB
2001	2	7	31,28	115,16	0,43	38	33,50	436,55	0,21	114	0,64	47	no	W
2015	11	2	42,08	151,65	0,56	15	11,50	148,39	0,07	348	0,64	48	no	IB
2013	3	7	33,2	93,39	0,35	72	46,72	595,17	0,28	71	0,63	50	no	IB
2000	11	5	24,32	88,4	0,33	85	39,76	581,42	0,28	72	0,61	51	no	N
1987	1	12	39,46	157,92	0,59	11	1,92	21,70	0,01	1057	0,60	52	no	IB
2001	1	5	34,31	102,1	0,38	50	35,52	453,98	0,22	102	0,60	53	yes	N
2004	3	29	39,86	154,93	0,58	14	3,23	38,38	0,02	827	0,60	54	no	IB
1996	1	21	33,4	130,16	0,48	27	15,94	212,28	0,10	249	0,59	55	no	W
1996	1	8	32,49	100,2	0,37	54	34,71	445,07	0,21	107	0,59	56	no	W
1991	3	7	40,16	139,75	0,52	24	11,20	136,79	0,07	377	0,59	57	no	IB
2014	1	4	5,45	12,88	0,05	847	66,30	1103,06	0,53	18	0,58	58	no	H
1987	1	10	20,99	64,95	0,24	152	45,11	685,32	0,33	57	0,57	59	no	IB
2018	3	2	25,23	87,61	0,33	87	33,30	501,59	0,24	95	0,57	60	no	W
2017	2	4	24,02	84,63	0,32	96	37,44	523,21	0,25	89	0,57	61	no	N
1982	2	15	37,64	148,44	0,55	18	1,31	13,81	0,01	1217	0,56	62	no	IB
1980	3	21	41,57	140,76	0,52	23	5,85	69,06	0,03	610	0,56	63	no	IB
2016	1	4	25,83	94,11	0,35	68	32,59	419,86	0,20	121	0,55	64	yes	H
1989	11	19	34,61	122,1	0,45	33	15,74	190,06	0,09	282	0,55	65	no	W
1995	12	25	33,4	119,57	0,45	37	17,56	196,03	0,09	274	0,54	67	yes	IB
1996	1	6	20,08	51,71	0,19	218	51,97	718,14	0,34	50	0,54	68	no	W
1986	2	14	41,68	126,68	0,47	31	11,50	134,07	0,06	385	0,54	69	no	N
1985	2	11	14,53	38,86	0,14	342	58,32	786,57	0,38	37	0,52	71	no	N
2012	12	14	28,76	92,39	0,34	74	29,97	369,31	0,18	144	0,52	72	yes	H
2017	2	3	15,34	48,57	0,18	250	44,10	704,08	0,34	53	0,52	73	no	W
2003	3	27	40,87	137,31	0,51	25	0,81	9,75	0,00	1355	0,52	74	no	IB
2018	3	17	28,46	93,5	0,35	70	25,43	349,43	0,17	150	0,52	75	no	IB
1996	2	6	14,23	41,3	0,15	309	55,10	751,79	0,36	44	0,51	76	no	N
2017	3	13	18,77	110,96	0,41	42	16,04	201,10	0,10	264	0,51	77	no	H
2009	12	24	24,22	76,86	0,29	113	34,51	443,84	0,21	108	0,50	78	yes	IB
1999	12	27	2,02	5,51	0,02	1275	58,22	995,15	0,48	21	0,50	79	yes	N
2016	2	12	28,76	98,08	0,37	62	20,79	260,40	0,12	206	0,49	80	yes	H
1997	11	25	36,63	113,39	0,42	40	10,90	139,62	0,07	366	0,49	81	no	IB
2007	11	20	39,46	125,1	0,47	32	3,43	38,76	0,02	825	0,48	82	no	N
2013	3	31	35,02	120,26	0,45	34	6,16	74,16	0,04	577	0,48	83	no	W

2014	11	29	26,24	129,34	0,48	28	0,20	2,19	0,00	1899	0,48	84	no	W
2002	11	13	5,45	14,28	0,05	807	57,21	893,17	0,43	28	0,48	85	no	H
1996	12	5	30,27	127,96	0,48	30	0,20	2,28	0,00	1878	0,48	87	no	IB
1979	2	14	13,52	31,25	0,12	432	46,42	754,49	0,36	43	0,48	88	no	IB
1979	2	2	34,11	120	0,45	36	4,14	45,96	0,02	754	0,47	89	no	IB
1998	12	31	26,44	72,31	0,27	127	18,37	413,35	0,20	122	0,47	90	no	IB
1990	1	27	28,96	98,49	0,37	59	18,16	208,83	0,10	252	0,47	91	no	N
2010	12	7	30,68	98,26	0,37	61	17,56	207,62	0,10	255	0,47	92	no	IB
1994	12	31	22,7	68,14	0,25	143	32,90	437,47	0,21	113	0,46	94	no	IB
2007	2	8	37,34	109,8	0,41	45	8,48	109,33	0,05	440	0,46	96	no	IB
2006	2	18	15,14	38,51	0,14	345	46,01	634,66	0,30	64	0,45	97	no	N
2005	12	2	31,28	90,4	0,34	79	17,86	225,49	0,11	235	0,44	98	no	N
1984	11	13	27,25	109,93	0,41	43	6,26	71,41	0,03	598	0,44	99	no	IB
1986	2	16	11,5	27,67	0,10	482	53,68	699,88	0,33	55	0,44	100	no	IB
1986	11	14	36,73	95,48	0,36	66	14,23	169,21	0,08	316	0,44	101	no	W
2016	11	23	25,93	114,98	0,43	39	0,61	6,93	0,00	1485	0,43	102	no	H
2006	3	5	3,13	8,39	0,03	1066	48,13	833,36	0,40	31	0,43	103	no	H
2014	2	6	0,81	1,76	0,01	1784	57,72	884,68	0,42	29	0,43	104	no	W
2002	1	23	33,5	80,14	0,30	103	19,88	267,65	0,13	200	0,43	105	no	N
1984	11	30	35,62	105,43	0,39	48	4,84	67,50	0,03	617	0,42	106	no	W
2018	3	24	7,06	20,08	0,07	629	53,48	730,85	0,35	46	0,42	107	no	IB
1989	12	18	15,94	42,53	0,16	294	37,94	554,48	0,27	79	0,42	109	no	W
2006	10	25	21,19	70,1	0,26	134	21,39	338,23	0,16	155	0,42	110	no	W
2006	3	23	24,82	85,43	0,32	93	18,26	209,41	0,10	251	0,42	111	no	W
2018	3	9	28,56	87,58	0,33	88	14,23	178,18	0,09	305	0,41	112	no	W
2000	12	30	0,2	0,49	0,00	2226	58,83	845,77	0,40	30	0,41	114	no	IB

Table 3.2.S. Frequencies (%) of cyclone trajectories for top100 and top20 (in brackets) extreme concurrent events, including potential sub-categories. The categories are: IB (Iberia), IBsw (Iberia southwest), N (north), W (West), Wslow (West slow-moving), H (Hybrid), Hmed (Mediterranean Hybrid).

Traj	IP	SP	PT	Minho	Douro	Tejo	Guad	Guadalq	Ebro	NW	NE	SW	SE
IB	41 (45)	42 (50)	40 (45)	22 (35)	30 (45)	38 (55)	45 (45)	49 (65)	31 (35)	28 (30)	34 (50)	47 (65)	37 (30)
IBsw	2 (0)	4 (0)	0 (0)	0 (0)	1 (0)	1 (0)	5 (0)	3 (0)	3 (5)	0 (0)	3 (10)	1 (0)	6 (10)
N	18 (5)	17 (15)	17 (15)	35 (35)	23 (25)	15 (5)	14 (10)	14 (15)	12 (15)	30 (25)	14 (5)	14 (10)	14 (25)
W	20 (35)	17 (30)	32 (30)	30 (15)	27 (30)	26 (35)	20 (30)	19 (10)	6 (5)	29 (30)	7 (5)	28 (20)	6 (0)
Wslow	5 (0)	4 (0)	4 (0)	1 (0)	3 (0)	7 (0)	5 (5)	6 (10)	1 (0)	2 (0)	2 (5)	6 (5)	3 (5)
H	14 (15)	16 (5)	7 (10)	12 (15)	16 (0)	11 (5)	10 (10)	8 (0)	34 (40)	11 (15)	29 (25)	4 (0)	16 (25)
Hmed	0 (0)	0 (0)	0 (0)	0 (0)	0 (0)	2 (0)	1 (0)	1 (0)	13 (0)	0 (0)	11 (0)	0 (0)	18 (5)

In addition to the four recurrent patterns for the cyclones' trajectories (Fig. 3.4 in Section 3.3.3), the following sub-categories have been identified:

- IB from the SW (included in the IB category): a small percentage (around 5%) of the events that affect the southern river basins (Guadiana, Guadalquivir) and Ebro is related to situations where a strong high-pressure ridge extends in the Central Atlantic Ocean blocking the westerly flow, and a typically weak low approaches the IP from the SW (Madeira Island), making landfall on its Mediterranean coastline. Because of its exposition to the Mediterranean Sea, events belonging to this category are also found in the SE sector's top events.

- W slow systems (included in W category): these events are associated with a very slow-moving low-pressure system located to the west of the IP, embedded in between a high-pressure ridge on its western side and an extended and strong high pressure to the East, over Central Europe. The trajectories associated with those cyclones extend meridionally without even making landfall. This specific configuration of the W class shows overall frequencies of 5%, 6% and 7%, for the Guadiana, Guadalquivir and Tejo river basins, respectively. A similar frequency is thus observed in the SW sector.

- H med (included in H category): this sub-category mainly affects the Ebro river basin (13% of the total number of events, more than one-third of the H occurrences for the basin). For these events, it still holds that a pronounced pressure gradient develops across the IP, as prescribed in Karremann et al. (2016), but its axis is rather latitudinally

oriented, eventually enhanced by the Pyrenees mountain chain. This is due to the presence of a Mediterranean low on the eastern side of IP and a high-pressure ridge to the West. Events characterized by cut-off lows in the Mediterranean also fall into this category. This explains the strong signal of Hmed configurations in both the SW and SE sectors (11% and 18% of the top100 events, respectively).

However, it is worth noting that very few instances of the top20 most extreme concurrent events rankings are associated with the patterns described above, as for two (one) occurrences of W slow, for the Guadalquivir (Guadiana) river basin. Therefore, despite the importance of each recurrent pattern for the local weather and climatology, we conclude that the 4-class scheme suggested in Karremann et al. (2016) is robust enough to characterize properly the most extreme precipitation and wind concurrent events affecting the IP.

4

Assigning precipitation to fronts on the North Atlantic and European Sector

This chapter is based on a manuscript that is an original contribution of this thesis published in the International Journal of Climatology, in 2018, under the title *"Assigning precipitation to mid-latitudes fronts on sub-daily scales in the North Atlantic and European sector: Climatology and trends"*, with the DOI: 10.1002/joc.5808.

The research included in this chapter was supported by the Portuguese Science and Technology Foundation (Fundação para a Ciência e a Tecnologia - FCT) and Portugal Horizon2020 through the projects UID/GEO/50019/2013 and PTDC/CTA-MET/29233/2017 (WEx-Atlantic). Riccardo Hénin was supported by an FCT doctoral grant (PD/BD/114479/2016) and Alexandre M. Ramos was supported by an FCT postdoctoral grant (FCT/DFRH/SFRH/BPD/84328/2012). S.S. acknowledges funding from the Swiss National Science Foundation (P300P2_167745 and P3P3P2_167747).

Graphical Abstract

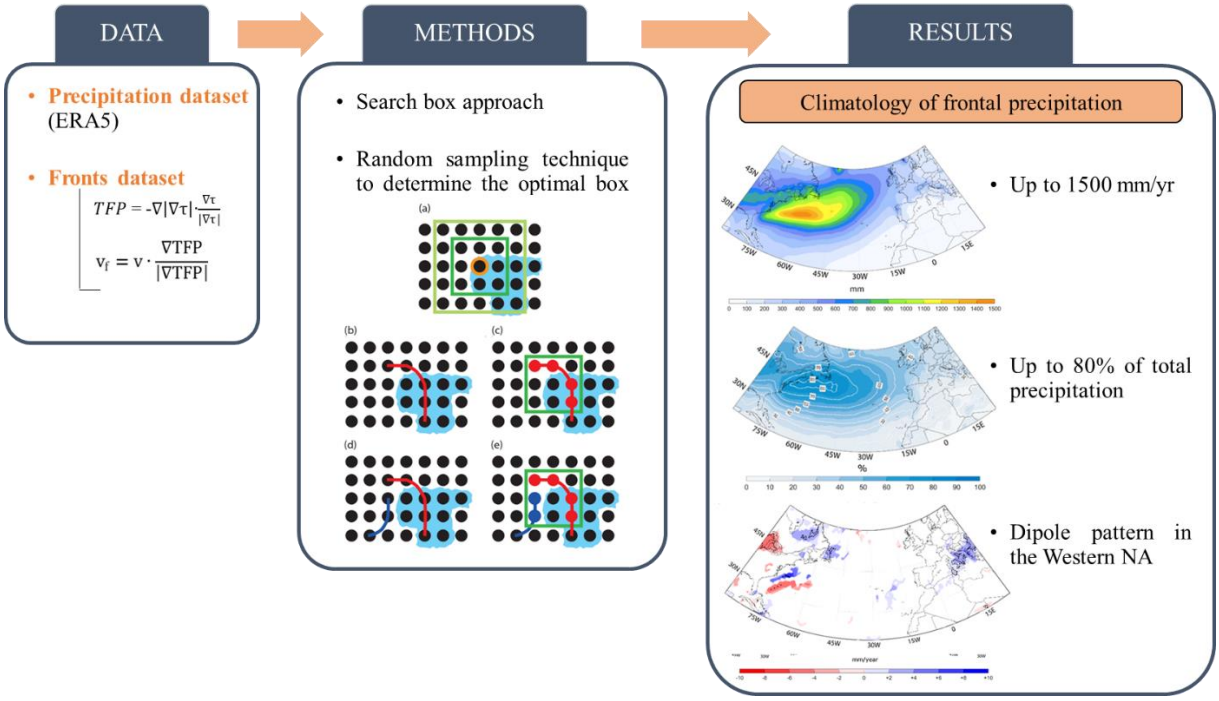

Highlights

- Context and motivation

Atmospheric fronts are fundamental features of the weather variability in the mid-latitudes and are typically associated with high-impact weather events such as extreme precipitation, hail and wind gusts. In gridded data, it is not straightforward to assign a spatial quantity as precipitation to pointy or stingy objects as cyclones or fronts. Most of the studies in the literature evaluate the precipitation amount that is systematically relatable to the cyclones as a whole and only a few explore the finer structure of precipitation bands in the neighborhood of fronts.

- Data (period considered: 1979-2016)

- Precipitation from ECMWF ERA-Interim reanalysis;
- Fronts database (Schemm et al., 2015).

- Methods

A search-box approach to co-locate precipitation and fronts on a sub-daily time scale is described. The procedure includes criteria to distinguish cold and warm fronts and their respective associated precipitation. A sensitivity test based on a random sampling technique is performed to search for the optimal box size.

- Results

The methodology is demonstrated with a real case study that affected Western Europe. Annual and seasonal cycles of frontal precipitation are presented and confirm, in agreement with previous studies, that a large fraction of all precipitation (up to 80% in the North Atlantic mid-latitudes, up to 60% in western European extremities) can be objectively associated to fronts, especially during autumn and winter. A negative trend in frontal precipitation, mainly driven by cold fronts, is identified over the Gulf Stream region.

Keywords: frontal climatology, frontal precipitation, fronts, midlatitudes, North Atlantic storm track.

4.1 Introduction

High impact weather events in the North Atlantic and European sector include wind and precipitation extremes causing flooding, landslides, human casualties and extensive property damage (e.g., Ulbrich et al., 2003; Pitt, 2008; Swiss Re, 2008; Papagiannaki et al., 2013; Liberato and Trigo, 2014). Over the Iberian Peninsula (IP), extreme precipitation events have been extensively studied through case studies (e.g., Fragoso et al., 2010; Vicente-Serrano et al., 2011; Liberato et al., 2011; Trigo et al., 2016) on daily (Ramos et al., 2014a) and multi-daily scales (2 to 10 accumulated days as defined in Ramos et al., 2017). These events are usually associated with low-pressure systems over the North Atlantic propagating eastward towards Europe (e.g., Hodges et al., 2003; Karremann et al., 2012; Pfahl, 2014; Liberato, 2014).

It is known that extratropical cyclones are often attended by atmospheric fronts (Schemm et al., 2018). It is therefore not surprising that in parts of the midlatitudes storm track regions, more than 90% of all precipitation extremes are associated with fronts (Catto and Pfahl 2013). Indeed, fronts have been recognized as a potential driver behind precipitation trends (Catto et al., 2012), in particular since their intensity scales with frontal precipitation rates (Schemm et al., 2017). Hence, atmospheric fronts are important weather components as they are frequently associated with significant weather changes.

Methodologies for automated objective frontal analysis (comprehensive reviews are provided by Simmonds et al., 2012 and Schemm et al., 2018) often rely on the definition of a thermal frontal parameter as defined by Clarke and Renard (1966) and Renard and Clarke (1965). Later, further improvements have been introduced to apply these earlier concepts to gridded data (Hewson, 1997; Hewson 1998). Several regional, as well as global, climatologies rely on the refined thermal-front-parameter approach (Berry et al., 2011a; Jenker et al., 2010; Schemm et al., 2015), along with analysis of trends for the recent past and for future projections (e.g., Berry et al., 2011b; Catto et al., 2014; Schemm et al., 2017). Berry et al. (2011a) and Berry et al. (2011b) showed that the midlatitude storm track regions are associated with the highest frequencies of fronts worldwide. Studies suggest that fronts will become less frequent in the storm track region under global warming scenarios (Catto et al., 2014). However, over the land, Schemm et al. (2017) found that the number of extremely strong fronts over Europe has increased in recent decades. A trend that is not observed over North America.

While many previous studies linked precipitation with extratropical cyclones (e.g., Hawcroft et al., 2012; Neu et al., 2013; Pfahl and Wernli, 2012; Lombardo et al., 2015), the

number of studies that specifically link precipitation with fronts is low and exists only for daily precipitation sums (e.g., Catto et al., 2012; Catto and Pfahl, 2013). To the authors' knowledge, a more regional analysis of frontal precipitation on sub-daily time scales (i.e., 6-hourly precipitation sums) is missing for the North Atlantic storm track region.

The present study aims at exploring the relationship between fronts and 6-hourly precipitation sums over the North Atlantic and European sectors. The main purposes are:

(i) develop a method for objectively associating, in time and space, precipitation with synoptic-scale fronts (warm and cold fronts separately) along with sensitivity analysis on the spatial criteria for their co-location;

(ii) test the method using a real case study, selected among the most intense that occurred over Western Europe;

(iii) compute and discuss seasonal and annual climatological means;

(iv) identify trends in frontal precipitation over the North Atlantic and European sectors.

Data and methods are presented in Section 4.2. The data sets for fronts and for the precipitation field are described in subsections 4.2.1 and 4.2.2. The technique to associate fronts and precipitation is explained and discussed in subsection 4.2.3. Results, including a detailed case study, annual and seasonal cycles and trend analysis, are discussed in section 4.3. Finally, conclusions are presented in section 4.4.

4.2 Data and Methods

4.2.1 Precipitation Dataset

The ERA-Interim reanalysis by the European Centre for Medium-Range Weather Forecast (ECMWF; Dee et al., 2011a) is used for the period 1979-2016 over the North Atlantic and European sector (20°N-60°N and 90°W-25°E). ERA-Interim provides accumulated precipitation on a 1º latitude-longitude grid at 6-hour intervals, based on the forecast model. In this study, both the 00 UTC and 12 UTC forecast times are used along with the accumulated precipitation given by all the forecast steps (00 UTC+3h to 00 UTC+12h and 12 UTC+3h to 12 UTC+12h). At first, the accumulated precipitation over 3-hour intervals are computed, as follows:

- 00 UTC to 03 UTC: equal to time step 00 UTC+3h;

- 03 UTC to 06 UTC: 00 UTC+6h - 00 UTC+3h;
- 06 UTC to 09 UTC: 00 UTC+9h - 00 UTC+6h;
- 09 UTC to 12 UTC: 00 UTC+12h - 00 UTC+9h;
- 12 UTC to 15 UTC: equal to time step 12 UTC+3h;
- 15 UTC to 18 UTC: 12 UTC+6h - 12 UTC+3h;
- 18 UTC to 21 UTC: 12 UTC+9h - 12 UTC+6h;
- 21 UTC to 00 UTC: 12 UTC+12h - 12 UTC+9h.

Then, the 3-hour values are aggregated in four intervals, centered in the middle of the accumulation period. For day *n* it follows:

- 00 UTC: from 21 UTC (day n^{-1}) to 03 UTC (day *n*)*;*
- 06 UTC: 03 UTC (day *n*) to 09 UTC (day *n*);
- 12 UTC: 09 UTC (day *n*) to 15 UTC (day *n*);
- 18 UTC: 15 UTC (day *n*) to 21 UTC (day *n*).

It is known that reanalysis data sets are affected by inaccuracies and by spin-up and spin-down effects of the associated forecast model (Dee et al., 2011a). For example, Kållberg (2011) analyzed the forecast drift for the precipitation field in the ERA-Interim product and found that the storm track regions are prone to the spin-up effect. Also, as moist processes are considerably approximated in the representation of the hydrological cycle of the forecast model, the humidity field may be inaccurate, leading to erroneous precipitation estimates (Uppala et al., 2005). Despite the above-mentioned limitations, good agreement has been found among ERA-Interim, ground-based observations and gridded records from different sources on both global and regional scales (e.g., Simmons et al., 2010; Donat et al., 2014; de Leeuw et al., 2014). Some literature is still critical about the suitability of reanalysis data for characterizing the long-term climate trends (e.g., Bengtsson et al., 2004; Thorne and Vose, 2010; Dee et al., 2011b; Cornes and Jones, 2013). For example, Thorne and Vose (2010) argue that current reanalysis account for many non-climatic behaviors and biases caused by changes in the observing system and they empathize with the need for a new "climate quality" reanalysis product. However, as Dee et al. (2011b) point out, concrete proposals about how to further improve the quality of reanalysis at climate scale have not been implemented yet. As the debate is still open, the here reported trends in frontal precipitation must be interpreted with caution.

4.2.2 Frontal system dataset

The front dataset is similar to that by Schemm et al. (2015). It is designed to identify synoptic-scale mobile fronts in the lower troposphere. Cold and warm fronts are distinguished using an advection criterion. Occluded fronts are detected if they are stronger than a pre-defined front threshold. Occluded fronts are categorized either as a cold or warm front and not classified into a distinct category. More specifically, the procedure is based on a thermal field of choice, following the suggestions outlined in Hewson (1998). The method locates fronts where the Thermal Front Parameter (TFP) is zero. The TFP is defined as follows

$$TFP = -\nabla|\nabla\tau|\cdot\frac{\nabla\tau}{|\nabla\tau|} \tag{4.1}$$

where τ is the thermal field chosen. The method requires the a priori definition of a minimum threshold for the thermal gradient. Schemm et al. (2015) suggest, in agreement with earlier studies, using equivalent potential temperature at 850 hPa as the underlying thermal field and a minimum front threshold of 4K/100km for the thermal gradient. The criteria to distinguish warm from cold fronts is

$$v_f = v \cdot \frac{\nabla TFP}{|\nabla TFP|} \tag{4.2}$$

where v is the vector representing the horizontal wind and $v_f > 0$ ($v_f < 0$) is associated with cold (warm) fronts. With this formulation, a front is treated as an object advected by the flow (Jenkner et al., 2010) and hence the sign of vf depends on whether the wind has the same direction of the temperature gradient or not. The focus of this method lies on the detection of mobile fronts as they are typically associated with extratropical cyclone development. Thermal methods are often flawed outside midlatitudes, along the steep topography or coastlines, where strong thermal gradients can develop during the daily radiation cycle (e.g., land-sea breezes or valley winds - see Schemm et al., 2015). For these reasons, a minimum threshold for the advection speed (3 ms^{-1}) and a minimum length criterion (500 km) are applied. However, depending on the chosen domain and on its typical weather features, the method can be made more effective by tuning these thresholds. In this study, quasi-stationary fronts are considered for comparison with the solely-mobile fronts dataset and a lowered threshold for the thermal gradient is also used. The length criterion is maintained throughout the analysis to avoid the detection of non-synoptic fronts.

4.2.3 Assigning precipitation to fronts

In the following, the method to link fronts with precipitation is discussed and the precipitation assigned to a front is hereafter referred to as frontal precipitation. The assignment is formerly based on a procedure that parallels that of Catto et al. (2012). In the present study, however, different precipitation data on a sub-daily scale is used and a sensitivity test is performed. Firstly, grid points with 6-hourly accumulated precipitation below 1mm are excluded. Secondly, for the remaining grid points, a predefined front-search box is set (Fig. 4.1a). This front-search box is centered on the grid point, consistently with parallels and meridians arcs that is, it extends by 1 degree-steps on either side of the grid point under consideration. Hence, the smallest feasible box is a 2°x2°, which corresponds to 3x3 grid points (dark green box represented in Fig. 4.1a). The next box is a 4°x4°, which corresponds to 5x5 grid points (light green box represented in Fig. 4.1a) and similarly for the larger boxes. Then, if a front is identified inside the front-search box, the 6-hourly accumulated precipitation at the grid point is tagged as frontal. The 6-hourly accumulation period is centered in time, that is, for a front at time t, the associated precipitation is taken from a t±3h time interval. The simplest situation occurs when only one front type is co-located with a precipitation spot, as shown in Fig. 4.1b. In this case, the assignment of frontal precipitation is straightforward as all the precipitation of the grid point under consideration is assigned to the only front type that is detected within the box, according to Eq. 4.2 (red solid circles in Fig. 4.1c). On the contrary, ambiguity may arise if different front types are detected, as shown in Fig. 4.1d. In those cases, the precipitation is attributed to the fronts according to the lengths of the fronts inside the search box. For example, if in a 2°x2° (3x3 grid points) search box a warm front is detected at 4 grid points (solid red circles in Fig. 4.1e) and a cold front is detected at 2 grid points (solid blue circles in Fig. 4.1e), then 66.6% of the precipitation of the grid point is associated with the cold front and 33.3% with the warm front. This ad-hock approach is efficient and assumes that inside the search box all front grid points contributed equally to the precipitation, i.e., precipitation is not varying strongly along the fronts. However, because it is known that frontal intensity scales with frontal precipitation (Schemm et al., 2017) and that warm and cold fronts produce different amounts of precipitation, more sophisticated approaches could attribute precipitation according to front intensity or front type. However, as both variants add new uncertainty, e.g., a front-type classification according to temperature advection can change the front type from warm to cold front along the same front, we prefer for the purpose of this study the *ad-hoc* approach.

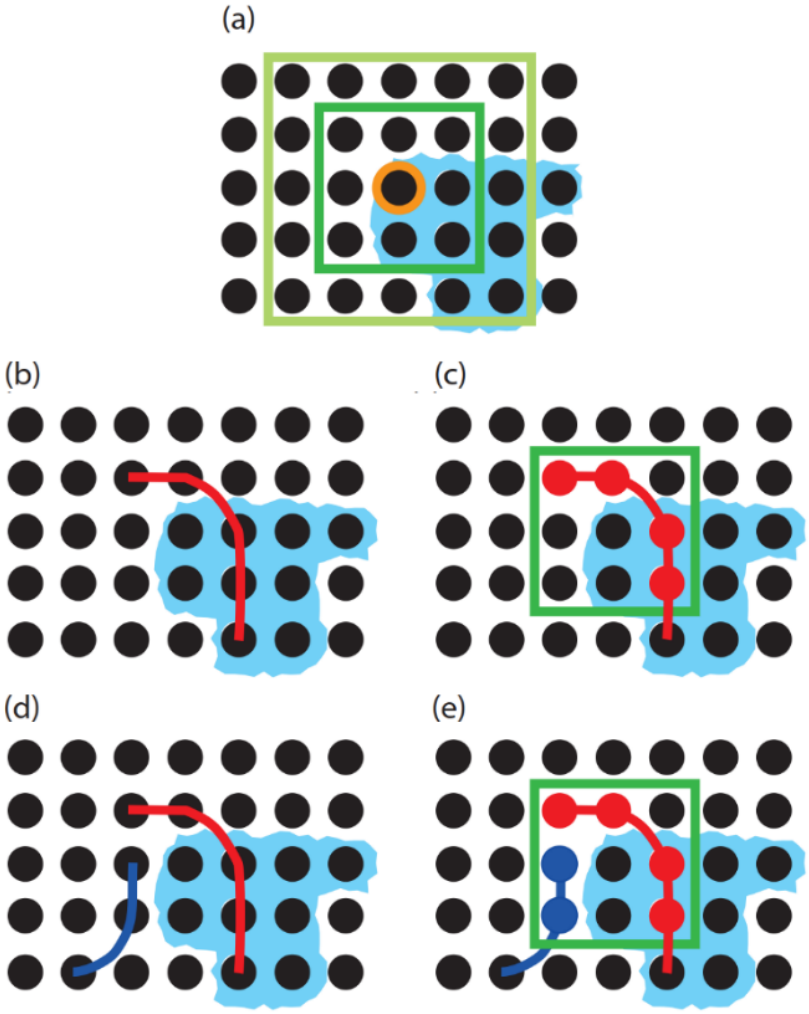

Figure 4.1. Sketch of the assigning method for frontal precipitation. (a) shows how the search box is defined. The black solid circles represent 1° evenly spaced grid points. The light blue spot represents precipitation. The orange dot is the considered grid point at time t, tagged for precipitation over a certain threshold (1mm over t±3h). The squares represent a 2°x2° (dark green) and a 4°x4° (light green) search boxes (3x3 and 5x5 grid points, respectively). The search continues similarly for the following grid points. (b) shows the idealized case of one warm front (red line) co-located with precipitation and (c) shows the related assignment of precipitation to the detected front type (warm front - red solid circles) within the search box. (d) shows the idealized case of both a cold and a warm front co-located with precipitation (blue and red lines, respectively) and (e) shows the related weighting of precipitation between the detected front types (blue and red solid circles for cold and warm fronts, respectively) within the search box. In this example, one-third of precipitation is assigned to cold fronts and two-thirds are assigned to warm fronts.

To define the search box optimally, a sensitivity analysis is performed, where the box size is increased in steps of 2° (one degree on either side of the grid point considered) from 2°x2° to 10°x10° that is, from 3x3 to 11x11 grid points (hereinafter, only the notation in degrees is used). An undersized search box may not catch the 6-hourly motion of a front and miss frontal precipitation which often covers large parts of the pre- and post-frontal areas. In this case, a certain underestimation of the precipitation can be expected as the front may pass through the box without being detected and the precipitation would not be tagged as frontal. Fig. 4.2 shows

this inaccuracy for two well-defined frontal systems, both originated by the splitting of a large Atlantic low, on 26th October 2004: the northern secondary low is approaching Ireland whereas the southern one just made landfall over central Portugal. In both cases, the warm front is slightly ahead of the cold one. The precipitation associated with the warm front decreases with increasing box size (from 2°x2° box in panels a-b to 10°x10° box in panels e-f) as larger amounts of rainfall are associated with the nearby cold front. On the other hand, it is important that the search box is not so large as to catch precipitation unrelated to the front.

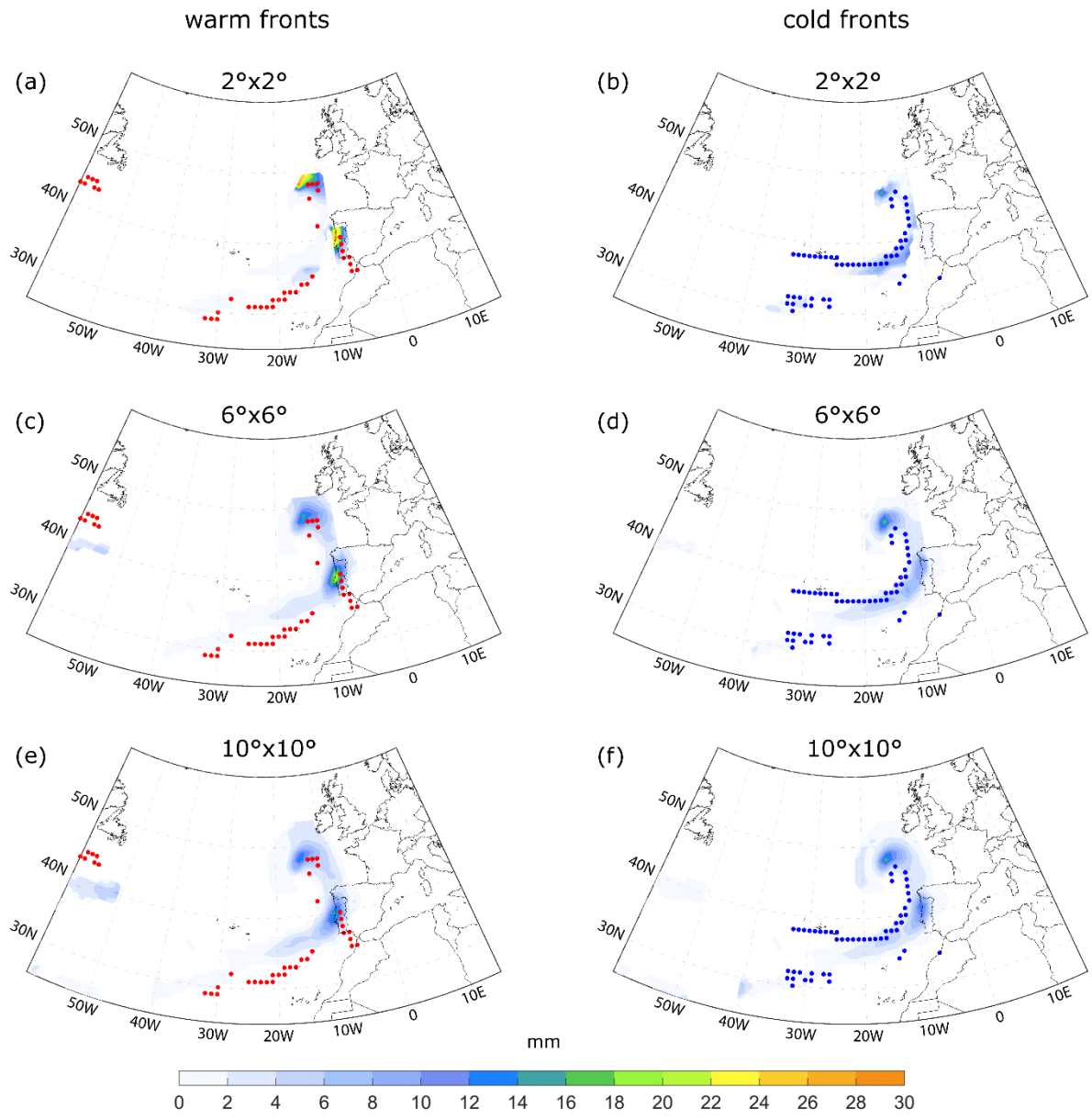

Figure 4.2. Example of application of the method for assigning precipitation to warm (left column) and cold (right column) fronts. Red (blue) dots correspond to warm (cold) fronts. Color shading corresponds to assigned precipitation for boxes of different sizes: (a-b) 2ºx2º; (c-d) 6ºx6º; (e-f) 10ºx10º. Event of the 27th October 2004, 00 UTC.

In order to evaluate more systematically the influence of the search box size on the results, the 1979-2016 mean of annual frontal precipitation is calculated for increasing search box sizes (2°x2° to 10°x10°) at every grid point. Therefore, five values of climatological mean frontal precipitation are obtained. Then, the interquartile range of the obtained values is computed (Fig. 4.3). The spread ranges up to 600 mm over the North Atlantic storm track region and up to 300 mm all over the rest of the domain except for North Africa where, however, frontal precipitation is negligible. This result calls for a more objective way to identify the optimal box size, besides any hypothesis that can be drawn from empirical experience.

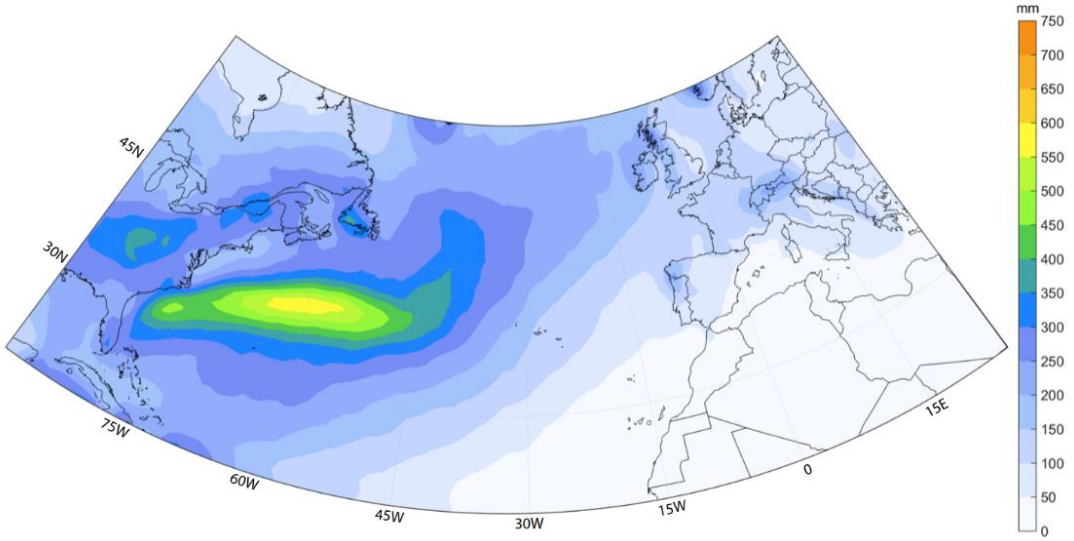

Figure 4.3. Interquartile range of mean climatological (1979-2016) frontal precipitation for five increasing search box sizes (2°x2° to 10°x10°).

A first choice to define an optimal search box could be based on the typical propagation speed that characterizes a synoptic-scale front. The maximum propagation speed of a front in the North Atlantic midlatitudes has been estimated to be 50/60 km/h (Anderson, 1990), which corresponds to approximately 300/360 km over a 6-hourly interval. This suggests a maximum box size with a width of 5°. Alternatively, an optimal front-search box could be based on the synoptic length scale of approximately 1000 km (Holton, 1972). Assuming that an extratropical cyclone typically has two fronts, it appears plausible to start with half of the synoptic length scale in order to associate half of the total precipitation to each of the two fronts: that is a 6° long box. Indeed, for the case studies performed throughout this analysis, a 6°x6° search box always yielded qualitatively good results.

However, a more consistent approach to identify an optimal box size is to test every box size with a randomized precipitation field and to see whether the added precipitation (precipitation is always added when increasing the box size) is still physically meaningful. The

new precipitation dataset is generated by mixing and randomly reassigning all the available 6-hourly accumulated values all over time and space. The attribution is then applied to both the real and the randomized precipitation dataset and, for each search-box size, the average amount of precipitation associated with all fronts is evaluated. The stepwise increase in frontal precipitation, that is the difference between a box size and a 2°x2° smaller box, is shown in Fig. 4.4. The threshold beyond which the added precipitation is not physically justifiable and deviates from noise corresponds to the point where the two curves intersect. The thereby identified optimal box size is 6°x6°, which is half the synoptic length scale (see the previous discussion). Consequently, we use a 6°x6° front-search box.

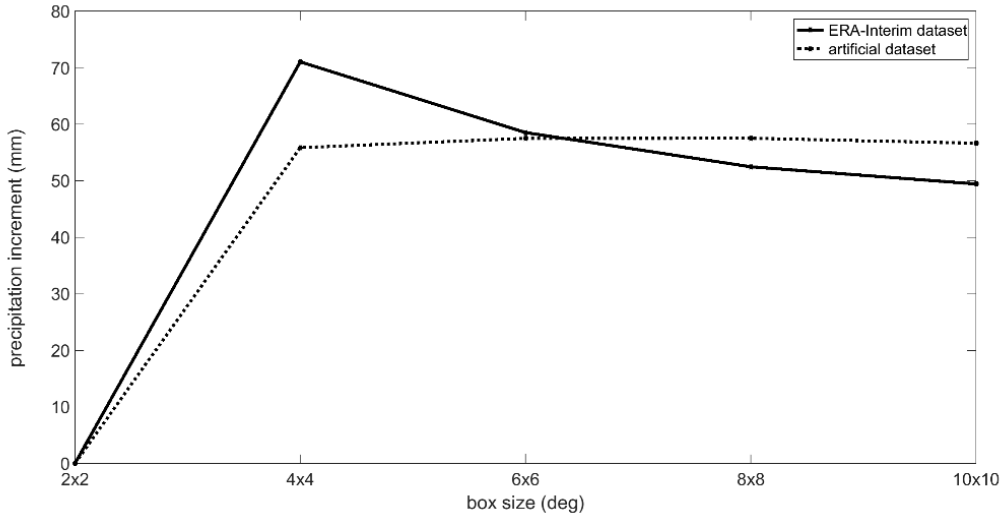

Figure 4.4. Relative increase in frontal precipitation (mm) with increasing search box. This quantity is evaluated stepwise by comparing the frontal precipitation obtained with an N°xN °and an N-2°xN-2° search box, respectively. The solid line indicates the relative increase based on ERA-Interim dataset and the dashed line the relative increase using a random sampling technique (see text for details).

The described method is applied to the domain 20°N-60°N and 90°W-25°E, an area that encompasses the North Atlantic storm track region and the western European coast. Areas north of 60° N are not considered, as the distortion of the box due to the poleward convergence of the meridians would be too large (e.g. Catto et al., 2012). Actually, the distortion might be overcome by using a dynamic search box defined by metric units (km). However, the fronts frequency beyond this latitude is relatively small compared to the extra-tropics (Schemm et al., 2015) and it is partly due to non-synoptic fronts (Berry et al., 2011a). Furthermore, the frontal activity at the synoptic scale beyond 60° N is more properly related to high-latitude (polar) cyclones, which are not the focus of this study, rather than extratropical cyclones (Tilinina et al., 2014). A couple of further technical notes complement this section. The method is independent of the direction the search box scans the grid. Precipitation is measured at the

surface whereas fronts are detected at 850 hPa. Therefore, it is possible, especially in strong baroclinic conditions, that the ground-based precipitation is not matched with the corresponding front. The front detection is not reliable in the vicinity of steep topography or where the topography intersects the 850-hPa surface.

4.3 Results and Discussion

4.3.1 Application of the method to a case study

A case study that illustrates the method to relate fronts with precipitation is presented below. The episode between 26th-27th October 2004 is characterized by distinct low-pressure systems attended by a warm and a cold front located over the eastern Atlantic. Fig. 4.5a-c shows the manual surface analysis of the German Weather Service (DWD) for comparison with the automated front detection shown in Fig. 4.5d-i. In Fig. 4.1.S figures are provided for warm and cold fronts separately.

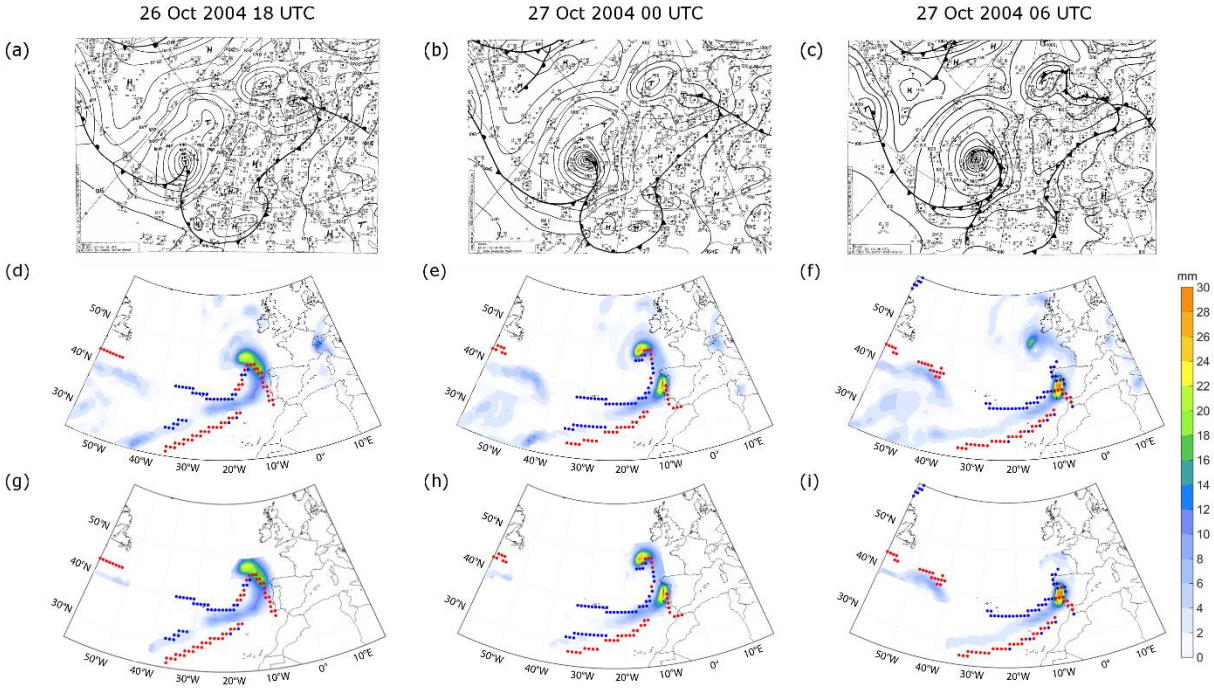

Figure 4.5. Case study 26th-27th October 2004. Left, central and right columns correspond respectively to 18 UTC, 00 UTC and 06 UTC on 26th-27th October 2004. (a-c) Synoptic analysis of surface pressure by German Meteorological Office (DWD). Color shading refers to (d-f) total precipitation and (g-i) frontal precipitation. Fronts are detected if they exceed a minimum thermal gradient threshold for θe of 4K [100km]$^{-1}$. Red (blue) dots correspond to warm (cold) fronts.

At 18 UTC on 26th October 2004, an extratropical cyclone is propagating eastwards across the North Atlantic and is heading towards the English Channel (cf. Figs. 4.5a and 4.5d). Six

hours later, at 00 UTC on 27th on October 2004, the low splits into two different frontal structures: the first one propagates towards the British Islands and the second one, south of the low near the front triple point, is moving towards Portugal (cf Figs. 4.5b and 4.5e). At 06 UTC on 27th October 2004, the northernmost frontal structure disappears in the automated front detection, and the one affecting Portugal turns into a rather complex pattern, reflecting an occlusion (cf Figs. 4.5c and 4.5f). Further south, a zonally elongated front extends over the ocean west of the African coastline. At 18 UTC on 26th October 2004, the frontal precipitation affects a wide area ahead of the low and an elongated area in the cyclone's warm sector (Fig. 4.5g). As the low splits, precipitation also separates into two distinct maxima (Fig. 4.5h). From 00 to 06 UTC on 27th October 2004, the precipitation maximum over Portugal is almost stationary, with values exceeding 60mm/12h. On the other hand, as the northernmost frontal system is no longer detected, the related precipitation pattern between France and Ireland is not tagged as frontal precipitation (cf. Figs. 4.5f and 4.5i). Further, the manual DWD analysis indicates a front over central Europe connected to a low over the Alps which, however, is not detected by the automated front identification. Consequently, the precipitation over the Alps is not identified as frontal. Those fronts are likely filtered by the constraints of the method, mainly the minimum thermal gradient and the minimum advection speed, as described in Sec. 2.2.

Indeed, Fig. 4.6 shows how the results are sensitive to the specific setting of the fronts detection method. The fronts over the English Channel that were missing in the front dataset (Fig. 4.5i) are eventually identified when the threshold of the thermal gradient is lowered from 4K $[100km]^{-1}$ to 3.5K $[100km]^{-1}$ (Fig. 4.6c). Additionally, a cold front is identified also over Italy, in agreement with the manual DWD analysis. The number of frontal grid points rather increases when quasi-stationary fronts are included in the dataset, either with the stricter threshold for the thermal gradient (Fig. 4.6d-f) or with the more lenient one (Fig. 4.6g-i). The identified frontal systems are more likely zonally-elongated in these cases, especially over the ocean. On the contrary, in the neighborhood of the main precipitation spots, ambiguity arises as to whether the detected fronts are cold or warm (e.g., Figs. 4.5f and 4.5i). In the case of stationary fronts and a low threshold for the thermal gradient, a fraction of precipitation west to Ireland is also missed (Fig. 4.6h-i). As pointed out in previous studies (Jenker et al., 2009; Schemm et al., 2015; Schemm et al., 2016), the rules for the tuning of the thresholds strictly depend on the spatial resolution and, eventually, on the needs of the end-users.

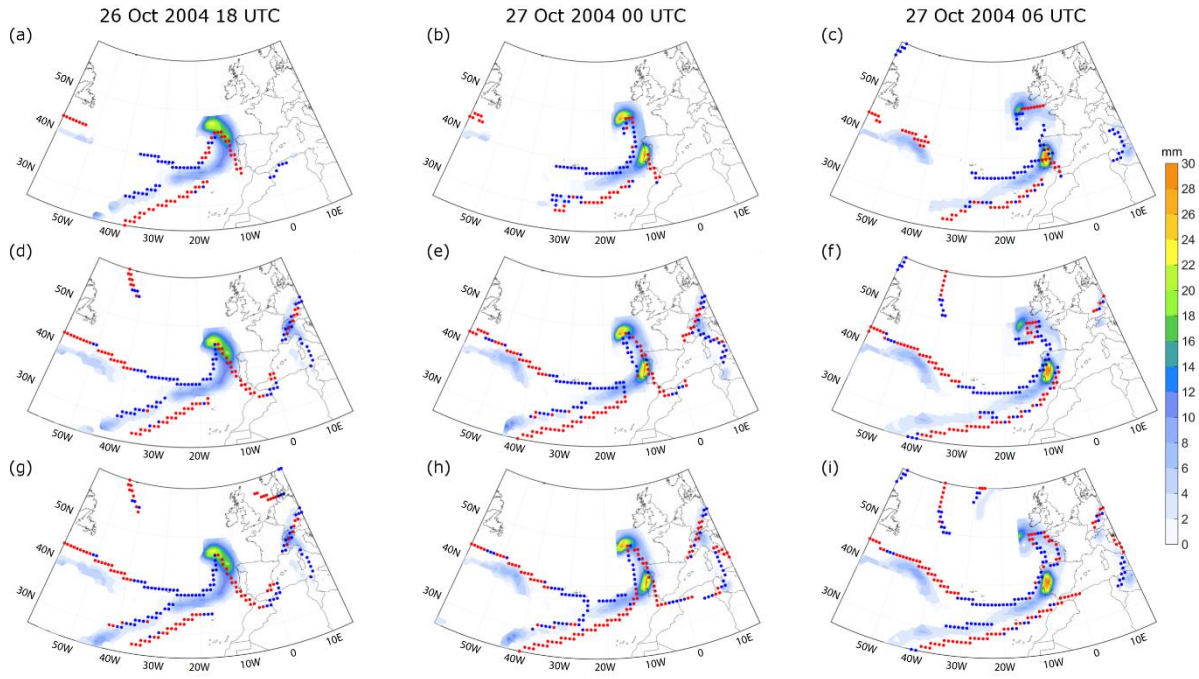

Figure 4.6. Case study 26th-27th October 2004. Red (blue) dots correspond to warm (cold) fronts. Left, central and right columns correspond respectively to 18 UTC, 00 UTC and 06 UTC on 26th-27th October 2004. Color shading corresponds to precipitation assigned to all fronts. In (a-c) mobile fronts are detected if they exceed a minimum thermal gradient threshold for θ_e of 3.5K [100km]$^{-1}$. Quasi-stationary fronts are included in the dataset with a threshold of (d-f) 4K [100km]$^{-1}$ and (g-i) 3.5K [100km]$^{-1}$.

4.3.2 Annual cycle of frontal precipitation

The long-term mean for annual frontal precipitation is shown and discussed in this section (Fig. 4.7). Both the 4K [100km]$^{-1}$ and the 3.5K [100km]$^{-1}$ thresholds are considered for mobile fronts whereas the results for the data sets including quasi-stationary fronts are shown in the Supplementary Material (Fig. 4.2.S). Over the North Atlantic, frontal precipitation peaks over the Gulf Stream region, with values exceeding 1500 mm/year, which is approximately 80% of total precipitation (Fig. 4.7a-b). Maximum frontal precipitation follows the center of the North Atlantic storm track region towards higher latitudes, in agreement with Berry et al. (2011a). The overall pattern is consistent with other measures of storm track activity such as heat flux or cyclone tracks (Pfahl 2014; Hodges et al., 2003). Over Western Europe, frontal precipitation accounts for around 400 mm/year, corresponding to a fraction of 40% of the total precipitation.

The front types contribute differently to the total amount of frontal precipitation. Over the ocean, maximum cold-front precipitation is more zonally oriented and shifted equatorward relative to warm-front precipitation (cf. Figs 4.7c and 4.7e). This pattern is consistent with previous studies (Berry et al., 2011a; Catto et al., 2012). Overall, annual cold-front precipitation

(up to 900 mm/year) exceeds warm-front precipitation (up to 700 mm/year). The difference of approximately 200 mm/year corresponds to 3 times the year-to-year standard deviation.

Over the land, approximately 60% of total precipitation is identified as frontal precipitation, in particular over the northern United States, southern Canada and at the western domain boundary. Major contributions for inland precipitation come from cold fronts as they are associated with up to 500mm/year and 40% of total precipitation. Warm fronts affect coastal areas and the Great Lakes region (cf. Figs. 4.7c-e and 4.7d-f). Continental Europe is less affected by frontal precipitation than North America, but precipitation associated with cold fronts is still prevailing. Cold-front precipitation is even larger along the European western coast compared to central Europe, due to the frequent landfall of deep low-pressure systems. The prevalence of cold-front precipitation is likely due to the fact that cold fronts are sharper, hence more frequently detected by the scheme, and because they often trigger strong convection along their leading edge.

The estimates on a sub-daily scale presented here expand the findings of Catto et al. (2012). According to their results, precipitation associated with cold and warm fronts accounts for 57% of total precipitation over the northern midlatitudes, with values up to 60% over Western Europe and peaks of up to 90% over the storm track regions. The differences with our findings are likely related to:

- different precipitation data. Their study on frontal precipitation used daily Global Precipitation Climatology Project (GPCP) precipitation sums at 2.5° horizontal resolution for the period 1997-2008;
- different settings in the front detection;
- different attribution boxes (5° instead of 6° used here).

Therefore, our findings highlight how attribution studies are sensitive to the underlying definition of fronts and precipitation data.

When the front threshold is lowered from 4K $[100km]^{-1}$ to 3.5K $[100km]^{-1}$ more precipitation is attributed to fronts (Fig. 4.7 – right column) because more real fronts are detected, as shown for the case study. The increase is strongest over North America, where more than 60% of total precipitation is labeled as frontal, compared to 50% observed with the stricter threshold. Based on the reduced threshold, more than 40% of precipitation is associated with fronts over Western Europe. Maximum precipitation associated with fronts increases from 80% to 90% over the Gulf Stream. The increase equally affects warm and cold fronts.

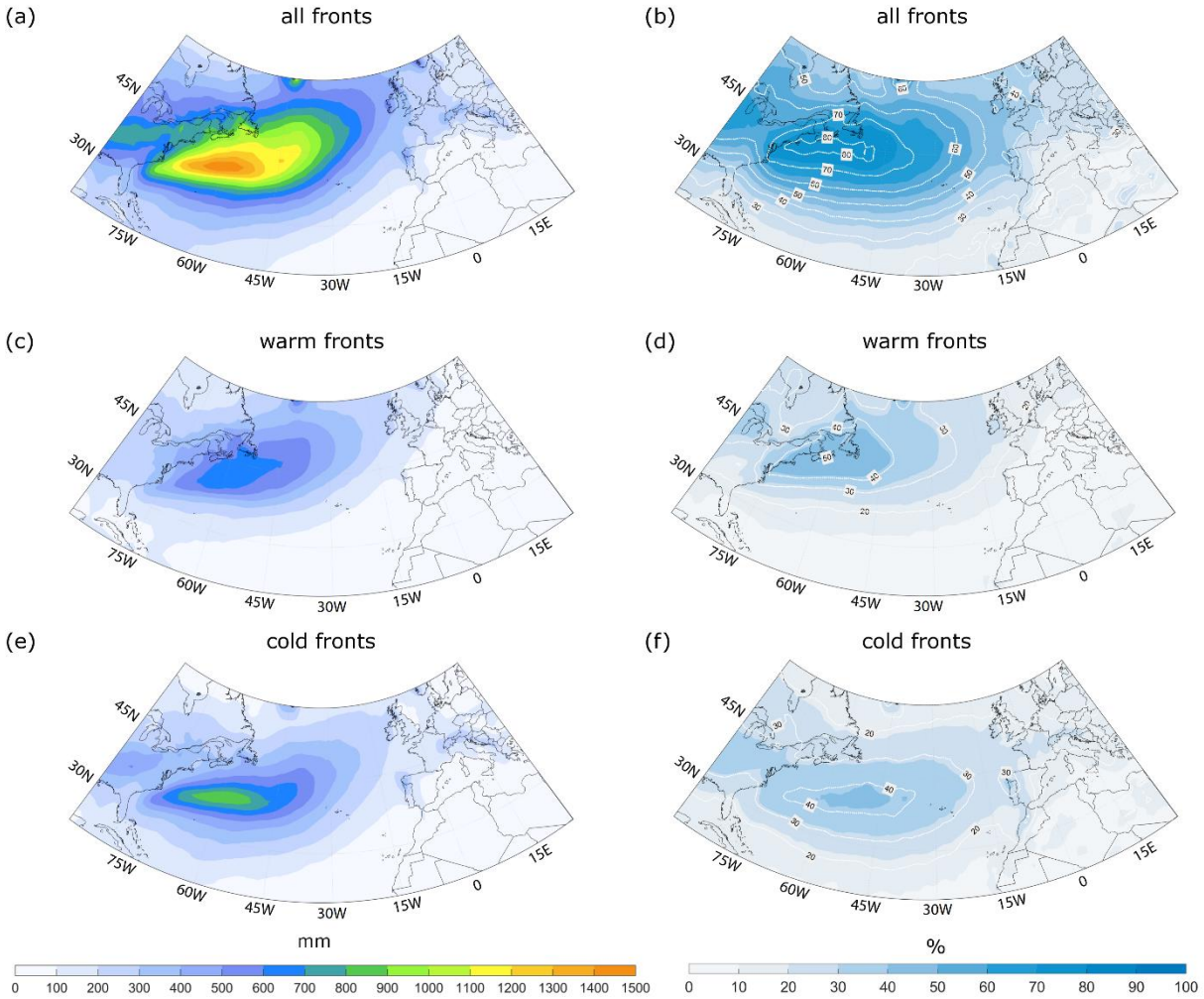

Figure 4.7. Annual cycle of frontal precipitation. Precipitation assigned to (a-b) all fronts, (c-d) warm fronts and (e-f) cold fronts in mm/year (left column) and fraction of frontal over total precipitation (right column). Color shading for percentages corresponds to a threshold of 4K $[100km]^{-1}$ for the minimum thermal gradient used to detect fronts. White contours correspond to the lower threshold 3.5K $[100km]^{-1}$ (only values over 20%).

4.3.3 Seasonal cycle of frontal precipitation

The seasonal cycle of frontal precipitation is shown in Fig. 4.8 for December to February (DJF), March to May (MAM), June to August (JJA) and September to November (SON). The largest fraction of front-related precipitation is located over the North Atlantic midlatitudes during all the seasons, but maxima shift towards the north (south) during autumn (summer) for both warm and cold fronts (consistent with the seasonal cycle in other storm track measures). Winter (Fig. 4.8a-b) and autumn (Fig. 4.8g-h) are the seasons that contribute mostly to the annual amount of frontal precipitation. During winter, the 3-month accumulated values exceed 200 mm and 300 mm for precipitation assigned to warm and cold fronts respectively, which corresponds to almost 90% of the total precipitation (Fig. 4.3.S). During half of the year, from September to February, the belt of maximum precipitation over the Atlantic Ocean is less

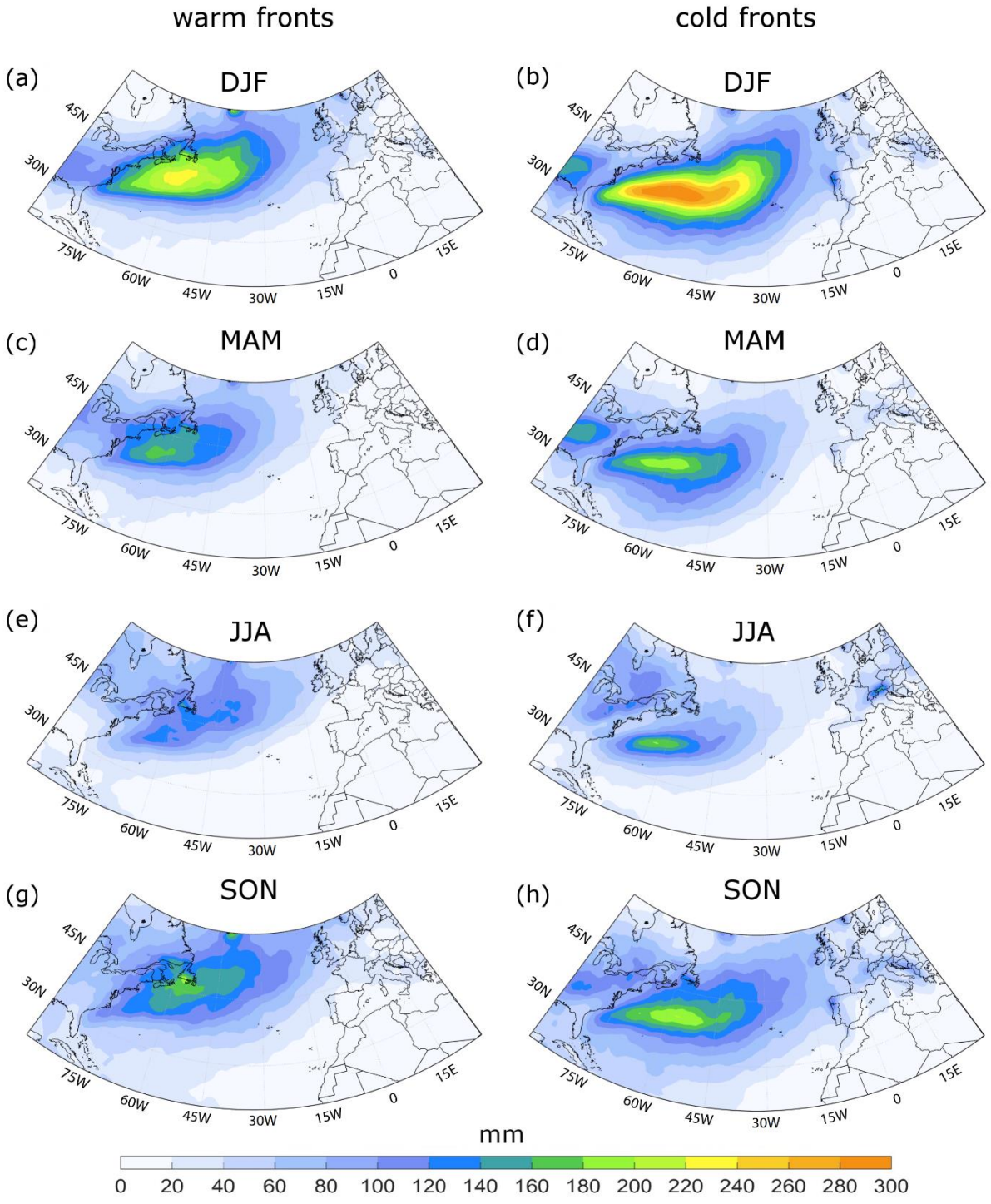

Figure 4.8. Seasonal cycle of frontal precipitation. Assigned precipitation to warm (left) and cold (right) fronts for (a-b) December to February; (c-d) March to May; (e-f) June to August and (g-h) September to November.

zonally oriented and tilts towards the northeast. Notable amounts of frontal precipitation are spread out to western Europe (almost 50% and 60% of total precipitation in front of northwestern Spain during autumn and winter respectively). On the contrary, during spring (Fig. 4.8c-d) and summer (Fig. 4.8e-f), the belt is restricted to the western side of the North

Atlantic. Spring accounts also for a local maximum of cold-front precipitation over the continent in North America whereas summer exhibits a local maximum over the Alps and Central Europe that tends to smooth in autumn. The Alpine region is known to be affected by several thermal local fronts that originate from orographic lifting and from the diurnal evolution of the planetary boundary layer (Jenkner et al., 2010; Schemm et al., 2016). Indeed, cold fronts globally account for more precipitation than warm fronts and this gap is higher in winter.

4.3.4 Trends in frontal precipitation

The annual trend for frontal precipitation (all fronts, warm fronts and cold fronts) is extracted from the 38-year ERA-Interim climatology. Berry et al. (2011b) found an overall decrease of fronts in the Northern Hemisphere during the period 1989-2009, along with a poleward shift of the frequency maxima. Schemm et al. (2017) showed that extremely strong fronts over Europe have increased in number during the last decades.

Trends are estimated using linear regression with a least-square fit and the trend probability is estimated using a Mann-Kendall (MK) test that accounts for serial auto-correlation (Wilks, 2006). To account for field significance, a control level of 10% is set for the false discovery rate (FDR), following Wilks (2016). The control level indicates the maximum fraction of locally significant grid points that are erroneously rejected in the domain: in addition to the several independent hypothesis tests for the grid points, a new field significance level is defined by acting on the collection of p-values and depending on a control level for the false discovery rate. The FDR procedure yields a global p-value threshold ($p^* = 0.009$) based on the distribution of p values obtained from the MK test. Given the above, a decreasing trend is found south of the main Gulf Stream Sea Surface Temperature (SST) zone, partially driven by changes in frontal precipitation (cf. Figs. 4.9a and 4.9b). The trend estimates a decrease in precipitation by 8mm/year, which corresponds to almost a net loss of 300mm during the 38-year period from 1979 to 2016. Localized negative trends also affect southern Canada and France where frontal precipitation decreases more slowly but still up to 5 mm/year. The trend estimates a weaker decrease of frontal precipitation, up to 4 mm/year in the Gulf Stream SST zone where changes are significant only according to the Mann-Kendall test not taking into account the field significance constraint (Fig. 4.9b). Cold fronts explain most of the above-mentioned variations whereas warm fronts have an overall weaker impact (cf. Figs. 4.9c and 4.9d). Only southeastern Europe and northern Canada are characterized by some areas of significant increasing trends, up to 4mm/year and up to 6mm/year for total and frontal

precipitation respectively. Both warm-front and cold-front precipitation are driving these changes.

Along the storm track region (30°N-35° N and 80°W-70°W) there is a weak but significant signal for a poleward displacement of frontal precipitation (Fig. 4.9b). Past studies showed this tendency for front frequencies (Berry et al., 2011b; Catto et al., 2014), as well as for the path of extratropical cyclones (Zappa et al., 2013). Our findings suggest that the decrease of precipitation over this area is mainly associated with a significant decrease of cold-front precipitation, whereas the warm fronts are driving the northward increase. The trend for the number of hours a front covers each grid point is also calculated and no significant changes are found over the Gulf Stream SST zone. That is, frontal precipitation is decreasing even though the number of frontal grid points detected by the method is not changing. This means that less precipitation is associated, on average, to the fronts. Considering the full domain, frontal precipitation can be considered as the main driver for most precipitation trends, except for the decrease over the Gulf of Mexico and France.

A separate analysis shows that the trends are significant mostly for convective frontal precipitation (Fig. 4.10). It is worth pointing out that our results are entirely based on precipitation taken from ERA-Interim reanalysis data and it is not clear whether these trends are also seen in observation or satellite estimates.

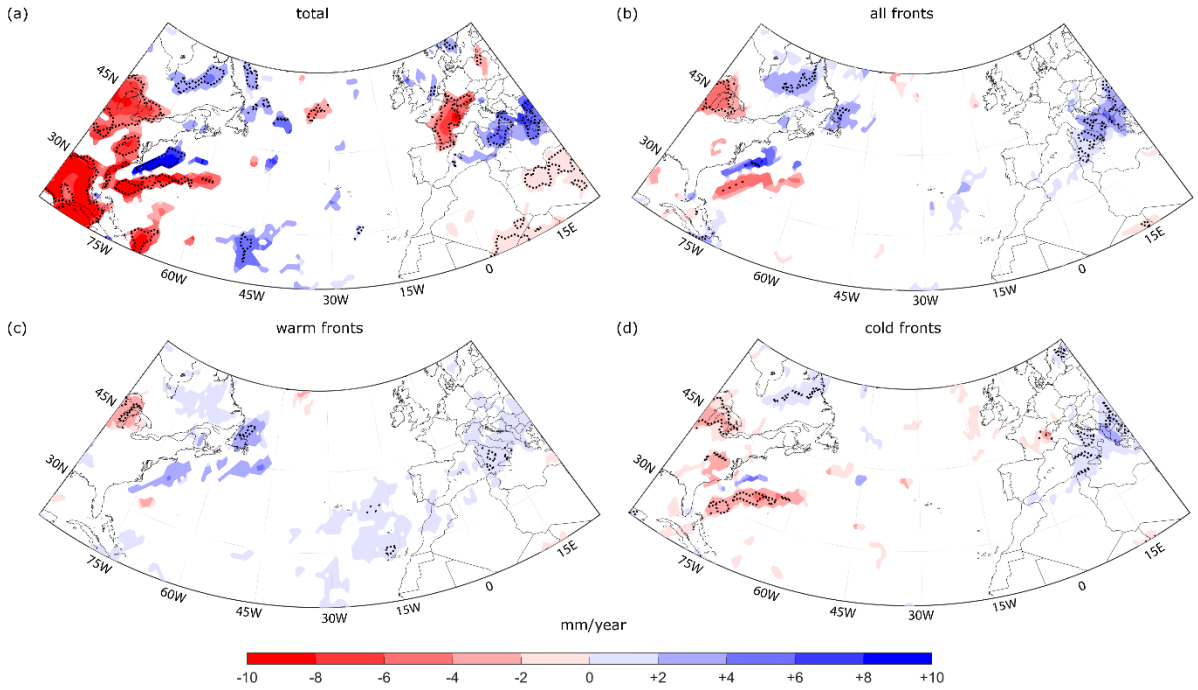

Figure 4.9. Annual trend for (a) total precipitation and for precipitation assigned to (b) all front, (c) warm fronts and (d) cold front. Only regions with statistical significance higher than 10% are plotted (modified Mann-Kendall test). Contoured regions are statistically significant according to the criterion for field significance of Wilks et al. (2016).

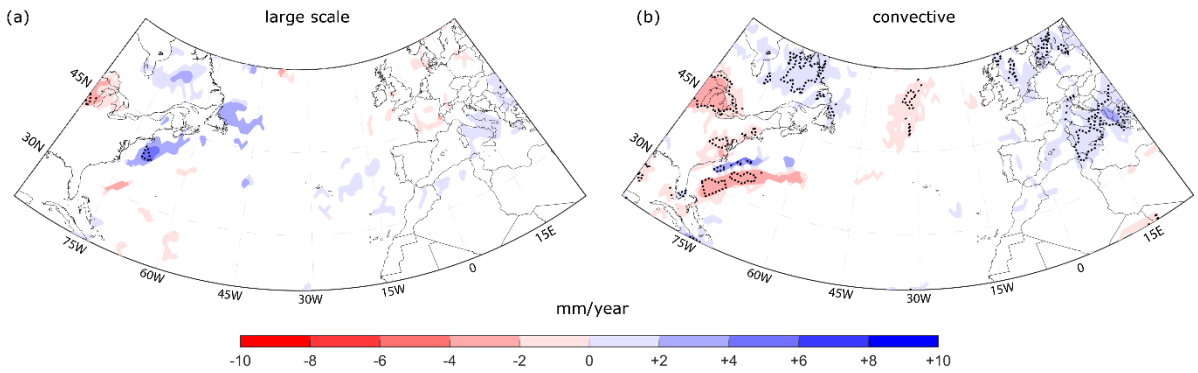

Figure 4.10. Annual trend for (a) large-scale frontal precipitation and (b) convective frontal precipitation. Only regions with statistical significance higher than 10% are plotted (modified Mann-Kendall test). Contoured regions are statistically significant according to the criterion for field significance of Wilks et al. (2016).

4.4 Summary and conclusions

In this study, a method to relate fronts with precipitation on 6-hourly time scales was developed, tested and discussed. Fronts are identified through an automated objective method based on a thermal approach as presented by Schemm et al. (2015). For consistency, precipitation, as well as the front detection, are based on ERA-Interim data (Dee et al., 2011a).

The method to relate fronts with precipitation is based on the co-location of 6-hourly accumulated precipitation, centered at each time step, and fronts inside a *search box*. Precipitation is assigned to the specific front type (cold and warm front) according to the length each front covers inside the search box. The optimal size for the search box is identified using random sampling techniques. A 6°x6° search box was found to be optimal because beyond this size, which corresponds approximately to half the synoptic length scale, the amount of added frontal precipitation is no longer distinguishable from added noise. The case of an extreme event illustrates that the presented method is capable of linking fronts with precipitation even in rapidly evolving situations. Further, based on a separation of cold and warm fronts according to temperature advection, the method allows for distinguishing warm-front from cold-front precipitation.

Analyses of annual and seasonal cycles show that the fraction of frontal precipitation is up to 80% (1500 mm/year) relative to the total amount of precipitation over the North Atlantic storm track region. High relative fractions of frontal precipitation (approximately 40%; 400 mm/year) extend all over the North Atlantic up to Western Europe, especially during autumn (circa 50%; 160 mm/3 months) and winter (circa 70%; 200 mm/3 months). This is not surprising because autumn and winter correspond to those seasons with the most active storms.

Finally, a trend analysis of frontal precipitation shows a statistically significant decrease of frontal precipitation over the past 38 years for the Gulf Stream region, mostly driven by cold fronts and owing to a poleward shift of fronts and related storms in this region (Berry et al., 2011b).

However, it remains unclear whether the trends in frontal precipitation are also seen in observation or if they are a result of the model-derived precipitation in the reanalysis data.
For the study of midlatitudes weather variability, the capacity to objectively link precipitation to the specific weather pattern or flow features is becoming increasingly useful (Hawcroft et al., 2012). The here described approach can be adapted and applied to extratropical cyclones, fronts, or any other objectively identified flow feature (e.g., atmospheric rivers). This has the potentiality to improve risk assessments of extreme weather events. Therefore, priority for future work will be given to the dynamics of specific case studies occurring over the North Atlantic storm track region, the area that accounts for the main identified climatological patterns. Further observational data sets will be used for precipitation as reanalysis may not represent properly extreme and localized events.

4.5 Supplementary Material

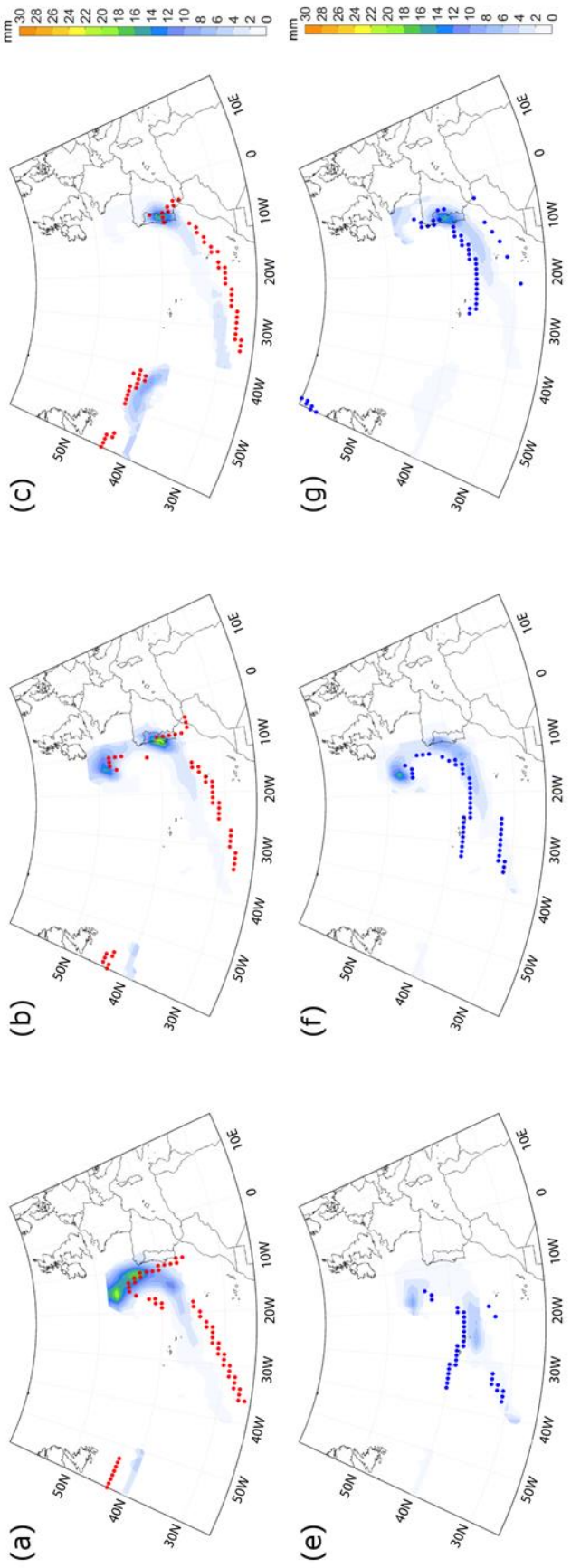

Figure 4.1.S. Case study 26th-27th October 2004. Red (blue) dots correspond to warm (cold) fronts. Left, central and right columns correspond respectively to 18 UTC, 00 UTC and 06 UTC on 26th-27th October 2004. Color shading corresponds to assigned precipitation to warm (a-c) and to cold (d-f) fronts.

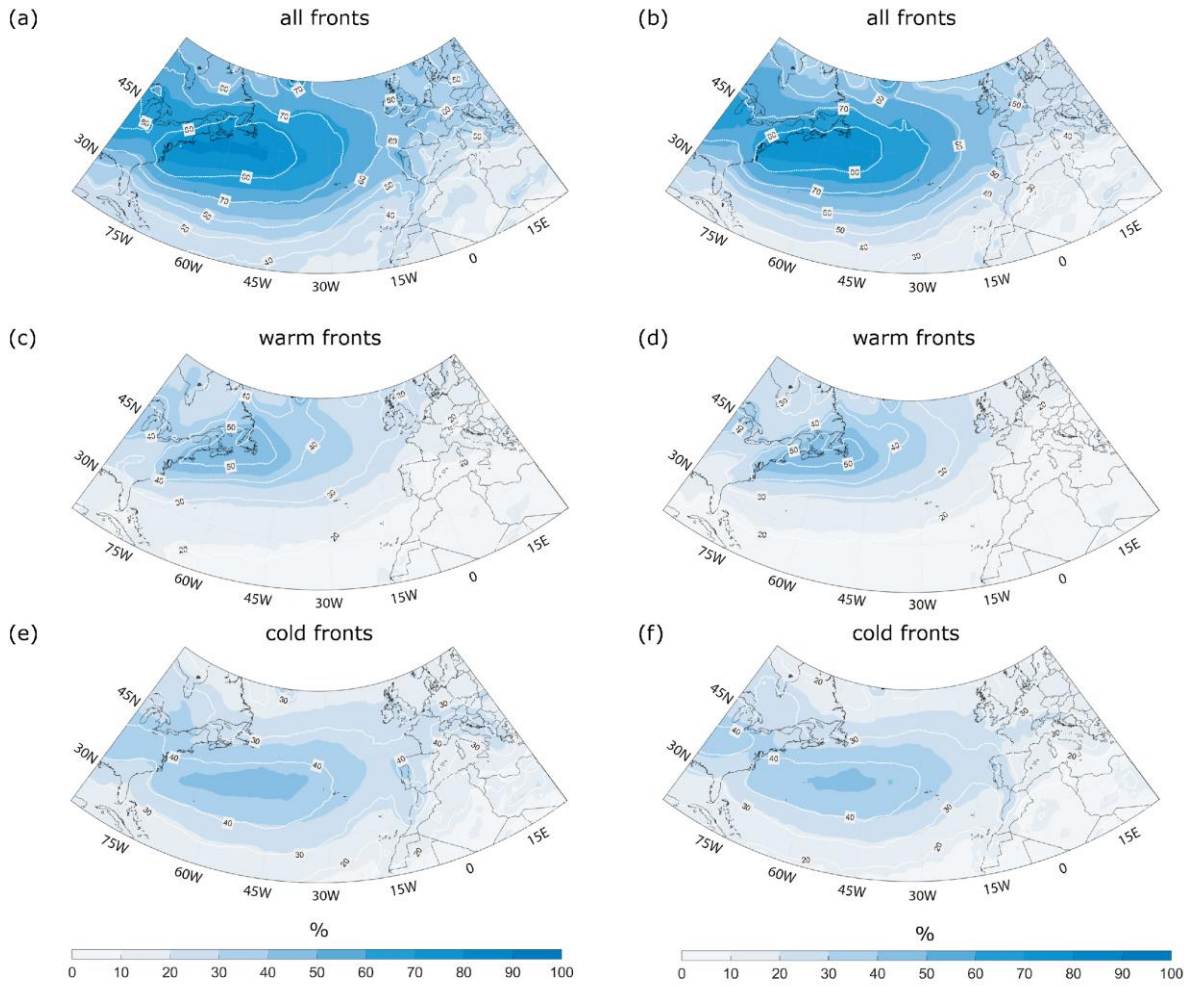

Figure 4.2.S. Annual cycle of frontal precipitation. In the left column color shading corresponds to fractions of frontal over total precipitation with a 4K $[100km]^{-1}$ threshold for the minimum thermal gradient used to detect fronts. White contours correspond to a dataset that includes quasi-stationary fronts (only values over 20%). In the right column same as for the left column but with a 3.5K $[100km]^{-1}$ threshold.

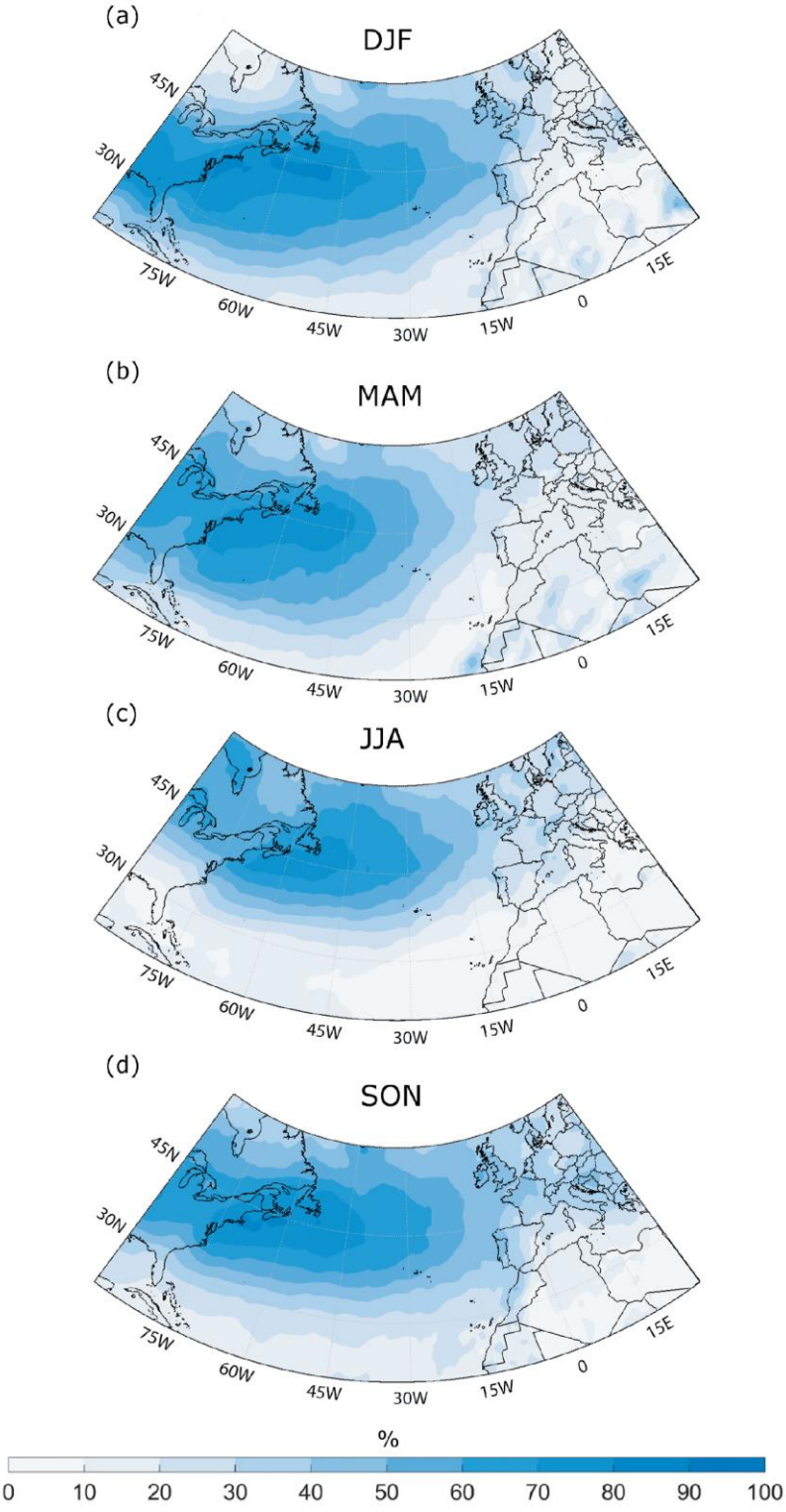

Figure 4.3.S. Seasonal climatology of assigned precipitation based on 34-year ERA-Interim dataset. Percentage of total precipitation assigned to all fronts for (a-b) December to February; (c-d) March to May; (e-f) June to August and (g-h) September to November**.**

5

Final Remarks and Conclusions

5.1 Outlook of the main results

The motivation behind this thesis was the characterization of high-impact weather events affecting the Iberian Peninsula (IP). To do so, this thesis analyses the North-Atlantic storms variability, its link to large-scale frontal system variability and how it affects the local weather of the IP. In addition, the relationship between storms, precipitation and wind extremes, in a compound weather extreme perspective producing multiple hazards was also established.

The results of this thesis are presented in three main chapters that characterize the North-Atlantic storms variability and its impacts. This section highlights the main findings for these chapters, and it answers the research questions mentioned in Chapter 1.

Chapter 2. Precipitation data sets and extreme events on the IP

This chapter is focused on the reliability of several precipitation data sets (from reanalysis to satellite observations) for the Iberian Peninsula (IP). The precipitation data sets considered include both reanalysis (from ECMWF) and satellite products (from TRMM mission). Data was aggregated in daily sum and days were also grouped in classes of precipitation to analyze the extreme events. The first research question for this topic is whether the most widely used precipitation data sets are adequate to represent extreme precipitation events on the IP. In fact, for the days characterized by very large anomalies of accumulated precipitation, most of the data sets showed large biases and errors, especially those satellite-based. In general, precipitation is underestimated, and extreme precipitation is even greatly underestimated. Among the satellite products, the near-real-time version of the TRMM 3B42 series outperformed the post-real-time version for the most extreme classes, although the latter is commonly considered more suited for research purposes. In this regard, another important question concerns the added value of ERA5, especially if compared to ERA-Interim. Indeed, ERA5 showed massive improvements in all the metrics with respect to its predecessor (larger correlation, lower bias and notably reduction of the error metrics) and turned out as the best choice to study precipitation extremes in the IP. The third research question for this chapter was about the main error sources that still affect precipitation data sets on the IP. Through bias decomposition, it was shown that the false negatives (false positives) still represent a considerable limitation in the accuracy of satellite (reanalysis) products, although ERA5 clearly outperforms all the other data sets also from this perspective. Whereas there are no noticeable differences in bias error sources between the TRMM 3B42 near-real-time and post-real-time

products, it is striking how ERA5 improved with respect to ERA-Interim, mostly in the hit bias error.

Chapter 3. A ranking of concurrent precipitation and wind extreme events for the IP

In Chapter 3, a ranking of concurrent precipitation and wind events is computed for the IP during the period 1979-2019. Given the results of the previous chapter, ERA5 data is used. The meteorological extremes, namely daily precipitation and daily maximum wind speed are ranked according to magnitude indices. For precipitation, the index considers both the extent of the anomaly and the area affected by the anomaly. For wind, the index is based on the exceedance of a percentile threshold for the maximum daily wind speed. By summing and normalizing, a new index is computed for concurrent events. The top100 concurrent extreme events are detailed in terms of cyclone properties, Atmospheric Rivers (ARs) and the spatial pattern of meteorological extremes. The first research question for this chapter is about how often concurrent extreme precipitation and wind events affect the IP. A novel insight that emerged in this study is that wind events are more independent from precipitation than the contrary. The frequency of both as that of concurrent events is higher during the canonical winter months even though a slight shift in time towards late winter/early spring is observed over the very last years. Secondly, we want to know which are the cyclones' properties associated with such events. This study clearly showed that around 85 out of the top100 concurrent extreme events in this region do have associated cyclones. Of these, half do have a trajectory that directly crosses the IP whereas all the others affect the IP while passing over the ocean. The last question addresses the existence of any potential regional variability or trend of concurrent precipitation and wind events. In this study, a specific sector of the northwestern IP, roughly corresponding to the Minho and Douro river basins, emerged as the top affected area by concurrent precipitation and wind extremes. The co-occurrence of Atmospheric Rivers (ARs) with precipitation and wind extremes is higher here than anywhere else in the IP (up to 40%).

Chapter 4. Assigning precipitation to atmospheric fronts on the North-Atlantic and European Sector

In the IP, precipitation and wind extremes are very often driven by a clear cyclonic feature, as shown in the abovementioned ranking. Moreover, the meteorological impacts do follow the cyclone's trajectory. Indeed, the cyclone lifecycle is typically described employing frontal

structures, along which precipitation develops and wind intensifies. This close connection is further investigated here through a methodology to objectively relate atmospheric fronts and precipitation at a sub-daily basis. The main research question addressed here is about the existence and robustness of such a methodology. Precipitation is related to fronts according to a spatial and temporal criterion. A random sampling technique is applied to determine the optimal dimension of the search box used to spatially relate frontal grid points and the 6h-accumulated precipitation at the same point, in the framework of gridded products such as reanalysis. It is found that for search boxes larger than 6°x6° (ERA-Interim data) it is no more possible to distinguish if the added precipitation is due to the vicinity of the fronts or to random noise instead, answering the main research question addressed about the existence and robustness of such a methodology. Given this approach, the next question is about the fraction of total precipitation associated with fronts, and about any potential regional difference and/or trend in frontal-related precipitation. A higher ratio of frontal to total precipitation (up to 80%) is found along the storm track region where a poleward shift of frontal precipitation is also observed. This tendency is mainly driven by cold fronts. Focusing on land areas, frontal precipitation mainly affects the western extremities of the IP (in consensus with previous chapters) and the historical trend is more contrasting.

5.2 Discussion and Future work

The general aim of the thesis was to explore the variability and mechanisms of precipitation and wind extreme events, focusing on a pre-defined geographical domain that includes the North Atlantic (NA) Ocean and the continental IP. Despite the quite broad subject, the thesis deals specifically with extratropical cyclones leading to weather extremes and extreme impacts. On one side, the outcomes of this thesis represent a novel characterization of extreme events on the IP, to consider in further studies on the region. On the other side, this thesis provides for a suite of research tools that can be easily adapted to other studies in the context of weather extremes, or to other domains.

In Chapter 2 it was assessed if ERA5 is the best gridded product for estimating precipitation on the IP and if this holds also for extreme precipitation events. It is known that extreme precipitation events, as for convective storms, are typically localized and of short duration. Therefore, a certain benefit from the ERA5 improvements in grid spacing and the

hourly reporting of accumulated precipitation was expected. The recent ERA5 reanalysis was released in 2019 (Hersbach et al., 2020) and this work was among the firsts to assess its potential over the IP. Despite it ranked best among the data sets considered, ERA5 still accounts for some caveats, as shown for the contribution of false alarms to the total bias. Increasing attention is given to false alarms in the literature (Tang G et al., 2020), in the context of future projections and usage of precipitation prediction for risk assessment. This comes especially true over complex terrain such as over the Alpine region (Sharifi et al., 2019). Tang G et al. (2020) have performed a comparison of several precipitation products, ranging from TMPA TRMM mission to the new Global Precipitation Measurement (GPM) mission, towards reanalysis, and false alarms are the main source of error, indeed. Moreover, the reanalysis scored worse than satellite products in their study.

In this regard, two satellite precipitation products from the TMPA TRMM mission, which have been largely studied worldwide at tropical latitudes, are examined in this thesis. The exploration of similar products to such a high latitudinal band as for the IP is quite a novelty in the literature. Most of the previous studies, as referred to in Chapter 2, assume that the post-real-time version (TRMM) is more suited for research purposes than the near-real-time (TRMM RT). However, according to the results of this thesis, it rather depends on which events are considered: for example, when dealing with extreme events or with extreme beyond-average anomalies, TRMM RT equals or even outperforms its counterpart version (and also ERA-Interim) in terms of both precipitation bias and error metrics. An increasing number of studies are now showing that the near-real-time products, as for any other satellite product, do have their strengths and limitations and that they are not better or worse than post-real-time products in absolute terms (e.g., Palharini et al, 2020; Mossaffa, 2020; Huang et al., 2021). Their performance strictly depends on the domain of interest instead, with the orography playing a key role (Derin et al., 2019). This is a vivid branch of research, for which extensive studies are missing, especially at the extratropical latitudes and for the European domain.

Currently, the TMPA TRMM mission is not active anymore and its products have been incorporated under the new GPM umbrella (Huffman et al., 2020), with the Integrated Multi-satellitE Retrievals for GPM (IMERG) algorithm. In the framework of GPM, an IMERG early run and an IMERG final run are still released, following the TRMM scheme. Therefore, the findings of this work easily extend to the new series. Indeed, the first (and very recent) published studies on GPM products also suggest that the early-released product has better timeliness, making it appealing to flood forecast, early warning and monitoring (e.g., Tang S et al., 2020; Arshad et al., 2021; Ramos et al., 2020).

Even though Chapter 2 dealt exclusively with precipitation, it is acknowledged that weather extremes do not always occur independently, conversely, they are often associated with the same large-scale feature, as for extratropical cyclones in the IP. The research pursued in Chapter 3 is part of the bigger picture of "compound events", a multi-hazard approach to extreme events that emerged in the scientific community over the last decade. This approach considers the interdependence and the co-occurrence of several potential meteorological extremes within the very same episode (e.g., Leonard et al., 2014; Zscheischler et al., 2018; Ridder et al, 2020).

A characterization of concurrent precipitation and wind events, classified as a compound event, is addressed in terms of common temporal and spatial patterns in chapter 3. According to the new classification typology suggested in Zscheischler et al. (2020a), these events are considered as "temporally and spatially compounding", to distinguish from the multivariate and preconditioned ones for which a statistical dependency is assessed.

Through the analysis of concurrent precipitation and wind events, several aspects of IP climatology also emerged. For example, it was shown that over the very last years extreme concurrent precipitation and wind events are shifting in time towards late winter/early spring. This was referred to as evidence of changes in the seasonal cycle, as for the intensification of heatwaves and persistence of drought conditions (e.g., Pereira et al., 2017; Ribeiro et al., 2020b, Páscoa et al., 2021; Liberato et al., 2021) that often overrun the canonical summer thus delaying the establishment of the autumn and winter typical atmospheric circulation patterns. Another novel insight of this study is that wind events are more independent from precipitation than the contrary. There was no previous evidence of this, but indeed it is known that wind extremes might be caused by external forcings other than cyclones, including large-scale pressure gradients (Karremann et al., 2016) or local steep topography (Durran, 2003; Huang et al., 2019). In this study, a specific sector of the northwestern IP, roughly corresponding to the Minho and Douro river basins, emerged as the top affected area by concurrent precipitation and wind extremes. This sector of the IP is well known for its high annual precipitation total and also for being often hit by NA extratropical cyclones (Gómez-Gesteira et al., 2011; Saez de Cámara et al., 2015; Lavers et al., 2018). This study clearly showed that almost all cyclones that approach Iberia, regardless of their specific trajectories, do have meteorological impacts on this region. In a recent study from Martins et al. (2020), wind extreme events are projected to increase during the century, especially in NW Iberia. In the same study, projected wind-

shear and wind helicity will also increase, mainly in SW Iberia. It is exactly where most of the exclusive wind extremes were observed in this thesis. These similarities deserve more in-depth analysis as they might indicate a different nature of wind events and their drivers among neighboring IP regions.

Another crucial aspect that emerged from this study is the presence of Atmospheric Rivers (Ars) attending the concurrent precipitation and wind events (up to 40% of the top100 concurrent events in NW Iberia do have an attended AR). This opens up new perspectives for future research, namely on (1) the potential broadening of compound events studies in the IP to ARs and other weather features, (2) the study of ARs as potential drivers for the intensification of extratropical cyclones and (3) the necessity to better characterize and classify the ARs occurrences, as they are becoming important players in impact and risk assessment studies. Whereas there is vivid research regarding the last argument, including studies on future projections (e.g., Gimeno et al., 2021; Eiras-Barca et al., 2021), the other topics are not yet fully addressed in the literature, and they represent a compelling line of research for the near future. For example, ARs have been considered so far as proxies for the precipitation enhancement; on the other side, it is demonstrated that a lack of ARs does produce the opposite effect, that is it strengthens drought conditions on the IP (e.g., Payne et al., 2020; Sousa et al., 2020; Sorì et al., 2020). Eventually, back to the compound events theoretical framework, further analysis can be pursued to define the statistical dependency between the probabilities of extreme rain and extreme wind. This is similar to what Bevacqua et al. (2020b) have recently done for precipitation and storm surges, to study compound coastal flooding. Linking the weather extremes to exposure and vulnerability analysis would also meet that demand for causal interconnections studies and bottom-up approaches that are strongly recommended by the compound events scientific community (Zscheischler et al., 2020b).

In Chapter 3 it was shown that at least 80% of concurrent precipitation and wind extreme events in the IP are clearly associated with an extratropical cyclone. The spatial patterns of precipitation and wind extremes were derived from reanalysis data, independently from the location of the potential leading cyclone. To define the relationship between meteorological extremes and larger-scale weather features as for precipitation and cyclones, objective criteria are needed. The cyclone lifecycle is typically described employing frontal structures, along which precipitation develops (Field and Wood, 2007). Several studies (e.g., Hawcroft et al., 2012; Neu et al., 2013; Lombardo et al., 2015) have quantified the total amount of precipitation and extreme precipitation associated with cyclones, typically by defining a radius of influence around the cyclone center, tracking its path and the corresponding precipitation falling inside.

However, only a few (Catto et al., 2012; Catto and Pfhal, 2013), including this thesis, tried to separate the frontal contributions.

The analysis pursued in chapter 4 represents a step forward in this context. The added value of using a random sampling technique to obtain the optimal box size for the allocation of precipitation to fronts potentially applies to other recent studies. In Dowdy and Catto (2017) precipitation is associated with the mutual fronts, cyclones and thunderstorms: this study is an interesting systematic analysis of all potential severe precipitation events, but it is based on a-priori established thresholds for the spatial association. Another recent work, by Rüdisühli et al. (2020) makes use of subjective thresholds, in this case to distinguish near-frontal and far-frontal precipitation. Nevertheless, it presents new potential skills derived from this methodology, as for the distinction between cold and warm frontal precipitation and between frontal and cyclonic precipitation.

In chapter 4 a long-term climatology of frontal precipitation is explored for the NA North Atlantic and European domains. New insights are provided for the historical trend of the amount of frontal to total precipitation: not only frontal precipitation is shifting poleward, but this tendency is shown to be mostly driven by cold fronts. The poleward shift of the North Atlantic storm track region is being discussed in the literature for both tropical (Shan and Yu, 2020) and extratropical cyclones (Tamarin-Brodsky and Kaspi, 2017), mainly based on cyclones tracking techniques. In this thesis, it is observed also for frontal-related precipitation. However, this still leaves room for different hypotheses regarding the underlying mechanisms: whether this trend is due to global circulation patterns, SST changes, or rather to the precipitation cycle itself whose variability is revealed through fronts-related analysis. These aspects represent a priority for future studies. On one side, the analysis can be improved by using ERA5 data. This would increase both the spatial and temporal accuracy of the methodology as for the sensitivity analysis for the search box. Moreover, new insights will be found while extending the trend analysis back in time, as soon as ERA5 will be definitely released back to 1950. On the other side, the main limitation of this analysis is that it is able to label a certain amount of precipitation as frontal precipitation, but it does not provide information on the specific front. While this is enough for the long-term assessment of frontal precipitation, it represents a caveat for short-term applications and case studies analysis: as the methodology applies to each time-step independently, there is no tracking over time.

Within this framework, Artificial Intelligence (AI) and Machine Learning (ML) approaches represent an enormous potential for improvement. Potentially, this refers to all kinds of association routines, involving a range of atmospheric flow features and/or weather variables, such as precipitation and cyclones, fronts and cyclones and so on. As described above, these routines typically rely on (1) the detection and tracking methods (iterative identification procedures) of the weather features to associate and (2) the definition of the spatial and temporal frame for the association to be straightforward. Regarding detection and tracking, novel approaches include, for example, deep learning neural networks for the automated detection of weather fronts (Biard and Kunkel, 2019), deep learning for explicit prediction of synoptic-scale fronts (Lagerquist et al., 2019) and machine learning-based cyclones labeling from satellite data (Bonfanti et al., 2018). Eventually, further efforts are needed towards integrating the detection and tracking techniques for the weather features with the association procedure.

In summary, this thesis highlighted how the occurrence of precipitation and wind extremes is tidily related to extratropical cyclones in the Iberian Peninsula. This analysis leads to a novel characterization of these events by investigating the temporal and spatial common patterns of both the meteorological extremes and the associated larger-scale weather features such as cyclones and atmospheric fronts. The Atlantic coast and specifically the northwestern Iberia emerged as hotspots for these events. This thesis presented novel and portable routines to objectively describe and classify these relationships, based on the most common gridded available data sets for the region. It is expected that some of these results will serve as benchmarks for future studies on weather extremes in the IP.

References

Abhigna BS, Nitasha S, Shilpa D, Crowdsourcing – A Step Towards Advanced Machine Learning. *Procedia Computer Science.* 2018; Volume 132, Pages 632-642, doi: 10.1016/j.procs.2018.05.062.

Acero FJ, Parey S, García JA, Dacunha-Castelle D. Return level estimation of extreme rainfall over the Iberian Peninsula: Comparison of methods. *Water (Switzerland)*. 2018; *10*(2), doi: 10.3390/w10020179.

Adler RF, Huffman GJ, Chang A, et al. The version 2 global precipitation climatology project (GPCP) monthly precipitation analysis (1979–present). *J. Hydrometeorol.* 2003; 4, 1147-1167, doi: 10.1175/1525-7541(2003)004<1147:TVGPCP>2.0.CO;2.

Ai P, Yuan D, Xiong C. Copula-based joint probability analysis of compound floods from rainstorm and typhoon surge: A case study of Jiangsu Coastal Areas, China. *Sustainability*. 2018; 10(7), doi:10.3390/su10072232.

Alexander LV, Fowler HJ, Bador M, Behrangi A, Donat MG et al. On the use of indices to study extreme precipitation on sub-daily and daily timescales. *Environ. Res. Lett.* 2019; 14(12), 5008, doi: 10.1088/1748-9326/ab51b6.

Anderson C. Estimating the propagation velocity of atmospheric fronts from surface wind observations. *Atmosphere-Ocean*. 1990, 28:3, 330-344. doi: 10.1080/07055900.1990.9649381.

Andrade C, Santos JA, Pinto JG, Corte-Real J. Large-scale atmospheric dynamics of the wet winter 2009–2010 and its impact on hydrology in Portugal. *Clim. Res*. 2011; 46:29-41. doi: 10.3354/cr00945.

Aon-Benfield. Annual global climate and catastrophe report IF 2018. http://www.aon.com. Accessed: April 2020.

Arshad M, Xieyao M, Jun Y, et al. Evaluation of GPM-IMERG and TRMM-3B42 precipitation products over Pakistan. *Atmospheric Research.* 2021; Volume 249, 105341, doi: 10.1016/j.atmosres.2020.105341.

Athanasiadis PJ, Wallace JM, Wettstein JJ. Patterns of Wintertime Jet Stream Variability and Their Relation to the Storm Tracks. *J. Atmos. Sci*. 2010; 67, 1361–1381, doi: 10.1175/2009JAS3270.1.

Augusto S, Ratola N, Tarín-Carrasco P, Jiménez-Guerrero P, Turco M, Schuhmacher M, et al. Population exposure to particulate-matter and related mortality due to the Portuguese wildfires in October 2017 driven by storm Ophelia. *Environment International*. 2020; Vol. 144, 106056, doi; 10.1016/j.envint.2020.106056.

Azorin-Molina C, Vicente-Serrano SM, McVicar TR, et al. Homogenization and Assessment of Observed Near-Surface Wind Speed Trends over Spain and Portugal, 1961–2011. *J. Climate.* 2014; 27, 3692–3712, doi: 10.1175/JCLI-D-13-00652.1.

Barnett T, Zwiers F, Hegerl G, et al. Detecting and attributing external influences on the climate system: A review of recent advances. *Journal of Climate*. 2005; 18(9), 1291–1314, doi: 10.1175/JCLI3329.1.

Behrangi A, Hsu K-L, Imam B, Sorooshian S, Huffman GJ, Kuligowski RJ. PERSIANN-MSA: a precipitation estimation method from satellite-based multispectral analysis. *J. Hydrometeorol.* 2009; 10, 1414-1429, doi: 10.1175/2009JHM1139.1.

Belo-Pereira M, Dutra E, Viterbo P. Evaluation of global precipitation data sets over the Iberian Peninsula. *J. Geophys. Res*. 2011; 116, D20101. doi: 10.1029/2010JD015481.

Bengtsson L, Hagemann S, Hodges KI. Can climate trends be calculated from reanalysis data?. *J. Geophys. Res.* 2004; 109, D11111. doi: 10.1029/2004JD004536.

Benjamin SG, Brown JM, Brunet G, Lynch P, Saito K, Schlatter TW. 100 Years of Progress in Forecasting and NWP Applications. *Meteorological Monographs*. 2018; *59*, 13.1-13.67, doi:10.1175/amsmonographs-d-18-0020.1.

Berry G, Reeder MJ, Jakob C. A global climatology of atmospheric fronts. *Geophysical Research Letters.* 2011a; 38: L04809. doi: 10.1029/2010GL046451.

Berry G, Jakob C, Reeder M. Recent global trends in atmospheric fronts. *Geophys. Res. Lett.* 2011b; 38: L21812. doi: 10.1029/2011GL049481.

Bevacqua E, Maraun D, Hobæk Haff I, Widmann M, Vrac M. Multivariate statistical modelling of compound events via pair-copula constructions: Analysis of floods in Ravenna (Italy). *Hydrology and Earth System Sciences*. 2017; 21(6), 2701–2723, doi: 10.5194/hess-21-2701-2017.

Bevacqua E, Vousdoukas MI, Shepherd TG, Vrac M. Brief communication: The role of using precipitation or river discharge data when assessing global coastal compound flooding. *Nat. Hazards Earth Syst. Sci.* 2020a, 20, 1765–1782, doi; 10.5194/nhess-20-1765-2020.

Bevacqua E. Vousdoukas MI, Zappa G. et al. More meteorological events that drive compound coastal flooding are projected under climate change. *Commun. Earth Environ.* 2020b; 1, 47, doi: 10.1038/s43247-020-00044-z.

Bevacqua E, De Michele C, Manning C, Couasnon A, Ribeiro AFS, Ramos AM et al. Guidelines for studying diverse types of compound weather and climate events. *Earth's Future.* 2021; 9, e2021EF002340, doi: 10.1029/2021EF002340.

Biard JC, Kunkel KE. Automated detection of weather fronts using a deep learning neural network. *Advances in Statistical Climatology, Meteorology and Oceanography*. 2019; *5*(2), 147–160, doi: 10.5194/ascmo-5-147-2019.

Bolvin DT, Huffman GJ. Transition of 3B42/3B43 Research Product from Monthly to Climatological Calibration/Adjustment. Scientific Report, 2015. https://pmm.nasa.gov/sites/default/files/imce/3B42_3B43_TMPA_restart.pdf. Accessed date: Sept 24, 2018.

Bonfanti C, Trailovic L, Stewart J, Govett M. Machine Learning: Defining Worldwide Cyclone Labels for Training. *21st International Conference on Information Fusion.* 2018; 753–760, doi: 10.23919/ICIF.2018.8455276.

Bouwer LM. Observed and Projected Impacts from Extreme Weather Events: Implications for Loss and Damage. In: Mechler R., Bouwer L., Schinko T., Surminski S., Linnerooth-Bayer J. (eds) Loss and Damage from Climate Change. Climate Risk Management, Policy and Governance. 2019. Springer, Cham. Doi: 10.1007/978-3-319-72026-5_3.

Brown TM, Pogorzelski WH, Giammanco IM. Evaluating Hail Damage Using Property Insurance Claims Data, *Weather*. 2015; Climate, and Society, 7(3), 197-210, doi: 10.1175/WCAS-D-15-0011.1.

Cai Y, Jin C, Wang A, Guan D, Wu J, Yuan F, et al. Spatio-Temporal Analysis of the Accuracy of Tropical Multisatellite Precipitation Analysis 3B42 Precipitation Data in Mid-High Latitudes of China. *PLoS ONE*. 2015; 10(4): e0120026, doi: 10.1371/journal.pone.0120026.

Cardoso Pereira S, Marta-Almeida M, Carvalho AC, Rocha A. Extreme precipitation events under climate change in the Iberian Peninsula. *Int J Climatol.* 2020; 40: 1255– 1278, doi: 10.1002/joc.6269.

Catto JL, Shaffrey LC, Hodges KI. Can climate models capture the structure of extratropical cyclones? *Journal of Climate*. 2010; 23(7), 1621–1635, doi: 10.1175/2009JCLI3318.1.

Catto JL, Jakob C, Berry G, Nicholls N. Relating global precipitation to atmospheric fronts. *Geophysical Research Letters.* 2012; 39: L10805, doi: 10.1029/2012GL051736.

Catto JL, Pfahl S. The importance of fronts for extreme precipitation. *Journal of Geophysics Research: Atmospheres.* 2013; 118, 10,791–10,801, doi: 10.1002/jgrd.50852.

Catto JL, Nicholls N, Jakob C, Shelton KL Atmospheric fronts in current and future climates. *Geophysical Research Letters.* 2014; 41: 7642–7650, doi: 10.1002/2014GL061943.

Catto JL, Ackerley D, Booth J, Champion AJ, Colle BA, Pfahl S, et al. The Future of Mid-Latitude Cyclones, *Current Climate Change Reports*. 2019; 5, 407-420, doi: 10.1007/s40641-019-00149-4.

Changnon SA, Changnon D, Hilberg S. Hailstorm across the Nations. Illinois State Water Survey, Contract Report 2009-12. 2009.

Chen S, Hong Y, Cao Q, Gourley JJ, Kirstetter P-E, Yong B et al. Similarity and difference of the two successive V6 and V7 TRMM multisatellite precipitation analysis performance over China. *J. Geophys. Res. Atmos*. 2013; 118, 13060–13074, doi: 10.1002/2013JD019964.

Cherenkova E, Kononova N, Muratova N. Summer drought 2010 in the European Russia. *Geography, Environment, Sustainability*. 2013;6(1):55-66, doi: 10.24057/2071-9388-2013-6-1-81-92.

Clarke LC, Renard RJ. The U.S. Navy numerical frontal analysis scheme: further development and a limited evaluation. *Journal of Applied Meteorology*. 1966; 5: 764–777, doi: 10.1175/1520-0450(1966)005<0764:TUSNNF>2.0.CO;2.

Coll J, Aguilar E, Ashcroft L. Drought variability and change across the Iberian Peninsula. *Theor. Appl. Climatol*. 2017; 130, 901–916, doi: 10.1007/s00704-016-1926-3.

Coll-Hidalgo P, Pérez-Alarcón A, Fernández-Alvarez JC, Nieto R, Gimeno L. Moisture Sources for the Explosive Cyclogenesis of Extratropical Cyclone Miguel (2019) through a Lagrangian Approach. *Environmental Sciences Proceedings*. 2021; 8(1):19, doi: 10.3390/ecas2021-10331.

Cornes RC, Jones PD. How well does the ERA-Interim reanalysis replicate trends in extremes of surface temperature across Europe?. *J. Geophys. Res. Atmos. 2013;* 118, 10, 262–10,276, doi: 10.1002/jgrd.50799.

Daly C, Smith JW, Smith JI, McKane RB. High-Resolution Spatial Modeling of Daily Weather Elements for a Catchment in the Oregon Cascade Mountains, United States. *J. Appl. Meteor. Climatol.* 2017; 46, 1565–1586, doi: 10.1175/JAM2548.1.

Davolio S, Della Fera S, Laviola S, Miglietta MM, Levizzani V. Heavy Precipitation over Italy from the Mediterranean Storm "Vaia" in October 2018: Assessing the Role of an Atmospheric River, *Monthly Weather Review*. 2020; 148(9), 3571-3588, doi: 10.1175/MWR-D-20-0021.1.

de Leeuw J, Methven J, Blackburn M. Evaluation of ERA-Interim reanalysis precipitation products using England and Wales observations. *Quarterly Journal of the Royal Meteorological Society*. 2015; 141: 798–806, doi: 10.1002/qj.2395.

de Luis M, Brunetti M, Gonzalez-Hidalgo JC, Longares LA, Martin-Vide J. Changes in seasonal precipitation in the Iberian Peninsula during 1946-2005. *Glob. Planet. Change.* 2010; 74, 27–33, doi: 10.1016/j.gloplacha.2010.06.006.

Dee DP, Uppala SM, Simmons AJ, Berrisford P, Poli P, Kobayashi S, et al. The ERA-Interim reanalysis: configuration and performance of the data assimilation system. *Quarterly Journal of the Royal Meteorological Society.* 2011a; 137, 553–597, doi: 10.1002/qj.828.

Dee DP, Källén E, Simmons AJ, Haimberger L. Comments on "Reanalyses Suitable for Characterizing Long-Term Trends". *Bulletin of the American Meteorological Society*. 2011b; 92, 65–70, doi: 10.1175/2010BAMS3070.1.

Della-Marta PM, Pinto JG. Statistical uncertainty of changes in winter storms over the North Atlantic and Europe in an ensemble of transient climate simulations. *Geophys. Res. Lett.* 2009; 36, L14703, doi: 10.1029/2009GL038557.

DeMoss JD, Bowman KP. Changes in TRMM Rainfall due to the Orbit Boost Estimated from Buoy Rain Gauge Data. *J. Atmos. Oceanic Technol.* 2007; 24, 1598–1607, doi: 10.1175/JTECH2082.1.

Deveson ACL, Browning KA, Hewson TD. A classification of FASTEX cyclones using a height-attributable quasi-geostrophic vertical-motion diagnostic. *Quarterly Journal of the Royal Met. Society*. 2002; 128(579), 93–117, doi: 10.1256/00359000260498806.

Donat MG, Leckebusch GC, Wild S, Ulbrich U. Future changes in European winter storm losses and extreme wind speeds inferred from GCM and RCM multi-model simulations. *Nat. Hazards Earth Syst. Sci.* 2011; 11, 1351–1370, doi: 10.5194/nhess-11-1351-2011.

Donat MG, Sillmann J, Wild S, Alexander LV, Lippmann T, Zwiers FW. Consistency of Temperature and Precipitation Extremes across Various Global Gridded In Situ and Reanalysis Data sets. *J. Climate.* 2014; 27, 5019–5035, doi: 10.1175/JCLI-D-13-00405.1.

Dowdy AJ, Catto J. Extreme weather caused by concurrent cyclone, front and thunderstorm occurrences. *Scientific Reports*. 2017; 7, 40359, doi: 10.1038/srep40359.

Durán L, Barstad I. Multi-scale evaluation of a linear model of orographic precipitation over Sierra de Guadarrama (Iberian Central System). *Int J Climatol.* 2018; 38, 4127–4141, doi: 10.1002/joc.5557.

Durran DR. Downslope winds, James R. Holton, Encyclopedia of Atmospheric Sciences, Academic Press, 2003, Pages 644-650, doi:10.1016/B0-12-227090-8/00288-8.

Easterling DR, Kunkel KE, Wehner MF, Sun L. Detection and attribution of climate extremes in the observed record, *Weather and Climate Extremes*. 2016; Volume 11, Pages 17-27, doi: 10.1016/j.wace.2016.01.001.

Ebert EE, Janowiak JE, Kidd C. Comparison of Near-Real-Time Precipitation Estimates from Satellite Observations and Numerical Models. *Bull. Amer. Meteor. Soc*. 2007; 88, 47-64, doi: 10.1175/BAMS-88-1-47.

Eiras-Barca J, Lorenzo N, Taboada J, Robles A, Miguez-Macho G. On the relationship between atmospheric rivers, weather types and floods in Galicia (NW Spain). *Nat. Hazards Earth Syst. Sci*. 2018a; 18, 1633–1645, doi: 10.5194/nhess-18-1633-2018.

Eiras-Barca J, Ramos AM, Pinto JG, Trigo RM, Liberato MLR, Miguez-Macho G. The concurrence of atmospheric rivers and explosive cyclogenesis in the North Atlantic and North Pacific basins. *Earth Syst. Dynam.* 2018b; 9, 91–102, doi: 10.5194/esd-9-91-2018.

Eiras-Barca J, Ramos AM, Algarra I, Vázquez M, Dominguez F, Miguez-Macho G et al. European West Coast atmospheric rivers: A scale to characterize strength and impacts. *Weather and Climate Extremes.* 2021; Volume 31,100305, ISSN 2212-0947, doi: 10.1016/j.wace.2021.100305.

El Kenawy AM, Lopez-Moreno JI, McCabe MF, Vicente-Serrano SM. Evaluation of the TMPA-3B42 precipitation product using a high-density rain gauge network over complex

terrain in northeastern Iberia. *Global and Planetary Change.* 2015, Volume 133, 188-200, doi: 10.1016/j.gloplacha.2015.08.013.

Faccini F, Luino F, Paliaga G, Sacchini A, Turconi L, de Jong C. Role of rainfall intensity and urban sprawl in the 2014 flash flood in Genoa City, Bisagno catchment (Liguria, Italy), *Applied Geography*. 2018; Vol. 98, pp. 224-241, doi: 10.1016/j.apgeog.2018.07.022.

Ferreira JA, Liberato MLR, Ramos AM. On the relationship between atmospheric water vapour transport and extratropical cyclones development. *Physics and Chemistry of the Earth*. 2016; Parts A/B/C, 94, 56-65, doi: 10.1016/j.pce.2016.01.001.

Field PR, Wood R. Precipitation and cloud structure in midlatitude cyclones. *Journal of Climate*. 2007; 20(2), 233–254, doi:10.1175/JCLI3998.1.

Fink AH, Brücher T, Ermert V, Krüger A, Pinto JG. The European storm Kyrill in January 2007: synoptic evolution, meteorological impacts and some considerations with respect to climate change. *Nat. Hazards Earth Syst. Sci.* 2009; 9, 405–423, doi: 10.5194/nhess-9-405-2009.

Fischer EM, Knutti R. Observed heavy precipitation increase confirms theory and early models. *Nature Clim Change.* 2016; 6, 986–991, doi: 10.1038/nclimate3110.

Fischer EM, Sippel S, Knutti R. Increasing probability of record-shattering climate extremes. *Nat. Clim. Chang.* 2021; 11, 689–695, doi: 10.1038/s41558-021-01092-9

Fragoso M, Trigo RM, Zêzere JL, Valente MA. The exceptional rainfall event in Lisbon on 18 February 2008. *Weather*. 2010; 65: 31–35, doi: 10.1002/wea.513.

Francis JA, Vavrus SJ. Evidence linking Arctic amplification to extreme weather in mid-latitudes. *Geophysical Research Letters*. 2012; 39(6), 1–6, doi: 10.1029/2012GL051000.

Gallego MC, Trigo RM, Vaquero JM, Brunet M, García JA, Sigró J, Valente MA. Trends in frequency indices of daily precipitation over the Iberian Peninsula during the last century. *Journal of Geophysical Research Atmospheres*. 2011; 116(2), 1–18, doi: 10.1029/2010JD014255.

García-Herrera R, Garrido-Perez JM, Barriopedro D, Ordóñez C, Vicente-Serrano SM, Nieto, R. The European 2016/17 Drought. *Journal of Climate.* 2019; 32(11), 3169-3187, doi: 10.1175/JCLI-D-18-0331.1.

Gardiner B, Blennow K, Carnus J-M, Fleischer P, Ingemarsson F, et al.. Destructive storms in European forests: past and forthcoming impacts. [Contract] 2010. ⟨hal-02824530⟩

Gaume E, Borga M, Llassat MC, Maouche S, Lang M, et al. Mediterranean extreme floods and flash floods . The Mediterranean Region under Climate Change. A Scientific Update, IRD Editions, pp.133-144, 2016, Coll. Synthèses, 978-2-7099-2219-7. ffhal-01465740v2f.

Gimeno L, Algarra I, Eiras-Barca J, Ramos AM, Nieto R. Atmospheric river, a term encompassing different meteorological patterns. *Wiley Interdisciplinary Reviews: Water.* 2021; 8(6), e1558, doi: 10.1002/wat2.1558.

Giorgi F. Climate change hot-spots. *Geophysical Research Letters*. 2006; 33(8), 1–4, doi: 10.1029/2006GL025734.

Gómez-Gesteira M, Gimeno L, deCastro M, Lorenzo MN et al. The state of climate in NW *Iberia. Clim. Res.* 2011; 48:109-144, doi: 10.3354/cr00967.

Gouveia CM, Trigo RM, Beguería S, Vicente-Serrano SM. Drought impacts on vegetation activity in the Mediterranean region: An assessment using remote sensing data and multi-scale drought indicators. *Global and Planetary Change*. 2017; Vol. 151, Pag. 15-27, doi: 10.1016/j.gloplacha.2016.06.011.

Govekar PD, Jakob C, Catto J. The relationship between clouds and dynamics in Southern Hemisphere extratropical cyclones in the real world and a climate model. *Journal of Geophysical Research*. 2014; 119(11), 6609–6628, doi: 10.1002/2013JD020699.

Graf MA, Wernli H, Sprenger M. Objective classification of extratropical cyclogenesis. *Quarterly Journal of the Royal Meteorological Society*. 2017; 143(703), 1047–1061, doi: 10.1002/qj.2989.

Grise KM, Polvani LM. The response of midlatitude jets to increased CO2.Distinguishing the roles of sea surface temperature and direct radiative forcing. *Geophysical Research Letter*. 2014; 6863–6871, doi: 10.1002/2014GL061638.

Guerreiro S, Kilsb C, Fowler HJ. Rainfall in Iberian transnational basins: a drier future for the Douro, Tagus and Guadiana?. *Climatic Change.* 2016; 135: 467, doi: 10.1007/s10584-015-1575-z.

Guisado-Pintado E, Jackson Derek WT. Coastal Impact From High-Energy Events and the Importance of Concurrent Forcing Parameters: The Cases of Storm Ophelia (2017) and Storm Hector (2018) in NW Ireland. *Frontiers in Earth Science*. 2019; Vol.7, Pag. 190, doi: 10.3389/feart.2019.00190.

Habib E, Henschke A, Adler RF. Evaluation of TMPA satellite-based research and real-time rainfall estimates during six tropical-related heavy rainfall events over Louisiana, USA. *Atmospheric Research.* 2009*;* 94, 373-388, doi: 10.1016/j.atmosres.2009.06.015.

Hanley J, Caballero R. The role of large-scale atmospheric flow and Rossby wave breaking in the evolution of extreme windstorms over Europe. *Geophysical Research Letters*. 2012; 39(21), 2–7, doi:10.1029/2012GL053408.

Hao Z, Hao F, Singh VP, Xia Y, Shi C, Zhang X. A multivariate approach for statistical assessments of compound extremes. *Journal of Hydrology*. 2018; 565, 87-94, doi: 10.1016/j.jhydrol.2018.08.025.

Hari V, Rakovec O, Markonis Y. et al. Increased future occurrences of the exceptional 2018–2019 Central European drought under global warming. *Sci Rep.* 2020*;* 10, 12207, doi: 10.1038/s41598-020-68872-9.

Hawcroft MK, Shaffrey LC, Hodges KI, Dacre HF. How much Northern Hemisphere precipitation is associated with extratropical cyclones?. *Geophys. Res. Lett*. 2012; 39, L24809, doi:10.1029/2012GL053866.

Hénin R, Ramos AM, Schemm S, Gouveia C, Liberato MLR. Assigning precipitation to mid-latitudes fronts on sub-daily scales in the North Atlantic and European sector: Climatology and trends. *International Journal of Climatology*. 2018a; 39: 317– 330, doi: 10.1002/joc.5808.

Hénin R, Liberato MLR, Ramos AM, Gouveia CM. Assessing the Use of Satellite-Based Estimates and High-Resolution Precipitation Data sets for the Study of Extreme Precipitation Events over the Iberian Peninsula. *Water*. 2018b; 10, 1688, doi: 10.3390/w10111688.

Hénin R, Ramos AM, Pinto JG, Liberato MLR. A ranking of concurrent precipitation and wind events for the Iberian Peninsula. *Int. J. Climatol.* 2021; 41: 1421– 1437, doi: 10.1002/joc.6829.

Herrera S, Gutiérrez JM, Ancell R, Pons MR, Frías MD, Fernández J. Development and analysis of a 50-year high-resolution daily gridded precipitation dataset over Spain (Spain02*). Int. J. Climatol.* 2012; 32, 74–85, doi: 10.1002/joc.2256.

Herring SCN, Christidis A, Hoell MP, Hoerling, PA. Stott. Explaining Extreme Events of 2019 from a Climate Perspective. *Bull. Amer. Meteor. Soc.* 2021*;* 102 (1), S1–S112, doi: 10.1175/BAMSExplainingExtremeEvents2019.1.

Hersbach H, Bell B, Berrisford P, Hirahara S, Horányi A, Muñoz-Sabater J et al. The ERA5 global reanalysis. *Q. J. R. Meteorol. Soc*. 2020; 146: 1999– 2049, doi: 10.1002/qj.3803.

Hersbach H, Dee D. ERA-5 reanalysis is in production. *ECMWF Newsl*. 2016; 147, 7.

Hewson TD. Objective identification of frontal wave cyclones. *Meteorological Applications.* 1997; 4: 311–315, doi: 10.1017/S135048279700073X.

Hewson TD. Objective fronts. *Meteorological Applications. 1998;* 5: 37–65, doi: 10.1017/S1350482798000553.

Hewson TD, Neu U. Cyclones, windstorms and the IMILAST project. Tellus A: Dynamic Meteorology and Oceanography. 2015; 67:1, doi: 10.3402/tellusa.v67.27128.

Hidalgo-Muñoz JM, Argüeso D, Gámiz-Fortis SR, Esteban-Parra, MJ, Castro-Díez Y. Trends of extreme precipitation and associated synoptic patterns over the southern Iberian Peninsula, *Journal of Hydrology.* 2011; 409, Issues 1–2, 497-511, doi: 10.1016/j.jhydrol.2011.08.049.

Hirsch J, Braun T, Bienert V. Assessment of Hail Risk on Real Estate: First Estimations with Climate Data, ERES eres2013_249, 2013; European Real Estate Society (ERES).

Hodges KI, Hoskins BJ, Boyle J, Thorncroft C. A Comparison of Recent Reanalysis Data sets Using Objective Feature Tracking: Storm Tracks and Tropical Easterly Waves. *Mon. Wea.*

Rev. 2003; 131, 2012–2037, doi: 10.1175/1520-0493(2003)131<2012:ACORRD>2.0.CO;2.

Holton, JR. An introduction to dynamic meteorology. New York : Academic Press, 1972.

Houze RA. Clouds and Precipitation in Extratropical Cyclones, *International Geophysics, Academic Press.* 2014; Vol. 104, Ch. 11, Pages 329-367, doi: 10.1016/B978-0-12-374266-7.00011-1.

Huffman GJ. NASA/GSFC; Greenbelt, M.D.; Adler, R.F.; Stocker, E.F.; Bolvin, D.T.; Nelkin, E.J. Analysis of TRMM 3-hourly multi-satellite precipitation estimates computed in both real and post-real time, 12th Conference on Satellite Meteorology and Oceanography, Poster Session 4, Moisture, Fluxes and Retrievals, 2003.

Huffman GJ, Bolvin DT, Nelkin EJ, Wolff DB, Adler RF, Gu G, et al. The TRMM Multisatellite Precipitation Analysis (TMPA): Quasi-Global, Multiyear, Combined-Sensor Precipitation Estimates at Fine Scales. *J. Hydrometeor.* 2007; 8, 38–55, doi: 10.1175/JHM560.1.

Huffman GJ, Adler RF, Bolvin DT, Nelkin EJ. The TRMM Multi-satellite Precipitation Analysis (TMPA). *Satellite Rainfall Applications for Surface Hydrology.* 2009. Springer, Dordrecht, doi: 10.1007/978-90-481-2915-7_1.

Huffman GJ, Bolvin DT. https://gpm.nasa.gov/sites/default/files/document_files/3B42_3B43_doc_V7.pdf Published on 8 April 2015. Accessed on 25 Sept 2018.

Huffman GJ, et al. Integrated Multi-satellite Retrievals for the Global Precipitation Measurement (GPM) Mission (IMERG). In: Levizzani V., Kidd C., Kirschbaum D., Kummerow C., Nakamura K., Turk F. (eds) Satellite Precipitation Measurement. Advances in Global Change Research, vol 67. Springer, 2020, Cham. DOI: 10.1007/978-3-030-24568-9_19.

Hunt E, Femia F, Werrell C, Christian JI, Otkin JA, Basara J, et al. Agricultural and food security impacts from the 2010 Russia flash drought, *Weather and Climate Extremes*. 2021; Volume 34, 100383, doi: 10.1016/j.wace.2021.100383.

IPCC, 2012: Managing the Risks of Extreme Events and Disasters to Advance Climate Change Adaptation. A Special Report of Working Groups I and II of the Intergovernmental Panel on Climate Change [Field, C.B., V. Barros, T.F. Stocker, D. Qin, D.J. Dokken, K.L. Ebi, M.D. Mastrandrea, K.J. Mach, G.-K. Plattner, S.K. Allen, M. Tignor, and P.M. Midgley (eds.)]. Cambridge University Press, Cambridge, UK, and New York, NY, USA, 582 pp.

IPCC, 2014: Climate Change 2014: Synthesis Report. Contribution of Working Groups I, II and III to the Fifth Assessment Report of the Intergovernmental Panel on Climate Change [Core Writing Team, R.K. Pachauri and L.A. Meyer (eds.)]. IPCC, Geneva, Switzerland, 151 pp.

IPCC, 2021: Climate Change 2021: The Physical Science Basis. Contribution of Working Group I to the Sixth Assessment Report of the Intergovernmental Panel on Climate Change [Masson-Delmotte, V., P. Zhai, A. Pirani, S.L. Connors, C. Péan, S. Berger, N. Caud, Y. Chen, L. Goldfarb, M.I. Gomis, M. Huang, K. Leitzell, E. Lonnoy, J.B.R. Matthews, T.K. Maycock, T. Waterfield, O. Yelekçi, R. Yu, and B. Zhou (eds.)]. Cambridge University Press. In Press.

Jenkner J, Sprenger M, Schwenk I, Schwierz C, Dierer S, Leuenberger D. Detection and climatology of fronts in a high-resolution model reanalysis over the Alps. *Meteorological Applications.* 2010*;* 17**:** 1–18, doi: 10.1002/met.142.

Jerez S, Montavez JP, Gomez-Navarro JJ, Lorente-Plazas R, Garcia-Valero JA, Jimenez-Guerrero P. A multi-physics ensemble of regional climate change projections over the Iberian Peninsula. *Climate Dynamics*. 2013; *41*(7–8), 1749–1768, doi :10.1007/s00382-012-1551-5.

Jiang S, Zhang Z, Huang Y, Chen X, Chen S. Evaluating the TRMM Multisatellite Precipitation Analysis for Extreme Precipitation and Streamflow in Ganjiang River Basin, China. *Advances in Meteorology*. 2017; Article ID 2902493, 11 pages, doi: 10.1155/2017/2902493.

Joyce RJ, Janowiak JE, Arkin PA, Xie P. CMORPH: a method that produces global precipitation estimates from passive microwave and infrared data at high spatial and temporal resolution, *J. Hydrometeorol*. 2004, 5, 487-503, doi: 10.1175/1525-7541(2004)005<0487:CAMTPG>2.0.CO;2.

Kållberg P. 2011. Forecast drift in ERA-Interim. ERA Report Series, No. 10, ECMWF: Reading, UK.

Karremann MK, Pinto JG, Reyers M, Klawa M. Return periods of losses associated with European windstorm series in a changing climate. *Environ. Res. Lett.* 2014; 9 124016, doi: 10.1088/1748-9326/9/12/124016.

Karremann MK, Liberato MLR, Ordóñez P, Pinto JG. Characterization of synoptic conditions and cyclones associated with top ranking potential wind loss events over Iberia. *Atmos. Sci. Lett*. 2016; 17: 354–361, doi: 10.1002/asl.665.

Kendon M, McCarthy M. The UK's wet and stormy winter of 2013/2014. *Weather.* 2015; 70: 40-47, doi: 10.1002/wea.2465.

Kettle AJ. Storm Tilo over Europe in November 2007: storm surge and impacts on societal and energy infrastructure. *Adv. Geosci.* 2019*; 49*, 187–196, doi; 10.5194/adgeo-49-187-2019.

Kew SF, Selten FM, Lenderink G, Hazeleger W. The simultaneous occurrence of surge and discharge extremes for the Rhine delta. *Nat. Hazards Earth Syst. Sci.* 2013; 13, 2017-2029, doi: 10.5194/nhess-13-2017-2013.

Khodayar S, Kalthoff N, Kottmeier C. Atmospheric conditions associated with heavy precipitation events in comparison to seasonal means in the western mediterranean region. *C. Clim Dyn*. 2018; 51: 951, doi: 10.1007/s00382-016-3058-y.

Klawa M, Ulbrich U. A model for the estimation of storm losses and the identification of severe winter storms in Germany. *Natural Hazards and Earth System Sciences.* 2003; 3, 725-732, doi: 10.5194/nhess-3-725-2003.

Kummerow C, Barnes W, Kozu T, Shiue J, Simpson J. The Tropical Rainfall Measuring Mission (TRMM) Sensor Package. *J. Atmos. Oceanic Technol.* 1998; 15809–15817, doi: 10.1175/1520-0426(1998)015<0809:TTRMMT>2.0.CO;2.

Lagerquist R, Mcgovern A, John D, Ii G. Object-based Deep Learning for Detection of Synoptic-scale Atmospheric Fronts, AMS 2019 annual meeting.

Laurila TK, Sinclair VA, Gregow H. Climatology, variability, and trends in near-surface wind speeds over the North Atlantic and Europe during 1979–2018 based on ERA5. *Int J Climatol.* 2021; 41: 2253– 2278, doi: 10.1002/joc.6957.

Lavers DA, Allan RP, Wood EF, Villarini G, Brayshaw DJ, Wade AJ. Winter floods in Britain are connected to atmospheric rivers, *Geophys. Res. Lett.* 2011; 38, L23803, doi: 10.1029/2011GL049783.

Lavers DA, Villarini G, Allan RP, Wood EF, Wade AJ. The detection of atmospheric rivers in atmospheric reanalyses and their links to British winter floods and the large-scale climatic circulation. *J. Geophys. Res.* 2012; 117, D20106, doi: 10.1029/2012JD018027.

Lavers DA, Richardson DS, Ramos AM, Zsoter E, Pappenberger F, Trigo RM. Earlier awareness of extreme winter precipitation across the western Iberian Peninsula. *Meteorol Appl.* 2018; 25: 622– 628, doi: 10.1002/met.1727.

Lavers DA, Villarini G. The nexus between atmospheric rivers and extreme precipitation across Europe. *Geophysical Research Letters.* 2013; 40: 3259–3264, doi: 10.1002/grl.50636.

Lavers DA, Villarini G. The contribution of atmospheric rivers to precipitation in Europe and the United States. *J. Hydrol.* 2015; 522, 382–390, doi: 10.1016/j.jhydrol.2014.12.010.

Leitão P, Roulet B, Rey J. The European Forecaster September 2018, newsletter n.23. Available at www.euroforecaster.org.

Leonard M, Westra S, Phatak A, Lambert M, van den Hurk B, McInnes K, Risbey J, Schuster S, Jakob D, Stafford-Smith M. A compound event framework for understanding extreme impacts. WIREs Clim Change. 2014; 5: 113-128, doi: 10.1002/wcc.252.

Levizzani V, Bauer P, Turk FJ. Measuring Precipitation from Space: EURAINSAT and the Future. 2007. (722p) Springer, doi: 10.1007/978-1-4020-5835-6.

Liberato MLR, Pinto JG, Trigo IF, Trigo RM. Klaus – an exceptional winter storm over northern Iberia and southern France. *Weather*. 2011; 66(12): 330–334, doi: 10.1002/wea.755.

Liberato MLR, Ramos AM, Trigo RM, Trigo IF, Durán-Quesada AM, Nieto R, Gimeno L. 2012. Moisture Sources and Large-Scale Dynamics Associated with a Flash Flood Event, in Lagrangian Modeling of the Atmosphere (eds J. Lin, D. Brunner, C. Gerbig, A. Stohl, A. Luhar and P. Webley). American Geophysical Union. Washington, D. C., doi: 10.1029/2012GM001244.

Liberato, MLR, Pinto JG, Trigo RM, Ludwig P, Ordóñez P, Yuen D, Trigo IF. Explosive development of winter storm Xynthia over the subtropical North Atlantic Ocean, *Nat. Hazards Earth Syst. Sci.* 2013; 13, 2239–2251, doi: 10.5194/nhess-13-2239-2013.

Liberato MLR, Trigo RM. Extreme precipitation events and related impacts in Western Iberia. Hydrology in a Changing World: Environmental and Human Dimensions. IAHS Red Book. 2014; No 363, 171-176. ISSN: 0144-7815.

Liberato MLR. The 19 January 2013 windstorm over the North Atlantic: large-scale dynamics and impacts on Iberia. *Weather and Climate Extremes*. 2014; 5: 16-28, doi: 10.1016/j.wace.2014.06.002.

Liberato MLR, Hénin R, Ramos AM, Gouveia C. Evaluating extreme precipitation events on the Iberian Peninsula using TRMM data. First International Electronic Conference on the Hydrological Cycle. 2017, 4880, doi: 10.3390/CHyCle-2017-04880.

Liberato MLR, Montero I, Gouveia C, Russo A, Ramos AM, Trigo RM. Rankings of extreme and widespread dry and wet events in the Iberian Peninsula between 1901 and 2016. *Earth Syst. Dynam.* 2021; 12, 197–210, doi: 10.5194/esd-12-197-2021.

Lionello P. 2012. The Climate of the Mediterranean Region: From the Past to the Future; Elsevier: Amsterdam, The Netherlands.

Liu C, Zipser E. Differences between the Surface Precipitation Estimates from the TRMM Precipitation Radar and Passive Microwave Radiometer Version 7 Products. *J. Hydrometeor*. 2014; 15, 2157–2175, doi: 10.1175/JHM-D-14-0051.1.

Liu Z, Ostrenga D, Teng W, Kempler S. Tropical Rainfall Measuring Mission (TRMM) Precipitation Data and Services for Research and Applications. *Bull. Amer. Meteor. Soc.* 2012; 93, 1317–1325, doi: 10.1175/BAMS-D-11-00152.1.

Liu Z. Comparison of versions 6 and 7 3-hourly TRMM multi-satellite precipitation analysis (TMPA) research products. *Atmospheric Research.* 2015a; 163, 91-101, doi: 10.1016/j.atmosres.2014.12.015.

Liu Z. Comparison of precipitation estimates between Version 7 3-hourly TRMM Multi-Satellite Precipitation Analysis (TMPA) near-real-time and research products. *Atmospheric Research*. 2015b; Vol. 153, 119-133, doi: 10.1016/j.atmosres.2014.07.032.

Lo Conti F, Hsu K-L, Noto LV, Sorooshian S. Evaluation and comparison of satellite precipitation estimates with reference to a local area in the Mediterranean Sea. *Atmospheric Research.* 2014; 153, 119-133, doi: 10.1016/j.atmosres.2014.07.032.

Lombardo K, Colle BA, Zhang Z. Evaluation of Historical and Future Cool Season Precipitation over the Eastern United States and Western Atlantic Storm Track Using CMIP5 Models. *J. Climate.* 2015; 28, 451–467, doi: 10.1175/JCLI-D-14-00343.1.

López-Moreno JI, Vicente-Serrano, SM. Positive and negative phases of the wintertime North Atlantic Oscillation and drought occurrence over Europe: A multitemporal-scale approach. *Journal of Climate*. 2008; 21(6), 1220–1243, doi: 10.1175/2007JCLI1739.1.

Lorente P, Hernández E, Queralt S, Ribera P. The flood event that affected Badajoz in November 1997. *Advances in Geosciences.* 2008; 16, 73–80, https://doi.org/10.5194/adgeo-16-73-2008.

Lorente-Plazas R, Montávez JP, Jimenez PA, Jerez S, Gómez-Navarro JJ, García-Valero JA, Jimenez-Guerrero P. Characterization of surface winds over the Iberian Peninsula. *International Journal of Climatology*. 2015; 35(6), 1007–1026, doi: 10.1002/joc.4034.

Manning C, Widmann M, Bevacqua E, Van Loon AF, Maraun D, Vrac M. Soil Moisture Drought in Europe: A Compound Event of Precipitation and Potential Evapotranspiration on Multiple Time Scales. *J. Hydrometeor.* 2018*;* 19, 1255–1271, doi:10.1175/JHM-D-18-0017.1.

Martín-Vide J., Gomez L. Regionalization of Peninsular Spain based on the length of dry spells, *Int. J. Climatol*. 1999; 19,537-555, doi: 10.1002/(SICI)1097-0088(199904)19:5<537::AID-JOC371>3.0.CO;2-X.

Martius O, Pfahl S, Chevalier C. A global quantification of compound precipitation and wind extremes. *Geophys. Res. Lett.* 2016; 43, 7709–7717, doi: 10.1002/2016GL070017.

Mathias L, Ermert V, Kelemen FD, Ludwig P, Pinto JG. Synoptic Analysis and Hindcast of an Intense Bow Echo in Western Europe: The 9 June 2014 Storm, *Weather and Forecasting.* 2017; 32(3), 1121-1141, doi: 10.1175/WAF-D-16-0192.1.

Matthews T, Murphy C, Wilby RL and Harrigan S. Stormiest winter on record for Ireland and UK. *Nature Climate Change*. 2014; 4, 738–740, doi: 10.1038/nclimate2336.

McGovern A, Elmore KL, Gagne II DJ, Haupt SE, Karstens CD, Lagerquist R, et al. Using Artificial Intelligence to Improve Real-Time Decision-Making for High-Impact Weather, *Bulletin of the American Meteorological Society*. 2017; 98(10), 2073-2090, doi: 10.1175/BAMS-D-16-0123.1.

Merino A, Fernández-Vaquero M, López L, Fernández-González S, Hermida L, Sánchez JL, García-Ortega E, Gascón E. Large-scale patterns of daily precipitation extremes on the Iberian Peninsula. *Int. J. Climatol.* 2016; 36: 3873-3891, doi: 10.1002/joc.4601.

Messori G, Bevacqua E, Caballero R, Coumou D, De Luca P, Faranda D et al.. Compound Climate Events and Extremes in the Midlatitudes: Dynamics, Simulation, and Statistical

Characterization. *Bulletin of the American Meteorological Society*. 2021; 102(4), E774-E781, doi: 10.1175/BAMS-D-20-0289.1.

Moftakhari HR, Salvadori G, AghaKouchak A, Sanders BF, Matthew RA. Compounding effects of sea level rise and flooding. *Proceedings of the National Academy of Sciences*. 2017; 114 (37) 9785-9790, doi: 10.1073/pnas.1620325114.

Moore P. An analysis of storm Ophelia which struck Ireland on 16 October 2017. *Weather.* 2021; 76: 301-306, doi: 10.1002/wea.3978.

Mornet A, Opitz T, Luzi M, Loisel S. Index for Predicting Insurance Claims from Wind Storms with an Application in France. *Risk Analysis*. 2015; 35: 2029-2056, doi:10.1111/risa.12395.

Muchan K, Lewis M, Hannaford J, Parry S. The winter storms of 2013/2014 in the UK: hydrological responses and impacts. *Weather.* 2015; 70: 55-61, doi: 10.1002/wea.2469.

Muehleisen W, Eder GC, Voronko Y, Spielberger M, Sonnleitner H, Knoebl K, et al. Outdoor detection and visualization of hailstorm damages of photovoltaic plants, *Renewable Energy*. 2018; Volume 118, Pages 138-145, doi: 10.1016/j.renene.2017.11.010.

Munich Re: Loss events in Europe 1980–2014: 10 costliest winter storms ordered by insured losses, *Tech. rep., Münchener Rückversicherungs-Gesellschaft*. 2015. Geo Risks Research, NatCat- SERVICE.

Musolino DA, Massarutto A, de Carli A, Does drought always cause economic losses in agriculture? An empirical investigation on the distributive effects of drought events in some areas of Southern Europe, *Science of The Total Environment*. 2018; Volume 633,2018, Pages 1560-1570, doi: 10.1016/j.scitotenv.2018.02.308.

Neu U, Akperov MG, Bellenbaum N, Benestad R, Blender R, Caballero R et al. IMILAST: A Community Effort to Intercompare Extratropical Cyclone Detection and Tracking Algorithms. *Bulletin of the American Meteorological Society.* 2013; 94: 529–547, doi: 10.1175/BAMS-D-11-00154.1.

Nieto Ferreira R. Synoptic climatology of cut-off low events that produced extreme precipitation in Valencia, Spain. *Proceedings of the 1st Int. Electron. Conf. Hydrol. Cycle*, 12–16 November 2017; Sciforum Electronic Conference Series, Vol. 1., doi: 10.3390/CHyCle-2017-04858.

Nieto Ferreira R. Cut-Off Lows and Extreme Precipitation in Eastern Spain: Current and Future Climate. *Atmosphere*. 2021; 12(7):835, doi: 10.3390/atmos12070835.

Nieto R, Gimeno L, Añel J, De la Torre L, Gallego D, Barriopedro D et al. Analysis of the precipitation and cloudiness associated with COLs occurrence in the Iberian Peninsula. *Meteorol. Atmos. Phys.* 2007; 96: 103, doi: 10.1007/s00703-006-0223-6.

Nissen KM, Leckebusch GC, Pinto JG, Renggli D, Ulbrich S, Ulbrich U. Cyclones causing wind storms in the Mediterranean: Characteristics, trends and links to large-scale patterns.

Natural Hazards and Earth System Science. 2010; *10*(7), 1379–1391, doi: 10.5194/nhess-10-1379-2010.

Outten S, Sobolowski S. Extreme wind projections over Europe from the Euro-CORDEX regional climate models. *Weather and Climate Extremes*. 2021; Volume 33, 100363, doi: 10.1016/j.wace.2021.100363.

Owen LE, Catto JL, Stephenson DB, Dunstone NJ. Compound precipitation and wind extremes over Europe and their relationship to extratropical cyclones, *Weather and Climate Extremes.* 2021; Volume 33, 100342, doi: 10.1016/j.wace.2021.100342.

Papagiannaki K, Lagouvardos K, Kotroni V. A Database of High-Impact Weather Events in Greece: A Descriptive Impact Analysis for the Period 2001-2011. *Nat. Hazards Earth Syst. Sci.* 2013; 13: 727-736, doi: 10.5194/nhess-13-727-2013.

Paredes D, Trigo RM, Garcia-Herrera R, Trigo IF. Understanding Precipitation Changes in Iberia in Early Spring: Weather Typing and Storm-Tracking Approaches. *J. Hydrometeor.* 2006; 7, 101–113, doi: 10.1175/JHM472.1.

Payne AE, Demory ME, Leung LR. et al. Responses and impacts of atmospheric rivers to climate change. *Nat. Rev. Earth Environ. 2020;* 1, 143–157, doi: 10.1038/s43017-020-0030-5.

Peña-Ortiz C, Barriopedro D, García-Herrera R. Multidecadal variability of the summer length in Europe. *Journal of Climate*. 2015; *28*(13), 5375–5388, doi: 10.1175/JCLI-D-14-00429.1.

Pendergrass AG, Knutti R. The Uneven Nature of Daily Precipitation and Its Change. *Geophysical Research Letters*. 2018; *45*(21), 11, 980-11, 988, doi: 10.1029/2018GL080298.

Pereira CS, Marta-Almeida M, Carvalho AC, Rocha A. Extreme precipitation events under climate change in the Iberian Peninsula. *Int J Climatol.* 2020; 40: 1255– 1278, doi: 10.1002/joc.6269.

Pereira S, Ramos AM, Rebelo L, Trigo RM, Zêzere JL. A centennial catalogue of hydro-geomorphological events and their atmospheric forcing. *Advances in Water Resources.* 2018; 122, 98-112, doi: 10.1016/j.advwatres.2018.10.001.

Pereira SC, Marta-Almeida M, Carvalho AC, Rocha A. Heat wave and cold spell changes in Iberia for a future climate scenario. *International Journal of Climatology*. 2017; *37*(15), 5192–5205, doi: 10.1002/joc.5158.

Pfahl S, Wernli H. Quantifying the Relevance of Cyclones for Precipitation Extremes. *J. Climate.* 2012; 25: 6770–6780, doi: 10.1175/JCLI-D-11-00705.1.

Pfahl S. Characterising the relationship between weather extremes in Europe and synoptic circulation features. *Nat. Hazards Earth Syst. Sci.* 2014; 14: 1461–1475, doi: 10.5194/nhess-14-1461-2014.

Phibbs S, Toumi R. The dependence of precipitation and its footprint on atmospheric temperature in idealized extratropical cyclones, *J. Geophys. Res. Atmos*. 2016; 121, 8743–8754, doi:10.1002/2015JD024286.

Pinto JG, Fröhlich EL, Leckebusch GC, Ulbrich U. Changing European storm loss potentials under modified climate conditions according to ensemble simulations of the ECHAM5/MPI-OM1 GCM. *Nat. Hazards Earth Syst. Sci.* 2007; 7, 165–175, doi: 10.5194/nhess-7-165-2007.

Pinto JG, Zacharias S, Fink AH. Factors contributing to the development of extreme North Atlantic cyclones and their relationship with the NAO. *Clim Dyn*. 2009; 32: 711, doi: 10.1007/s00382-008-0396-4.

Pinto JG, Karremann MK, Born K, Della-Marta PM, Klawa M. Loss potentials associated with European windstorms under future climate conditions. *Clim. Res.* 2012; 54:1-20, doi: 10.3354/cr01111.

Pinto JG, Gómara I, Masato G, Dacre HF, Woollings T, Caballero R. Large-scale dynamics associated with clustering of extratropical cyclones affecting Western Europe. *J. Geophys. Res. Atmos*. 2014; 119, 13,704– 13,719, doi: 10.1002/2014JD022305.

Pinto JG and Ludwig P. Extratropical cyclones over the North Atlantic and western Europe during the Last Glacial Maximum and implications for proxy interpretation. *Clim. Past.* 2020; 16, 611–626, doi: 10.5194/cp-16-611-2020.

Pinto P, Belo-Pereira M. Damaging Convective and Non-Convective Winds in Southwestern Iberia during Windstorm Xola. *Atmosphere*. 2020; 11(7): 692, doi: 10.3390/atmos11070692.

Pitt M. 2008. The Pitt Reviews – Lessons Learned From the 2007 Summer Floods, Final Report, Environ. Agency, London.

Priestley MDK, Pinto JG, Dacre HF, Shaffrey LC. The role of cyclone clustering during the stormy winter of 2013/2014. *Weather,* 2017; 72: 187-192, doi: 10.1002/wea.3025.

Priestley MDK, Dacre HF, Shaffrey LC, Schemm S, Pinto JG. The role of secondary cyclones and cyclone families for the North Atlantic storm track and clustering over western Europe. *Q. J. R. Meteorol. Soc*. 2020; 146: 1184– 1205. Doi: 10.1002/qj.3733.

Púčik T, Castellano C, Groenemeijer P, Kühne T, Rädler AT, Antonescu B, Faust E. Large Hail Incidence and Its Economic and Societal Impacts across Europe, *Monthly Weather Review*. 2019; 147(11), 3901-3916, doi: 10.1175/MWR-D-19-0204.1.

Punge HJ, Kunz M. Hail observations and hailstorm characteristics in Europe: A review, *Atmospheric Research*. 2016; Volumes 176–177, Pages 159-184, doi: 10.1016/j.atmosres.2016.02.012.

Raible CC, Della-Marta PM, Schwierz C, Wernli H, Blender R. Northern Hemisphere extratropical cyclones: A comparison of detection and tracking methods and different

reanalyses. *Monthly Weather Review*. 2008; *136*(3), 880–897, doi: 10.1175/2007MWR2143.1.

Raible CC, Messmer M, Lehner F, Stocker TF, Blender R. Extratropical cyclone statistics during the last millennium and the 21st century. *Climate of the Past.* 2018; 14, 1499–1514, doi: 10.5194/cp-14-1499-2018.

Raible CC, Pinto JG, Ludwig P, Messmer M. A review of past changes in extratropical cyclones in the northern hemisphere and what can be learned for the future. *WIREs Clim Change*. 2021; 12:e680. Doi: 10.1002/wcc.680.

Ramos AM, Trigo RM, Liberato MLR. A ranking of high-resolution daily precipitation extreme events for the Iberian Peninsula. *Atmospheric Science Letters.* 2014a; 15: 328–334, doi: 10.1002/asl2.507.

Ramos AM, Cortesi N, Trigo RM. Circulation weather types and spatial variability of daily precipitation in the Iberian Peninsula. *Front. Earth Sci.* 2014b; 2, 25, doi: 10.3389/feart.2014.00025.

Ramos AM, Trigo RM, Liberato MLR, Tomé R. Daily precipitation extreme events in the Iberian Peninsula and its association with Atmospheric Rivers. *Journal of Hydrometeorology.* 2015; 16: 579–597, doi: 10.1175/JHM-D-14-0103.1.

Ramos AM, Nieto R, Tomé R, Gimeno L, Trigo RM, Liberato MLR, Lavers DA. Atmospheric rivers moisture sources from a Lagrangian perspective. *Earth Syst. Dynam.* 2016a; 7, 371–384, doi: 10.5194/esd-7-371-2016.

Ramos AM, Tomé R, Trigo RM, Liberato MLR, Pinto JG. Projected changes in atmospheric rivers affecting Europe in CMIP5 models. *Geophysical Research Letters*. 2016b; 43:9315–9323, doi: 10.1002/2016GL070634.

Ramos AM, Trigo RM, Liberato MLR. Ranking of multi-day extreme precipitation events over the Iberian Peninsula. *Int. J. Climatol*. 2017; 37: 607–620, doi: 10.1002/joc.4726.

Ramos AM, Trigo RM, Tomé R, Liberato MLR. Impacts of Atmospheric Rivers in Extreme Precipitation on the European Macaronesian Islands. *Atmosphere.* 2018; 9(8):325, doi: 10.3390/atmos9080325.

Ramos AM, Sousa PM, Dutra E, Trigo RM. Predictive skill for atmospheric rivers in the western Iberian Peninsula, *Nat. Hazards Earth Syst. Sci.* 2020; 20, 877–888, doi: 10.5194/nhess-20-877-2020.

Raveh-Rubin S, Wernli H. Large-scale wind and precipitation extremes in the Mediterranean: a climatological analysis for 1979–2012. *Q.J.R. Meteorol. Soc.* 2015; 141: 2404-2417, doi: 10.1002/qj.2531.

Raveh-Rubin S, Catto JL. Climatology and dynamics of the link between dry intrusions and cold fronts during winter, Part II: Front-centred perspective. *Climate Dynamics*. 2019; *53*(3–4), 1893–1909, doi:10.1007/s00382-019-04793-2

Reale M, Lionello P. Synoptic climatology of winter intense precipitation events along the Mediterranean coasts. *Nat. Hazards Earth Syst. Sci.* 2013; 13, 1707–1722, doi: 10.5194/nhess-13-1707-2013.

Reale M, Liberato MLR, Lionello P, Pinto JG, Salon S, Ulbrich S. A Global Climatology of Explosive Cyclones using a Multi-Tracking Approach. *Tellus A: Dynamic Meteorology and Oceanography.* 2019; 71:1, 1-19, doi: 10.1080/16000870.2019.1611340.

Rebelo L, Ramos AM, Pereira S, Trigo RM. Meteorological Driving Mechanisms and Human Impacts of the February 1979 Extreme Hydro-Geomorphological Event in Western Iberia. *Water*. 2018; *10*, 454.

Ren F-M, Trewin B, Brunet M, Dushmanta P, Walter A, Baddour O, Korber M. A research progress review on regional extreme events. *Advances in Climate Change Research*. 2018; Volume 9, Issue 3,Pages 161-169, doi: 10.1016/j.accre.2018.08.001.

Renard R, Clarke L. Experiments in numerical objective frontal analysis. *Monthly Weather Review. 1965;* 93: 547-556, doi: 10.1175/1520-0493(1965)093<0547:EINOFA>3E2.3.CO;2.

Rhodes RI, Shaffrey LC, Gray SL. Can reanalyses represent extreme precipitation over England and Wales? *Quarterly Journal of the Royal Meteorological Society.* 2015; 141 (689), 1114-1120, doi: 10.1002/qj.2418.

Ribeiro AFS, Russo A, Gouveia CM et al. Modelling drought-related yield losses in Iberia using remote sensing and multiscalar indices. *Theor Appl Climatol*. 2019*;* 136, 203–220; doi: 10.1007/s00704-018-2478-5.

Ribeiro AFS, Russo A, Gouveia CM, Páscoa P, Zscheischler J. Risk of crop failure due to compound dry and hot extremes estimated with nested copulas. *Biogeosciences*. 2020a, 17, 4815–4830, doi: 10.5194/bg-17-4815-2020.

Ribeiro AFS, Russo A, Gouveia CM, Pires CAL. Drought-related hot summers: A joint probability analysis in the Iberian Peninsula, *Weather and Climate Extremes*. 2020b; Volume 30, 100279, doi: 10.1016/j.wace.2020.100279.

Ridder N, de Vries H, Drijfhout S. The role of atmospheric rivers in compound events consisting of heavy precipitation and high storm surges along the Dutch coast. *Nat. Hazards Earth Syst. Sci*. 2018; 18, 3311–3326, doi: 10.5194/nhess-18-3311-2018.

Ridder NN, Pitman AJ, Westra S. et al. Global hotspots for the occurrence of compound events. *Nat. Commun.* 2020*;* 11, 5956, doi: 10.1038/s41467-020-19639-3.

Robine J-M, Cheung SLK, Le Roy S, Van Oyen H, Griffiths C, Michel J-P, Herrmann FR. Death toll exceeded 70,000 in Europe during the summer of 2003. *Comptes Rendus Biologies.* 2008; Vol. 331, Issue 2, Pages 171-178, doi: 10.1016/j.crvi.2007.12.001.

Rossi G, Cancelliere A. Managing drought risk in water supply systems in Europe: a review, *International Journal of Water Resources Development*. 2013; 29:2, 272-289, doi: 10.1080/07900627.2012.713848.

Rüdisühli S, Sprenger M, Leutwyler D, Schär C, Wernli H. Attribution of precipitation to cyclones and fronts over Europe in a kilometer-scale regional climate simulation, *Weather Clim. Dynam.* 2020; 1, 675–699, doi: 10.5194/wcd-1-675-2020.

Ruffault J, Moron V, Trigo RM, Curt T. Daily synoptic conditions associated with large fire occurrence in Mediterranean France: evidence for a wind-driven fire regime. *Int. J. Climatol*. 2017; 37: 524-533, doi: 10.1002/joc.4680.

Rummukainen M. Changes in climate and weather extremes in the 21st century. *WIREs Clim Change*. 2012; 3: 115-129, doi.org/10.1002/wcc.160.

Russo A, Gouveia CM, Páscoa P, DaCamara CC, Sousa PM, Trigo RM. Assessing the role of drought events on wildfires in the Iberian Peninsula. *Agricultural and Forest Meteorology*. 2017; *237–238*, 50–59, doi: 10.1016/j.agrformet.2017.01.021.

Sadegh M, Moftakhari H, Gupta HV, Ragno E, Mazdiyasni O, Sanders B, Matthew R, AghaKouchak A. Multihazard scenarios for analysis of compound extreme events. *Geophysical Research Letters.* 2018; 45, 5470– 5480, doi: 10.1029/2018GL077317.

Sáez de Cámara E, Gangoiti G, Alonso L, Iza J. Daily precipitation in Northern Iberia: Understanding the recent changes after the circulation variability in the North Atlantic sector, *J. Geophys. Res. Atmos*. 2015; 120, 9981– 10,005, doi: 10.1002/2015JD023306.

Salmoral G, Ababio B, Holman IP. Drought Impacts, Coping Responses and Adaptation in the UK Outdoor Livestock Sector: Insights to Increase Drought Resilience. *Land*. 2020; 9(6):202, doi: 10.3390/land9060202.

Sanders F, Gyakum JR. Synoptic-Dynamic Climatology of the "Bomb", *Monthly Weather Review*. 1980; *108*(10), 1589-1606, doi: 10.1175/1520-0493(1980)108<1589:SDCOT>2.0.CO;2.

Santos JA, Rochinha C, Liberato MLR, Reyers M, Pinto JG, Projected changes in wind energy potentials over Iberia. *Renewable Energy*, 2015; Volume 75, Pages 68-80, doi: 10.1016/j.renene.2014.09.026.

Santos M, Fragoso M. Precipitation variability in Northern Portugal: Data homogeneity assessment and trends in extreme precipitation indices. *Atmospheric research.* 2013; 131, 34-45, doi: 10.1016/j.atmosres.2013.04.008.

Santos M, Fonseca A, Fragoso M, Santos JA. Recent and future changes of precipitation extremes in mainland Portugal. *Theoretical and Applied Climatology*. 2019; *137*(1–2), 1305–1319, doi: 10.1007/s00704-018-2667-2.

Santos VM, Casas-Prat M, Poschlod B, Ragno E, van den Hurk B, Hao Z, Kalmár T et al. Statistical modelling and climate variability of compound surge and precipitation events in a managed water system: a case study in the Netherlands. *Hydrol. Earth Syst.* Sci. 2021; 25, 3595–3615, doi: 10.5194/hess-25-3595-2021.

Sanuy M, Rigo T, Jiménez JA, Llasat MC. Classifying compound coastal storm and heavy rainfall events in the north-western Spanish Mediterranean. *Hydrol. Earth Syst. Sci.* 2021; 25, 3759–3781, doi: 10.5194/hess-25-3759-2021.

Scheel MLM, Rohrer M, Huggel Ch, Santos Villar D, Silvestre E, Huffman GJ. Evaluation of TRMM Multi-satellite Precipitation Analysis (TMPA) performance in the Central Andes region and its dependency on spatial and temporal resolution. *Hydrol. Earth Syst. Sci.* 2011; 15, 2649-2663, doi: 10.5194/hess-15-2649-2011.

Schemm S, Rudeva I, Simmonds I. Extratropical fronts in the lower troposphere–global perspectives obtained from two automated methods. *Quarterly Journal of the Royal Meteorological Society*. 2015; 141: 1686–1698, doi: 10.1002/qj.2471.

Schemm S, Nisi L, Martinov A, Leuenberger D, Martius O. On the link between cold fronts and hail in Switzerland. *Atmos. Sci. Lett*. 2016; 17: 315–325, doi: 10.1002/asl.660.

Schemm S, Sprenger M, Martius O, Wernli H, Zimmer M. Increase in the number of extremely strong fronts over Europe? A study based on ERA-Interim reanalysis (1979–2014). *Geophysics Research Letters.* 2017; 44: 553–561, doi: 10.1002/2016GL071451.

Schemm S, Sprenger M, Wernli H. When during their life cycle are extratropical cyclones attended by fronts?. *Bulletin of the American Meteorological Society*. 2018; doi: 10.1175/BAMS-D-16-0261.1.

Schultz DM, Zhang F. Baroclinic development within zonally-varying flows. *Q. J. Roy. Meteorol. Soc.* 2017; 133: 1101-1112, doi: 10.1002/qj.87.

Screen JA, Simmonds I. Amplified mid-latitude planetary waves favour particular regional weather extremes. *Nature Climate Change*. 2014; *4*(8), 704–709, doi: 10.1038/nclimate2271.

Seneviratne SI, Nicholls N, Easterling D, Goodess CM, Kanae S, Kossin J, et al. Changes in climate extremes and their impacts on the natural physical environment. Managing the Risks of Extreme Events and Disasters to Advance Climate Change Adaptation. A Special Report of Working Groups I and II of the Intergovernmental Panel on Climate Change (IPCC). Cambridge University Press, Cambridge, UK, and New York, NY, USA; 2012, 109–230.

Serrano A, Garciacutea J, Mateos V, Cancillo ML, Garrido. J. Monthly modes of variation of precipitation over the Iberian Peninsula. *J. Clim.* 1999; 12, 2894–2919, doi: 10.1175/1520-0442(1999)012<2894:MMOVOP>2.0.CO;2.

Shan K and Yu X. Enhanced understanding of poleward migration of tropical cyclone genesis. *Environ. Res. Lett*. 2020; 15, 104062, doi: 10.1088/1748-9326/abaf85.

Sharifi E, Eitzinger J, Dorigo W. Performance of the State-Of-The-Art Gridded Precipitation Products over Mountainous Terrain: A Regional Study over Austria. *Remote Sensing.* 2019; 11(17):2018, doi: 10.3390/rs11172018.

Shields CA, Rutz JJ, Leung L-Y, Ralph FM, Wehner M, Kawzenuk B, et al. Atmospheric River Tracking Method Intercomparison Project (ARTMIP): project goals and experimental design. *Geoscientific Model Dev*elopment. 2018; 11, 2455–2474, doi: 10.5194/gmd-11-2455-2018.

Sillmann J, Thorarinsdottir T, Keenlyside N, Schaller N, Alexander LV, Hegerl G, et al. Understanding, modeling and predicting weather and climate extremes: Challenges and opportunities. *Weather and Climate Extremes.* 2017; 18, 65-74, ISSN 2212-0947, doi: 10.1016/j.wace.2017.10.003.

Simmonds I, Keay K, Bye JAT. 2012. Identification and climatology of Southern Hemisphere mobile fronts in a modern reanalysis. Journal of Climate 25: 1945-1962, doi: 10.1175/JCLI-D-11-00100.1.

Simmonds I and Govekar PD. What are the physical links between Arctic sea ice loss and Eurasian winter climate?, *Environ. Res. Lett.* 2014; 9 101003, doi: 10.1088/1748-9326/9/10/101003.

Simmons AJ, Willett KM, Jones PD, Thorne PW, Dee DP. Low-frequency variations in surface atmospheric humidity, temperature, and precipitation: Inferences from reanalyses and monthly gridded observational data sets. *Journal of Geophysical Research.* 2010*;* 115: D01110, doi: 10.1029/2009JD012442.

Sinclair VA, Rantanen M, Haapanala P, Räisänen J, Järvinen H. The characteristics and structure of extra-tropical cyclones in a warmer climate, *Weather Clim. Dynam.* 2020; 1, 1–25, doi: 10.5194/wcd-1-1-2020.

Skofronick-Jackson G, Petersen WA, Berg W, Kidd C, Stocker EF, Kirschbaum DB, et al. The Global Precipitation Measurement (GPM) Mission for Science and Society. *Bull. Amer. Meteor. Soc.* 2017; 98, 1679–1695, doi: 10.1175/BAMS-D-15-00306.1.

Sorooshian S, Hsu KL, Gao X, Gupta HV, Imam B, Braithwaite D. Evaluation of PERSIANN system satellite-based estimates of tropical rainfall. *Bulletin of the American Meteorological Society*. 2000; *81*(9), 2035–2046, doi: 10.1175/1520-0477(2000)081<2035:EOPSSE>2.3.CO;2.

Sousa PM, Barriopedro D, Trigo RM, Ramos AM, Nieto R, Gimeno L, Turkman KF, Liberato MLR. Impact of Euro-Atlantic blocking patterns in Iberia precipitation using a novel high-resolution dataset, *Climate Dynamics.* 2016; 46 (7-8), 2573-2591. doi: 10.1007/s00382-015-2718-7.

Sousa PM, Ramos AM, Raible CC, Messmer M, Tomé R, Pinto JG, Trigo RM. North Atlantic Integrated Water Vapor Transport—From 850 to 2100 CE: Impacts on Western European Rainfall, *Journal of Climate*. 2020. 33(1), 263-279. doi: 10.1175/JCLI-D-19-0348.1.

Stephenson DB, Pavan V, Collins M, Junge MM, Quadrelli R. North Atlantic Oscillation response to transient greenhouse gas forcing and the impact on European winter climate: A CMIP2 multi-model assessment. *Climate Dynamics*, 2006; *27*(4), 401–420, doi: 10.1007/s00382-006-0140-x.

Sutanto SJ, Vitolo C, Di Napoli C, D'Andrea, Lanen HAJ, Heatwaves, droughts, and fires: Exploring compound and cascading dry hazards at the pan-European scale, *Environment International*. 2020; Vol. 134,105276, doi: 10.1016/j.envint.2019.105276.

Swiss Re. Natural catastrophes and man-made disasters in 2007: high losses in Europe – Sigma, Nr. 1/2008. Swiss Re Publishing, 2008. Available at www.swissre.com/sigma/1_2008.html.

Tamarin-Brodsky T, Kaspi Y. Enhanced poleward propagation of storms under climate change. *Nature Geoscience. 2017;* 10, 908–913 (2017), doi: 10.1038/s41561-017-0001-8.

Tang G, Clark MP, Papalexiou SM, Ma Z, Hong Y. Have satellite precipitation products improved over last two decades? A comprehensive comparison of GPM IMERG with nine satellite and reanalysis data sets. *Remote Sensing of Environment*. 2020; Volume 240, 111697, doi: 10.1016/j.rse.2020.111697.

Tang S, Li R, He J, Wang H, Fan X, Yao S. Comparative Evaluation of the GPM IMERG Early, Late, and Final Hourly Precipitation Products Using the CMPA Data over Sichuan Basin of China. *Water.* 2020; 12(2):554, doi: 10.3390/w12020554.

Tervo R, Láng I, Jung A, Mäkelä A. Predicting power outages caused by extratropical storms, *Nat. Hazards Earth Syst. Sci*. 2021; 21, 607–627, doi: 10.5194/nhess-21-607-2021.

Thomas CM, Schultz DM. Global climatologies of fronts, airmass boundaries, and airstream boundaries: Why the definition of "front' matters. *Monthly Weather Review*. 2019; *147*(2), 691–717, doi: 10.1175/MWR-D-18-0289.1.

Thorne PW, Vose RS. Reanalyses suitable for characterizing long-term trends: Are they really achievable? *Bulletin of the American Meteorological Society.* 2010; 91, 353–361, doi: 10.1175/2009BAMS2858.1.

Tilinina N, Gulev SK, Bromwich DH. New view of Arctic cyclone activity from the Arctic system reanalysis. *Geophys. Res. Lett.* 2014; 41: 1766–1772, doi: 10.1002/2013GL058924.

Trigo IF. Climatology and interannual variability of storm-tracks in the Euro-Atlantic sector: a comparison between ERA-40 and NCEP/NCAR reanalyses. *Climate Dynamics*. 2006; 26: 127-143, doi: 10.1007/s00382-005-0065-9.

Trigo RM, Valente MA, Trigo IF, Miranda PMA, Ramos AM., Paredes D, García-Herrera R. The Impact of North Atlantic Wind and Cyclone Trends on European Precipitation and Significant Wave Height in the Atlantic. *Annals of the New York Academy of Sciences*. 2008; 1146: 212-234, doi:10.1196/annals.1446.014.

Trigo RM, Varino F, Ramos AM, Valente MA, Zêzere JL, Vaquero JM et al. The record precipitation and flood event in Iberia in December 1876: Description and synoptic analysis. *Front. Earth Sci.* 2014; 2, doi: 10.3389/feart.2014.00003.

Trigo RM, Ramos C, Pereira SS, Ramos AM, Zêzere JL, Liberato MLR. The deadliest storm of the 20th century striking Portugal: Flood impacts and atmospheric circulation. *Journal of Hydrolology*. 2016; 541: 597-610, doi: 10.1016/j.jhydrol.2015.10.036.

Uccellini LW. Processes Contributing to the Rapid Development of Extratropical Cyclones. In: Newton C.W., Holopainen E.O. (eds) Extratropical Cyclones. *American Meteorological Society*. 1990. Boston, MA, doi: 10.1007/978-1-944970-33-8_6.

Ulbrich U, Brücher T, Fink AH, Leckebusch GC, Krüger A, Pint JG. The central European floods of August 2002: Part 1 - Rainfall periods and flood development. *Weather. 2003;* 58 (10): 371-377, doi: 10.1256/wea.61.03A.

Ulbrich U, Leckebusch GC and Pinto JG. Extra-tropical cyclones in the present and future climate: a review. *Theor. Appl. Climatol.* 2009; 96 (1-2), 117-131, doi: 10.1007/s00704-008-0083-8.

Uppala SM, KÅllberg PW, Simmons AJ, Andrae U, Bechtold VDC, Fiorino M et al. The ERA-40 re-analysis. *Quarterly Journal of the Royal Meteorological* Society. 2005; 131: 2961–3012, doi: 10.1256/qj.04.176.

Vaglio Laurin G, Francini S, Luti T, Chirici G, Pirotti F, Papale D. Satellite open data to monitor forest damage caused by extreme climate-induced events: a case study of the Vaia storm in Northern Italy, *Forestry: An International Journal of Forest Research*. 2021; Volume 94, Issue 3, Pages 407–416, doi: 10.1093/forestry/cpaa043.

Van den Hurk B, van Meijgaard E, de Valk P, van Heeringen K-J, Gooijer J. Analysis of a compounding surge and precipitation event in the Netherlands. *Environ. Res. Lett.* 2015; 10 035001, doi: 1088/1748-9326/10/3/035001.

Veals PG, Steenburgh WJ. Climatological Characteristics and Orographic Enhancement of Lake-Effect Precipitation East of Lake Ontario and over the Tug Hill Plateau. *Mon. Wea. Rev.* 2015; 143, 3591–3609, doi: 10.1175/MWR-D-15-0009.1.

Vicente-Serrano SM, Trigo RM, López-Moreno JI, Liberato MLR, Lorenzo-LaCruz J, Beguería S et al. Extreme winter precipitation in the Iberian Peninsula in 2010: anomalies, driving mechanisms and future projections. *Climate Research.* 2011; 46: 51-65, doi: 10.3354/cr00977.

Vicente-Serrano SM, Rodríguez-Camino E, Domínguez-Castro F, El Kenawy A, Azorín-Molina C. An updated review on recent trends in observational surface atmospheric variables and their extremes over Spain. *Cuadernos de Investigacion Geografica*. 2017; *43*(1), 209–232, doi: 10.18172/cig.3134.

Villarini G. Evaluation of the Research-Version TMPA Rainfall Estimate at Its Finest Spatial and Temporal Scales over the Rome Metropolitan Area. J. *Appl. Meteor. Climatol.* 2010; 49, 2591-2602, doi: 10.1175/2010JAMC2462.1.

Wakimoto RM, Murphey HV, Nester A, Jorgensen DP, Atkins NT. High Winds Generated by Bow Echoes. Part I: Overview of the Omaha Bow Echo 5 July 2003 Storm during BAMEX. *Mon. Weather Review*. 2006; 134(10), 2793-2812, doi: 10.1175/MWR3215.1.

Wilks DS. Statistical Methods in the Atmospheric Sciences. 2006. 2nd ed. USA: Academic Press. ISBN: 0127519661.

Wilks DS. "The Stippling Shows Statistically Significant Grid Points": How Research Results are Routinely Overstated and Overinterpreted, and What to Do about It. Bull. Amer. Meteor. Soc. 2016; 97, 2263–2273, doi: 10.1175/BAMS-D-15-00267.1.

Woollings T, Czuchnicki C, Franzke C. Twentieth century North Atlantic jet variability. *Quarterly Journal of the Royal Meteorological Society*. 2014; *140*(680), 783–791, doi: 10.1002/qj.2197.

Wu W, McInnes K, O'Grady J, Hoeke R, Leonard M, Westra S. Mapping dependence between extreme rainfall and storm surge. *Journal of Geophysical Research: Oceans*. 2018; 123, 2461- 2474. doi: 10.1002/2017JC013472.

Yong B, Ren L-L, Hong Y, Wang J-H, Gourley JJ, Jiang S-H, et al. Hydrologic evaluation of Multisatellite Precipitation Analysis standard precipitation products in basins beyond its inclined latitude band: A case study in Laohahe basin, China. *Water Resour. Res.* 2010; 46, W07542, doi: 10.1029/2009WR008965.

Yong B, Chen B, Gourley JJ, et al. Intercomparison of the Version-6 and Version-7 TMPA precipitation products over high and low latitudes basins with independent gauge networks: Is the newer version better in both real-time and post-real-time analysis for water resources and hydrologic extremes?, *Journal of Hydrology*. 2014; Volume 508, 77-87, doi: 10.1016/j.jhydrol.2013.10.050.

Zappa G, Shaffrey LC, Hodges KI, Sansom PG, Stephenson DB. A Multimodel Assessment of Future Projections of North Atlantic and European Extratropical Cyclones in the CMIP5 Climate Models. *J. Climate.* 2013; 26, 5846–5862. doi: 10.1175/JCLI-D-12-00573.1.

Zscheischler J and Seneviratne SI. Dependence of drivers affects risks associated with compound events. *Nat. Science Advances.* 2017; 3, 6, doi: 10.1126/sciadv.1700263.

Zscheischler J, Westra S, van den Hurk BJJM, Seneviratne SI, Ward PJ, Pitman A, et al. Future climate risk from compound events. *Nature Climate Change*. 2018; doi: 10.1038/s41558-018-0156-3.

Zscheischler J, Martius O, Westra S. et al. A typology of compound weather and climate events. *Nat. Rev. Earth Environ*. 2020a; 1, 333–347, doi: 10.1038/s43017-020-0060-z.

Zscheischler J, van den Hurk B, Ward PJ, Westra S, Chapter 4 - Multivariate extremes and compound events, Editor(s): Jana Sillmann, Sebastian Sippel, Simone Russo, Climate Extremes and Their Implications for Impact and Risk Assessment, Elsevier, 2020b, Pages 59-76, ISBN 9780128148952, doi: 10.1016/B978-0-12-814895-2.00004-5.

Zscheischler J, Naveau P, Martius O, Engelke S, Raible CC. Evaluating the dependence structure of compound precipitation and wind speed extremes. *Earth Syst. Dynam.* 2021; 12, 1–16, doi: 10.5194/esd-12-1-2021.

List of contributions and publications

Publication to ISI Journals

Hénin R, Ramos AM, Schemm S, Gouveia C, Liberato MLR. 2018. Assigning precipitation to mid-latitudes fronts on sub-daily scales in the North Atlantic and European sector: Climatology and trends. *International Journal of Climatology*, 2018, 1-14, doi: 10.1002/joc.5808.

Hénin R, Liberato MLR, Ramos AM, Gouveia CM. 2018. Assessing the Use of Satellite-Based Estimates and High-Resolution Precipitation Data sets for the Study of Extreme Precipitation Events over the Iberian Peninsula. *Water*, 2018, 10, 1688, doi: 10.3390/w10111688.

Hénin R, Ramos AM, Pinto JG, Liberato MLR. A ranking of concurrent precipitation and wind events for the Iberian Peninsula. *International Journal of Climatology*, 2021; 41: 1421– 1437, doi:10.1002/joc.6829.

Conference Proceedings

Liberato MLR, Hénin R, Ramos AM, Gouveia C. 2017. Evaluating extreme precipitation events on the Iberian Peninsula using TRMM satellite data. *In Proceedings of the 1st Int. Electron. Conf. Hydrol. Cycle*, 12–16 November 2017; Sciforum Electronic Conference Series, Vol. 1, 2017. doi:10.3390/CHyCle-2017-04880.

Hénin R, Liberato MLR, Ramos AM, Gouveia CM. 2018. Caracterização da precipitação frontal associada aos eventos extremos na Península Ibérica. *In Proceedings of the 10º Simpósio de Meteorologia e Geofísica da APMG – 18º Encontro Luso-Espanhol de Meteorologia*, Lisbon, 22-27 Mar 2017 [in press].

Poster Communications and Oral Presentations at Conferences

Hénin R, Ramos AM, Pinto JG, Liberato MLR. A ranking of concurrent precipitation and wind events for the Iberian Peninsula, Workshop on Compound Weather and Climate Events, Bern, Switzerland, 12-15 January 2021. (oral communication)

Hénin R, Liberato MLR, Ramos AM, Gouveia CM. Assessing the Use of Satellite-Based Estimates and High-Resolution Precipitation Data sets for the Study of Extreme Precipitation Events over the Iberian Peninsula. EMS Annual Conference 2019. Copenaghen, Denmark, 9-13 September 2019. (oral communication)

Hénin R, Liberato MLR, Ramos AM. Objective assignment of precipitation and fronts to cyclones: application to extreme events on the Iberian Peninsula EGU - European Geosciences Union General Assembly 2019. Wien, 7-12 Apr 2019. (oral communication)

Liberato MLR, Paredes H, Ramos AM, Reis A, Hénin R, Barroso J. Expert Crowdsourcing for Semantic Annotation of Atmospheric Phenomena. AGU - American Geosciences Union Fall Meeting 2018. Washington, 10-14 Dec 2018. (poster)

Hénin R, Liberato MLR, Ramos AM. Variability of compound extreme events in the Euro-Atlantic region and its association to extratropical storms. 7th European Windstorm Workshop. Karlsruhe, 10-13 October 2018. (poster)

Liberato MLR, Ramos AM, Trigo R, Hénin R, Pinto J, Karremann MK, Paredes H, Reis A, Martins P, Barroso J. Consistent catalogues of extreme and high impact winter storms in Portugal. 7th European Windstorm Workshop. Karlsruhe, 10-13 October 2018. (oral communication)

Hénin R, Liberato MLR, Ramos AM. Assessing frontal and extreme precipitation over the Euro-Atlantic domain. EGU - European Geosciences Union General Assembly 2018. Wien, 8-13 Apr 2018. (poster)

Liberato MLR, Paredes H, Ramos AM, Hénin R, Martins P, Barroso J. Expert Crowdsourcing for Semantic Annotation of Extreme Meteorological and Hydrological Phenomena. EGU - European Geosciences Union General Assembly 2018. Wien, 8-13 Apr 2018. (poster)

Hénin R, Liberato MLR, Ramos AM, Gouveia CM. Caracterização da precipitação frontal associada aos eventos extremos na Península Ibérica. 10º Simpósio de Meteorologia e Geofísica da APMG – 18º Encontro Luso-Espanhol de Meteorologia, Lisbon, 22-27 Mar 2017 (poster).

Hénin R, Ramos AM, Liberato MLR, Gouveia CM. Relating precipitation to fronts at a sub-daily basis. EGU - European Geosciences Union General Assembly 2017 – Wien, 23-28 Apr 2017 (poster)